EXPERIMENTAL STUDY ON MICROWAVE ASSISTED CVD GROWTH OF CARBON NANOTUBES ON SILICON WAFER USING COBALT AS A CATALYST

By

MADHAN PRASATH RAMAKRISHNAN

Bachelor of Engineering

Bharathiar University

Coimbatore, India

May, 2000

Submitted to the Faculty of the
Graduate College of the
Oklahoma State University
in partial fulfillment of
the requirements for
the Degree of
MASTER OF SCIENCE
May, 2005

EXPERIMENTAL STUDY ON MICROWAVE

ASSISTED CVD GROWTH OF CARBON

NANOTUBES ON SILICON WAFER

USING COBALT AS A

CATALYST

Thesis Approved:

Dr. Ranga Komanduri

Thesis Advisor

Dr. Hongbing Lu

Dr. Lionel M. Raff

Dr. A. Gordon Emslie

Dean of the Graduate College

SUMMARY

Controlled growth of carbon nanotubes is an important step in the realization of practical nanoscale devices for applications in nanoelectronics, sensors, field emission displays, and microelectro mechanical systems (MEMS), among others. Microwave assisted Chemical Vapor Deposition (CVD) technique has been successfully used to synthesize carbon nanotubes on silicon wafer substrates. Since a transition metal catalyst, such as iron, nickel, cobalt is needed for growth of nanotubes, a thin film of cobalt catalyst (2 ~ 5 nm) is deposited on the silicon wafer substrates using Pulsed Laser Deposition (PLD) technique using an excimer laser (248nm). The CVD process conditions, including growth time, plasma pretreatment time, process gases, and flow rate of carbon source gas (methane) are studied towards obtaining controlled growth of nanotubes. Further, patterned catalyst film is formed by the PLD technique and vertically aligned nanotubes are successfully grown on patterned catalyst film. The carbon nanotubes are characterized using SEM, TEM, AFM and μ-Raman Spectroscopy.

ACKNOWLEDGEMENT

I would like to express indebtedness to my advisor and mentor, Dr.Ranga Komanduri, for his support, guidance, and advice. I truly appreciate his encouragement and advices in helping me grow, not only technically, but also in all aspects during the course of my M.S. study. I would like to thank my committee members, Dr. H.B. Lu and Dr. L.M.Raff, for kindly serving in my thesis committee.

I also wish to express my sincere gratitude to my teammates, Mr. Raju Nidadavolu and Mr. Devanathan Raghavan, for their contributions towards this project work. I would also like to thank Mr. Sony Varghese, for his valuable help with PLD technique, AFM characterization, and many useful suggestions. I would like to thank Mrs. Phoebe Doss, and Mr. Terry colberg for their help with SEM and TEM characterization. I would also like to extend my gratitude to Lee, Choo, Hari, Anand, Ganesh and all the members of our research group for their support and friendship.

I would like to thank the Department of Mechanical and Aerospace Engineering for providing me with the opportunity to pursue M.S at Oklahoma State University.

I am ever thankful to my parents and grandparents who were always a constant source of inspiration and encouragement for me at all times. Finally, I would like to extend my gratitude to my sister, brother-in-law and my twin little nieces for their inspiration and love.

TABLE OF CONTENTS

LIST OF TABLES

Table **Page**

LIST OF FIGURES

CHAPTER 1

INTRODUCTION

1.1 CARBON NANOTUBES

Carbon nanotubes (CNTs) were discovered by Iijima in 1991 while investigating the soot of an arc-discharge experiment used to create C_{60} buckyballs [1]. Soon after his discovery carbon nanotube is identified as the fourth allotropic form of carbon along with three other allotropic forms, namely, fullerenes, graphite and diamond [2]. Experimental investigations and theoretical studies have shown that carbon nanotubes possess unique properties, such as exceptionally high young's modulus (1-5 TPa) [3, 4], very high thermal conductivity (~2000 W/m/K) [5, 6, 7], least resistance for electrical conductivity (10^{-4} Ω-cm) [8,111], and ability to conduct remarkably huge amounts of current density (10^{13} A/m^2) [8]. As a result, carbon nanotubes can be used for a wide range of applications including, reinforcing fibers for composites [9], field emission displays [10, 11], and myriad of other applications such as interconnects in microelectronics, field effect transistors (FETs) [12, 13], hydrogen storage batteries and nanoprobes and sensors [14]. Additionally, newly reported applications include nanotube antennas for detecting and transmitting radio waves [15], nano scale mass conveyors [16], filters [17], and as electromechanical oscillators in nanoelectromechanical systems (NEMS) [18].

1.2 CARBON NANOTUBES- MORPHOLOGY

Carbon nanotubes can be visualized as a sheet of graphite that has been rolled into a tube. Since these tubes are found to have diameters varying from a few nanometers to a few hundreds of nanometers these tubes are commonly known as nanotubes. The nanotubes exist as single walled or multiwalled tubes as shown in Figure 1.1. In the case of a single walled carbon nanotube, a single sheet of graphite is rolled to form the tube, or when multiple single walled nanotubes are arranged concentrically along a common axis they result in the formation of multiwalled carbon nanotubes. Carbon atoms are arranged in a hexagonal array in a single sheet of graphite, with each carbon atom having three neighboring carbon atoms.

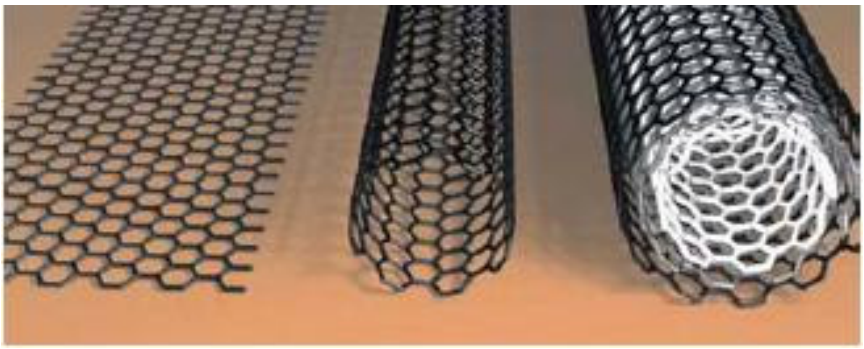

Figure 1.1 Illustration of a graphite sheet where carbon atoms are arranged in a hexagonal array, and a single wall (middle) and, multiwall carbon nanotubes (right) [19].

1.3 CARBON NANOTUBES STRUCTURE

The atomic structure of nanotubes is expressed in terms of the chiral vector, C_h which describes the structure in terms of the tube chirality (helicity) and the chiral angle θ. The chiral vector is described by the following equation:

$$C_h = n\hat{a}_1 + m\hat{a}_2$$

The integers (n, m) are the number of steps along the zig-zag carbon atoms on the hexagonal lattice and $\hat{a}_1$, $\hat{a}_2$ are the unit vectors as shown in Figure 1.2.

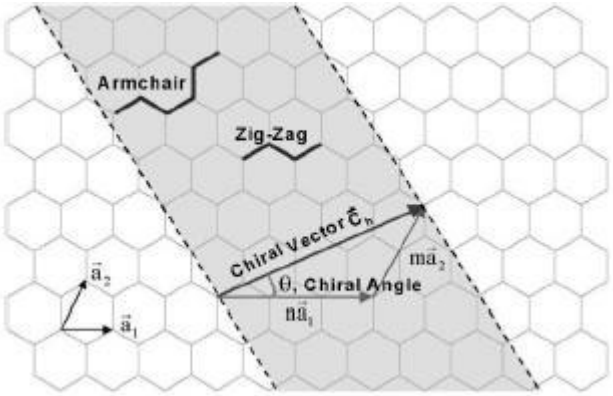

Figure 1.2. Schematic diagram showing the hexagonal sheet of graphite, rolled to form a carbon nanotube [20].

The chiral angle determines the amount of twist in the tube and two limiting cases occur when the chiral angle is 0° and 30°. These limiting cases are referred to as *zig-zag* and *armchair* based on the geometry of the carbon atoms around the circumference of the nanotube. The difference in armchair and zig-zag tubes is shown in Figure 1.3. In terms of the roll-up vector, the zig-zag nanotube is denoted by (n, 0) and the arm chair tube as (n, n) [20]. The chirality of the carbon nanotubes has significant implications on the material properties, in particular on the electronic properties of the carbon nanotubes. Depending on the chirality, the tubes can be either metallic or semiconducting [21].

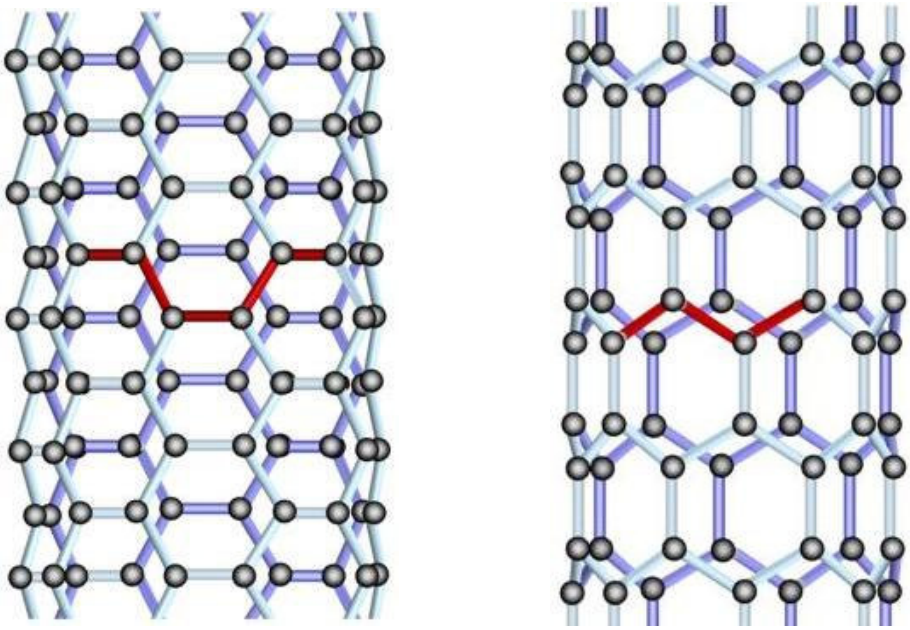

A. armchair B. zig-zag

Figure 1.3 Schematic diagram showing (A) armchair and (B) zigzag type nanotubes[21].

1.4 NANOTUBES - GROWTH METHODS

Arc-discharge and laser ablation methods were the early processes widely used for growth of nanotubes. Both these methods involve condensation of carbon atoms generated from evaporation of solid carbon sources. Temperature involved in these methods are close to the temperature of vaporization of graphite (3000- 4000^{o}C). Further details of these processes are available in literature [1, 4, 23]. Laser ablation process is not compatible for scaleup whereas the arc-discharge process has been used to produce large quantities of CNTs. However, the purity of nanotubes produced by arc-discharge is modest compared to those produced by the laser ablation technique, which can produce single walled nanotubes with purity as high as 90%. Apart from the above mentioned methods, chemical vapor deposition (CVD) is an important method to grow nanotubes [24, 25].

The chemical vapor deposition (CVD) process has been widely used for several years. In this process, a feedstock, such as carbon monoxide (CO) or hydrocarbon gas is heated to about 800 - 1000℃ in presence of a transition metal catalyst to promote nanotube growth. The chemical vapor deposition method is amenable for nanotube growth with control on patterned surfaces, and is reported to be suitable for fabrication for electronic devices, sensors, field emitters and other applications [26]. Despite all the reported advances in the CVD process, numerous challenges still exist in understanding the growth mechanisms and successful synthesis of carbon nanotubes in large scale. In this investigation, plasma enhanced microwave assisted CVD approach is used and an effort is made towards the vertically aligned growth of carbon nanotubes on patterned surface.

1.5 OUTLINE

After a brief introduction (Chapter 1), Chapter 2 contains the literature review on the mechanisms involved in growth of carbon nanotubes. It may be noted that team mate Raghavan's thesis [110] cover literature review on properties and synthesis methods of carbon nanotubes and team mate Nidadavolu's thesis [109] cover literature review on plasma assisted techniques for growth of nanotubes and applications and may be referred for those topics. Chapters 3 and 4 deal with problem statement and the experimental approach, respectively. Chapter 5 deals with the methodology and procedure used for the growth of nanotubes in this investigation. Chapter 6 presents the results, Chapter 7 discussion and Chapter 8 conclusions and future work.

CHAPTER 2

LITERATURE REVIEW

2.1 INTRODUCTION

Despite the development of a large body of literature on the subject of carbon nanotube growth mechanisms, a definitive model for the growth of nanotubes has not yet been determined, owing to lack of consistent experimental data [28]. Further, decades of research on carbon filaments growth and subsequent work on growth mechanisms following the discovery of carbon nanotubes by Iijima [1] have failed to decipher the atomic scale mechanisms by which these nanotubes grow [28]. However, considering the impact of these nanotubes on technology and due to lack of theoretical understanding of the growth of multiwalled and singlewalled nanotubes, a study of the literature on growth mechanisms has been pursued and reported in this chapter.

This chapter is organized in such a way that the earlier theories detailing the fundamentals of carbon filament growth mechanisms are discussed first, and then growth mechanism of multiwalled and singlewalled carbon nanotubes are discussed later under the categories of microscopic and macroscopic growth mechanisms.

2.2 HISTORY OF CARBON FILAMENTS

2.2.1 Earliest literature on the growth of carbon filaments

Carbon fibers or filamentous carbon has been the subject of investigation long before the discovery of carbon nanotubes by Iijima in 1991 [1]. The earliest available literature on carbon fibers dates back to 1889 when Hughes and Chambers [29] patented a process for pyrolyzing marsh gas in iron crucibles to produce macroscopic carbon fibers to be used in electric lamp filaments. It has also been reported that carbon fibers were prepared by Edison [57] to be used as filament for an early model of an electric light bulb. Further, Baker and Harris [35] in their report identify Schultzenberger as one of the first to observe the synthesis of carbon filaments growth as early as the 1890's during experimentation of passing cyanogen gas over red hot porcelain. Despite the availability of literature on carbon filament growth in the early 1900's, the filament growth mechanism and the exact role played by a catalyst in the formation of filaments was not explained and had to wait until the development of electron microscopy techniques in the 1950's [35].

2.2.2 Renewed Interest on Carbon filament growth in 1950's

In early 1953, Davis *et al.* [30] report an unusual form of carbon deposited on the brick work of a blast furnace which was causing the bricks to disintegrate. After careful investigation using electron microscopy and X-ray diffraction they reported the deposited carbon as minute vermicular growth formed by the interaction of carbon monoxide and iron oxide in the so called 'iron spots' in the brick. The observed carbon vermicules to have thicknesses ranging from 100 A to about 0.2 μmeters and after further identification of cementite (Fe_3C) and iron percarbide ($Fe_{20}C_9$) through X-ray examination they

suggested the occurrence of following chemical reactions for the growth of the carbon filaments.

$$3Fe+2CO \rightarrow Fe_3C+CO_2$$

$$Fe_3C \rightarrow 3Fe+C$$

$$20Fe_3C+14CO \rightarrow 3Fe_{20}C_9+7CO_2$$

$$3Fe_{20}C_9 \rightarrow 20Fe_3C+7C$$

The reaction $2CO \rightarrow CO_2+C$ was suggested to be catalyzed either by iron or cementite (Fe_3C). Further, they explained the origination of catalyst, iron or iron carbide as specks on the surface of the iron oxide and each speck giving rise to a thread of carbon. This work shed some light on the role of catalyst played in Hughes and Chambers work [29], but they were less certain to comment on the status of the catalyst once growth commenced [35].

2.2.3 Carbon filament deposition problem in Industry

During 1950's Baker *et al.* [32] investigated the synthesis and formation of carbon filaments on nuclear fuel pins using controlled atmosphere electron microscopy (CAEM) [32]. During their experimentation, they directly observed the growth of carbon filaments on various metal surfaces, including iron, cobalt, and nickel [31, 33]. Carbon deposition was a problem to the petrochemical industry as well, as they prevent the formation of clean fuels. In the nuclear field, the filaments constituted a large fraction of the carbonaceous materials deposited on metallic components during operation with a methane-carbon dioxide based coolant. Heat transfer efficiencies of metallic tubed heat exchangers were suffering due to carbon depositions [33, 35].

2.2.4 Earlier growth theories

Most of the published work on carbon filaments around that time investigated the parameters controlling their growth with a view to prevent their formation. Investigation of these deposits by Baker and others [32, 36, 37] reported the deposits to consist of three types of carbon: amorphous, filamentous, and graphitic. A mechanism was also proposed by Baker [34] in which particles of iron, nickel, or iron-nickel originating from the furnace tubes catalyze the formation of filamentous carbon. They even reasoned that if that mechanism was correct, they could inhibit the growth of filamentous carbon and in turn they could potentially reduce the accumulation of amorphous carbon and thereby overcome the plaguing problem of carbon deposition.

Growth mechanisms were broadly classified under the two categories, one theory was based on catalyzed decomposition or disproportionation of carbon monoxide and the second one was based on the idea of catalyzed decomposition of hydrocarbons [35]. Both theories irrespective of their differences required a catalyst.

2.2.5 Catalyzed disproportionation of carbon monoxide

Disproportionation of carbon monoxide take place through a complex reaction but the basic stoichiometric equation is given below [35].

$$2CO \leftrightarrow C + CO_2$$

The forward reaction producing carbon is exothermic and the attainment of equilibrium is reported to be sensitive to the reaction conditions and required catalytic surfaces, such as iron, cobalt, and nickel. Iron was the most studied catalyst and various studies are in agreement that the filaments formed in three shapes: 1. Helical, 2. Twisted,

and 3. Straight. The morphological details of the filaments were found to vary widely due to the catalyst employed and also owing to the reaction conditions [35, 37, 41].

Additionally, Hofer *et al.* [36] found that iron catalyst produced solid filaments, nickel catalysts produced tubes, and cobalt catalyst produced both solid threads and tubules. However, the most controversial aspect of the disproportionation of the carbon monoxide theory was the identification of the active catalyst which was responsible for the filament growth.

2.2.6 Catalyzed decomposition of hydrocarbons

A study by Fryer and Paal [39] reported the formation of filaments on platinum surfaces during thermal decomposition of hydrocarbon gases like methane and mixtures of nitrogen, benzene and 25% hydrogen. Baker *et al.* [31] investigated the development and growth of carbon filaments from the decomposition of acetylene over isolated particles of nickel, iron, cobalt, and chromium. Their experimental observations revealed that the filaments had metal particles at the growing end and they reported that the filaments stopped growing when the catalyst particle was totally enveloped by a layer of carbon.

2.3 PROPOSED GROWTH MECHANISM OF CARBON FILAMENT FORMATION

2.3.1 Baker's Model

Baker *et al.* [35] proposed a model for the growth of filamentous carbon on metal particles during decomposition of hydrocarbons. The proposed key step in the mechanism was the diffusion of carbon species through the particle from the hotter leading surface of

the metal catalyst on which the hydrocarbons comes into contact, to the cooler rear surfaces, where carbon is precipitated from solution. They suggest the temperature gradient created in the metal particle during the exothermic decomposition of the hydrocarbon at the exposed front surface and the endothermic reaction at the rear surface to be the driving force for carbon diffusion. The excess carbon accumulated at the exposed front surfaces is transported by surface diffusion around the peripheral surfaces of the particle to form the graphitic skin of the carbon filament.

If the process slows down, the available catalyst surface for adsorption and decomposition of hydrocarbon decreases and thereby the temperature gradient and carbon diffusion rate are also decreased reducing the growth rate of filaments. This process comes to a stop when the leading face of the catalyst is encapsulated by a layer of carbon preventing further hydrocarbon decomposition. They also report the metal catalyst to be carried away from the support surface to the tip of the filament during the growth process. Based on the observation of activation energies for filament growth and carbon diffusion, they proposed the diffusion of carbon through the catalyst particle as the rate determining step. Though the model attempts to explain the mechanism in detail, there were shortcomings and conflicts with other works. One of the assumptions was that they consider the reaction of catalyst decomposition of the hydrocarbon to be exothermic.

Figure 2.1 is a schematic of the growth mechanism of a carbon filament proposed by Baird *et al.* [47]. Baird *et al.* [47] proposed an explanation involving surface diffusion of metal-metal hydrocarbon species across the edge of carbon layer planes. Nucleation is reported to commence and growth of shell begins when hydrocarbons associated with the metal particles diffuse on the surface of the catalyst.

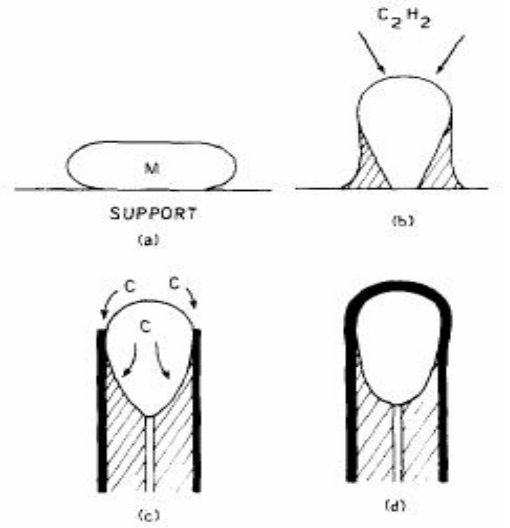

Figure 2.1 Growth mechanism schematic of a carbon filament [35].

As shown in Figure 2.1, when new metal hydrocarbon species dissociate on its edges, the carbon layers develop by lateral growth following the external surface of the catalyst. This lateral growth exerts a force strong enough to lift up the catalyst particle above the surface of the substrate. Layers are thought to progress laterally in the same way and result in a filament. The hollow channel in the center is explained by the fact that no carbon supply can reach the back of the liquid metal droplet. Growth of carbon layers continues as long as there is a supply of metal from the top of the catalyst. When the whole metal droplet is covered by carbon layers at the tip, diffusion stops and growth ends.

However, Rostrup-Nielsen and Trimm [41] argue the driving force responsible for diffusion of carbon to be due to the existence of a carbon concentration gradient rather than a temperature gradient within the particle as suggested by Baker *et al.* [35]. In contrast, Yang and Yang [42] report a temperature gradient as the driving force for the

diffusion process resulting in growth of carbon deposition when hydrocarbons interact with nickel.

2.3.2 VLS (Vapor-Liquid-Solid) theory based explanation for tubular nature of filaments

Since carbon filaments formed by gaseous decomposition of hydrocarbons were found to be invariably tubular, filament growth mechanisms generally considered the concepts of the VLS (Vapor-liquid-Solid) theory developed by Wagner and Ellis [48] to explain the tubular nature of carbon filaments. Based on VLS theory, whiskers or filaments grow because of supersaturation of catalytic liquid droplet by decomposition of vapor phase molecules, and also due to the solute getting continuously precipitated in the form of cylinders from the resulting super saturated liquid [48].

2.3.3 Tibbetts model

The reason proposed for tubular nature of carbon fibers is that it was energetically favorable for the newly formed surface of the growing fiber to precipitate as low-energy basal planes of graphite rather than as high-energy prismatic planes [50]. Further, the proposed model explained tubular “Tree ring” structure of carbon filaments to arise from the anisotropic surface free energy of graphite. In this model, a metal- metal hydrocarbon species diffuses across the catalytic particle allowing the carbon to precipitate in contact with the previous deposit, and the initial spacing and the inner diameter is determined by the contact angle between the catalyst metal particle and the substrate.

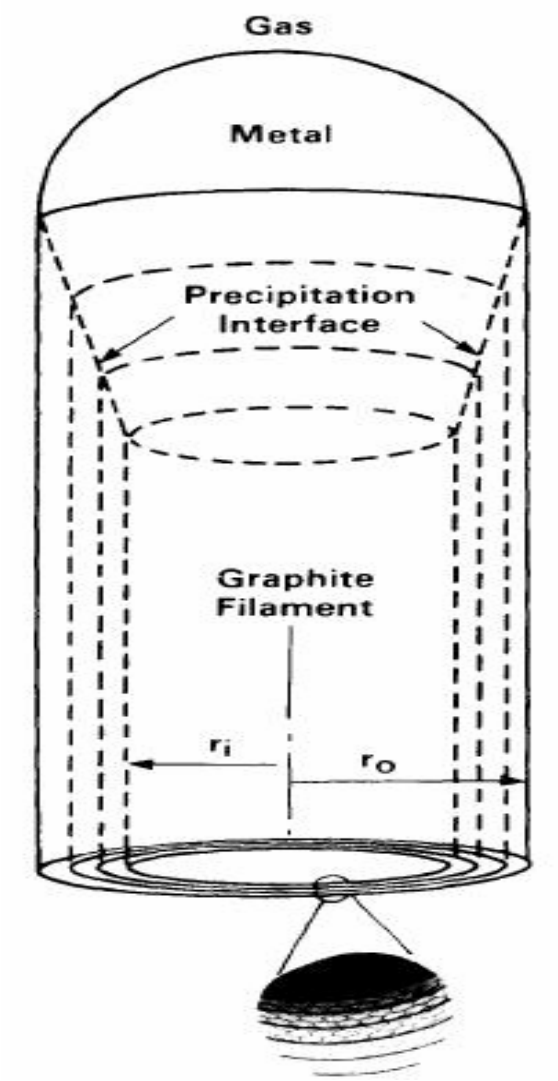

Figure 2.2 Tubular filament growth model [50]

2.3.4 Precipitation of filaments

Considering the precipitation process to occur at the bottom of the catalyst particle, the change in Gibbs free energy, δG, when a fiber length of d*l* is precipitated is given by 2.1 [50].

$$\delta G = 2\pi(r_o + r_i)\sigma dl + \tfrac{1}{12}\pi E a^2 \ln(r_o / r_i)dl - \Delta\mu_o d\upsilon / \Omega \qquad (2.1)$$

The first term on the right hand side represents the energy to form the surface of the filament and is proportional to σ, the energy required to form a unit area of (0001) graphite in equilibrium with the vapor phase. The second term is the elastic energy required to bend the graphite basal planes in the form of nested cylinders. The final term contains $\Delta\mu_o$, the chemical potential change when a carbon atom precipitates from the dissolved phase, the volume change dν, and the volume of carbon atom in graphite Ω. The number of carbon atoms in the precipitate is given by 2.2 [50].

$$dn = dv / \Omega = \pi (r_0^{\,2} - r_i^{\,2}) dl / \Omega \tag{2.2}$$

Thus the change in chemical potential Δμ driving the precipitation is given by 2.3 [50]

$$\Delta\mu = -\partial G / \partial n$$

$$= \Delta\mu_o - \frac{2\sigma\Omega}{r_o - r_i} - \frac{Ea^{\,2}\Omega}{12 (r_o^{\,2} - r_i^{\,2})} \ln(r_o / r_i) \tag{2.3}$$

Further, filaments are reported to form only when Δμ > 0. In the presence of catalyst particles of differing sizes, filaments having r_o and r_i values which give the largest Δμ will be most likely to form and grow more rapidly [51]. Since r_o is fixed by the size of the catalyst particle r_i adjusts itself to maximize Δμ. Thus r_i can be determined from the condition as shown in equation 2.4.

$$\left[\partial(\Delta\mu) / \partial r_i\right]_{r_o} = 0 \tag{2.4}$$

Thus, the model proposed by Tibbetts [50] for carbon filament growth morphology is closely related to the VLS theory and is based on the assumptions that

molecular decomposition and carbon solution occurs at one side of the catalytic particle. As soon as the catalytic particle becomes supersaturated, the subsequent gradient in chemical potential causes diffusion in the back face of the particle where precipitation takes place. So the model finally explains that it is energetically favorable for the fiber to precipitate with graphite basal planes parallel to the exterior planes and a hollow core. This model explains why the fiber structure is tubular and why the graphite basal planes are the exterior planes. Furthermore, it predicts that there will be a minimum diameter below which no filaments will grow. Also, owing to a weak maximum in chemical potential and also due to energy fluctuations during precipitation, graphite planes deposited on the inner diameter are prone to be more disordered than the exterior planes.

2.3.5 Tibbetts further discussions

Owing to high thermal conductivity of Iron (Fe), Tibbetts *et al.* [57] in their later work discuss the temperature gradient to be too small to account for the observed flux of carbon atoms in contrast to the mechanism suggested by Baker *et al.* [33]. They argue that the iron particles remain in the austenitic phase and they contend that surface diffusion takes place. Rather, they put forth a model that assumes that iron becomes super saturated with carbon atoms and propose that the flux is primarily driven by concentration gradient in agreement with Rostrup –Nielson and Trimm [41].

2.3.6 Phase of the metal catalytic particle-during the growth of filaments

Tibbetts *et al.* [57] proposed a model that assumes the catalytic particle to be in austenitic phase, but supersaturated with carbon. However Oberlin *et al.* [46] report

identification of Fe_3C as the phase of the catalyst particle during filament growth. Since carbide particles can also be formed when supersaturated austenitic particles are cooled, any post growth analysis may not necessarily indicate the true phase of the catalyst during the growth at high temperature. In agreement with Tibbetts' [57] assumption, Bradley *et al.* [52] have observed catalyst particles in the austenitic phase within the filament, even after cooling down from high temperatures during the growth. Further investigation by Sacco *et al.* [53] is consistent with the hypothesis that carbon supersaturated austenitic iron as the phase of catalytic particles during filament growth. Furthermore, the low diffusivity of carbon in Fe_3C, about four orders of magnitude less than that in iron [54], is reported to limit the growth rate of filaments.

Finally, Tibbetts *et al.* [57] argue that a feasible transport mechanism for carbon atoms from the gas phase to the lengthening of filament is adsorption of carbon atoms, followed by diffusion through the bulk of the particle. Diffusion through the particle is driven by a carbon concentration gradient and is considered rapid compared to adsorption of hydrocarbons on the surface of the catalyst particle.

2.3.7 Growth mechanism of nanotubes

Although there were several models proposed, after the discovery of carbon nanotubes by Iijima, there was a lack of real consensus between the experimental data and the pattern of growth of both multi-walled and single-walled nanotubes. Years of study of the growth of carbon filaments suggest that carbon filaments grow via precipitation of dissolved carbon from a catalyst particle, however notable differences exist between growth of carbon nanotubes and carbon filaments. Additionally,

differences exist in explaining the growth of singlewalled and multiwalled nanotubes as well. Therefore, the second part of the literature review will focus on microscopic growth mechanisms and macroscopic growth mechanisms, in a view to explain the differences behind the growth of SWNTs and MWNTs [66].

2.4 MICROSCOPIC GROWTH MECHANISMS

2.4.1 Growth mechanisms of multiwalled carbon nanotubes-Introduction

The earliest growth model for growth of multi-walled carbon nanotubes was reported by Iijima [65]. This model was based on topological considerations and emphasized the role of pentagonal and heptagonal rings capable of bending the straight hexagonal network of carbon atoms. But differences existed in understanding if the inner or the outer tubes grew first, and also in knowing if the different shells were assisting each other during the growth.

2.4.2 Close-ended growth

Endo *et al.* [60] report formation of carbon nanofibers based on their assumptions and observations that nanotubes remains closed during growth. They report that longitudinal growth of tube occurs by the continuous incorporation of small carbon clusters (C_2 dimers). Since this C_2 absorption process is assisted by the presence of pentagonal defects at the tube end, it allows bond-stitching in order to reconstruct the caps on the growing tubes. In support to this close-ended approach Saito *et al.* [61] also report that concentric tubules are formed by epitaxial carbon growth and report that there is always a closed cap at the end of each tubule.

A.

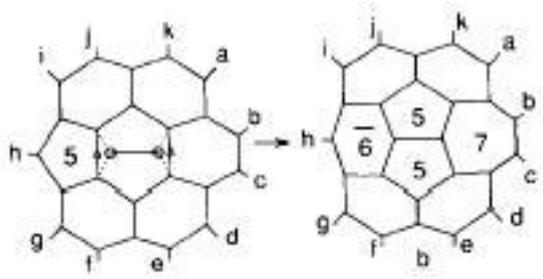

B.

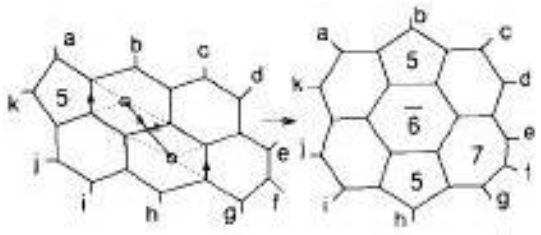

C.

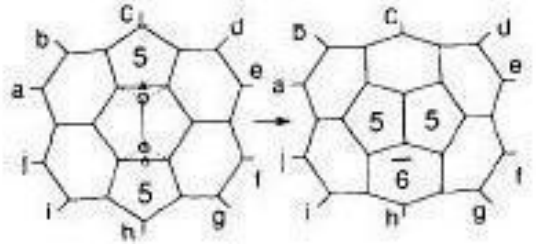

D.

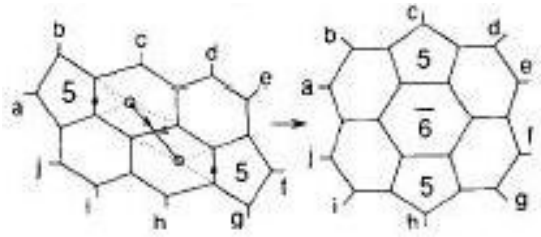

Figure 2.3. Possible reactions for the absorption of a C_2 cluster (a), (b) Near a single pentagon and (c), (d) near two pentagons [60].

Growth mechanism of MWNTs, where the tube ends are assumed to be closed during growth is illustrated in Figure 2.3. In the Figure, the two open circles and the dashed lines denote a C_2 molecule, newly formed bonds and deleted bonds, respectively. A new hexagon is denoted by 6 and a {7, 5} pair are created in the absorption process in both (a) and (b). The relative positions of the two pentagons, expressed as a linear combination of unit vectors of the honeycomb lattice, becomes closer after C_2 absorption in (c) and (d), respectively [64]. The closed-tube approach was favorable compared to the open one, because any dangling bond that might participate in an open tube growth would be unstable. But the closed tube approach failed to explain the multilayer tube growth and how the inside shells grow to a different length compared with the outer ones [64].

2.4.3 Tube ends open during growth-Iijima model

Iijima [65] proposed a microscopic model for tube growth, in which the tubules are open at their ends while growing. Most of the tubes have multiple shells of coaxially arranged cylinders, and carbon hexagons on individual tubes are arranged in a helical fashion with variable pitches. During the growth, the ends of the tubes are kept open, but they tend to be closed quickly when the growth condition becomes inappropriate. If the tube end is open, carbon atoms are deposited onto tube peripheries, and the tube grows. When the tube is enclosed by introducing six pentagons on the tube periphery, the tube cap becomes inactive and there will be no more growth on that particular tube shell. Furthermore growth of these tubes takes place on other tube shells which might start to grow on the outer side of the existing tube wall.

2.4.3.1 Role of pentagons and heptagons

When a kink or a defect site on the growing tube is supplied with two carbon atoms as shown in Figure 2.4, a new carbon hexagon is formed. This results in kink advancement and the tube grows [65]. This process is repeated and the tube growth is maintained in its original cylindrical shape. A helical structure promotes tube growth since it can provide an endless source of kinks. If a single atom is added to the kink site, a pentagon is formed as illustrated in the Figure [2.4 a] and it transforms the tube to a cone shape. Also, if rest of the kinks are furnished with hexagons, the resulting tube takes up a cone shape, whereas if three carbon atoms are added to the kink it results in the formation of heptagon. The heptagon is reported to play an important role in the transformation of a cone to a smaller tube.

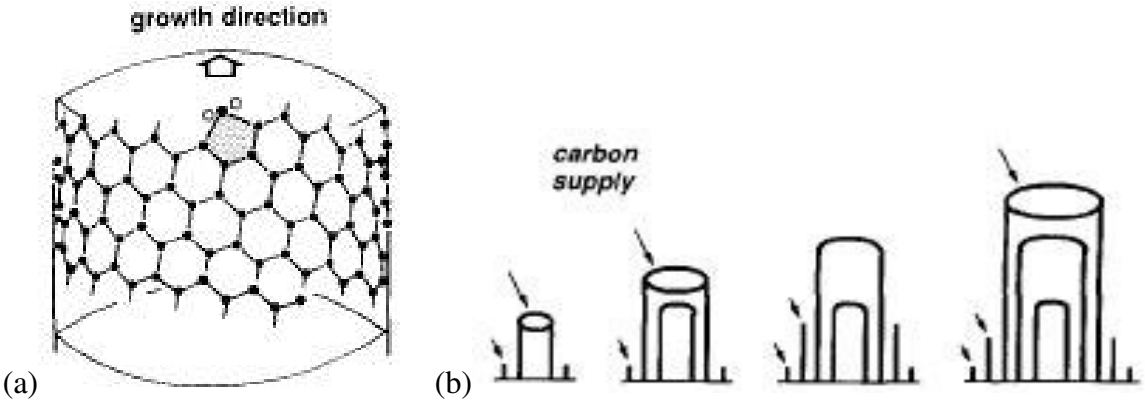

Figure 2.4. (a) Schematic representation of a kink-site on the tube end periphery. (b) Tube ends are open while growing by accumulation of carbon atoms at tube peripheries [65]

In an open ended model, all the growth layers of a tube remain open during growth and grow in the axial direction by the addition of carbon clusters to the network at the open ends to form hexagonal rings. Closure of the layer is caused by the nucleation of pentagonal rings due to local perturbations in growth conditions or due to the competition

between stable structures. Further thickening of the tubes occurs by layer growth on already grown inner-layer templates and the large growth anisotropy results from the vastly different rates of growth at the high energy open ends having dangling bonds in comparison to the unreactive basal planes.

Figure 2.5 summarizes various morphologies of nanotube tips. The open-ended tube is the starting form or the nucleus as shown in Fig 2.5 (a). A continuous supply of hexagons on the tube periphery results in a longer tube as shown in Fig 2.5 (b). The open ended tube can be enclosed when six pentagons are introduced which results in the formation of polygonal cap, shown in Fig 2.5 (c). The open circles represent pentagon locations and growth stops when the tube is enclosed. However, a second tube can be nucleated on the first tube sidewall and can cover it as shown in Fig 2.5 (d) and Fig 2.5 (e).

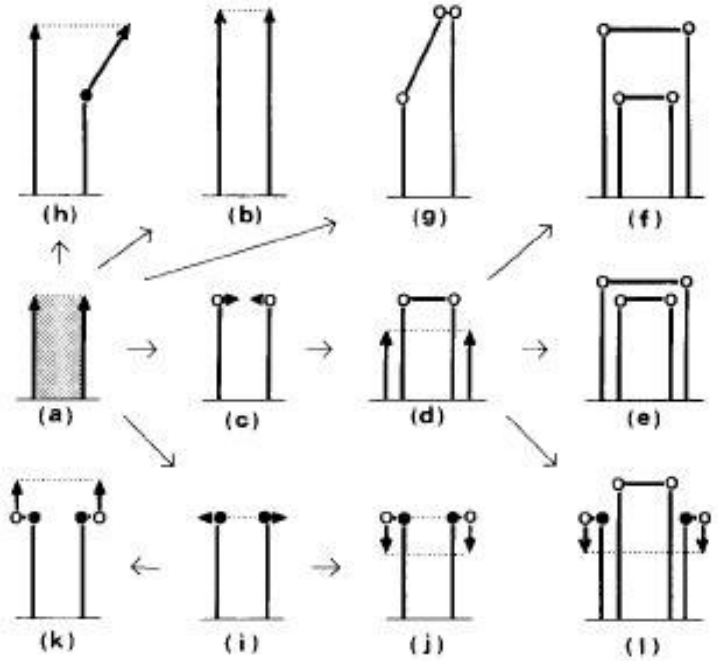

Figure 2.5. Carbon nanotube termination based on the open-end tube growth. Arrows represent termination of the tubes and also growth directions. Open and solid circles represent locations of pentagons and heptagons respectively [65]

Formation of a single pentagon on the tube periphery triggers the transformation of the cylindrical tube to a cone shape as show in Fig 2.5 (g). Introduction of single heptagon into an open cone periphery changes the cone shape into a tube but a reverse growth of this transformation is shown in Fig 2.5 (h). However, growth may be stopped in such a case because of an expanding periphery. This will cost too much free energy to stabilize the dangling bonds. Thus, controlling the formation of pentagons and heptagons is a crucial factor in the growth of carbon nanotubes. When six heptagons are formed on the periphery, it results in expansion of the circular brim as shown in Fig 2.5 (i). The circular brim is turned around when a set of six pentagons are formed on the periphery shown in Fig 2.5 (j).

2.4.4 Lip-lip Interaction models for growth of Multi-walled carbon nanotubes.

Guo *et al.* [75] proposed that chemisorbed carbon atoms bridge the dangling bonds between adjacent layers of multi walled structures thereby stabilizing an open edge of the growing multi-walled tube. This is illustrated in Figure 2.6.

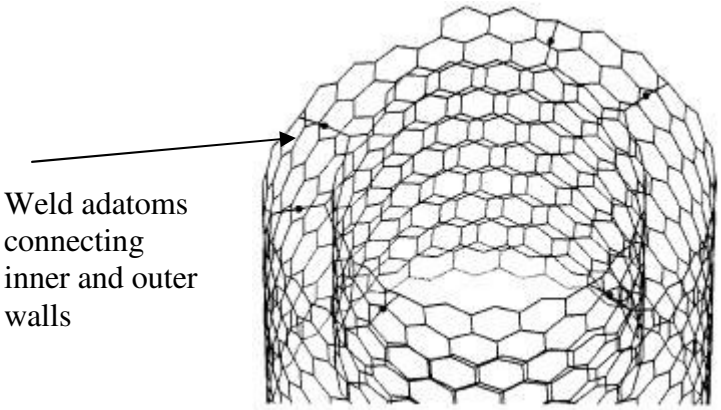

Figure 2.6. Representation of a multi-walled nanotube with an open tip. Only two of the many layers are shown and several spot weld adatoms are shown occupying sites between doubly coordinated edge atoms of adjacent layers [75].

The presence of outer walls is reported to stabilize the innermost wall in keeping it open for continued growth. As suggested by Guo *et al.* [75], an initial graphite flake is formed containing at least one pentagon and if the carbon density is high, the open shell nucleates a second layer before closing. The second layer grows much faster on the existing template (inner tube). Once the edge of the outer layer reaches the edge of the inner shell, an adatom spot weld forms stabilizing the open end. Additional carbon feedstock introduced adds to the open edges to form the body of the nanotube. Additional outer layers of tubes are reported to grow by island nucleation and anneal on the underlying nanotube template. Thickening takes place by over layer growth. This mechanism is illustrated in Figure 2.7.

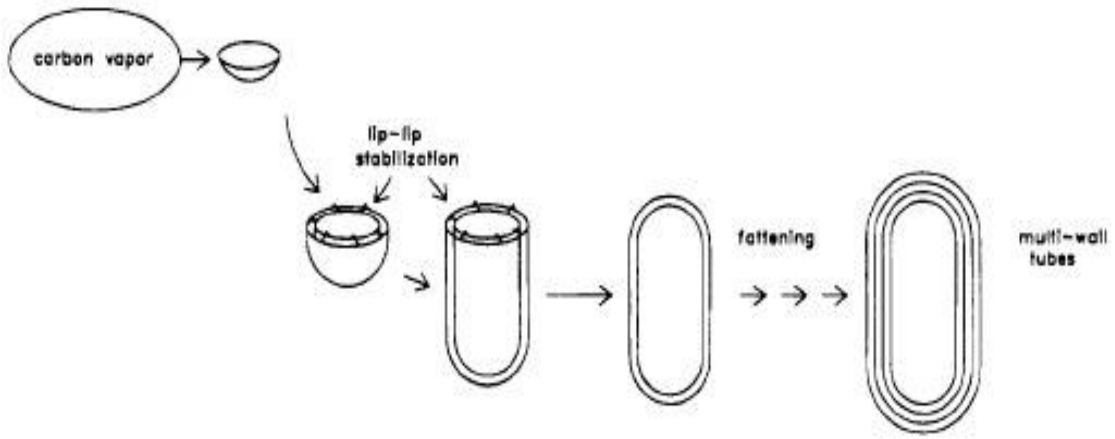

Figure 2.7 Lip-lip stabilization in multi-walled nanotube growth

Charlier *et al.* [66, 67] performed MD simulations to investigate the growth process of multi-walled carbon nanotubes. They report that dangling bonds of the inner and outer edges of a bilayer tube to rapidly move towards each other, forming several bonds to bridge the gap between the adjacent edges. Further, they report that the lip-lip

interaction as the stabilizing mechanism to inhibit the spontaneous dome closure of the inner tube. The end geometry is highly active chemically and it easily accommodates incoming carbon clusters, supporting growth by chemisorption from the vapor phase.

2.4.5 Microscopic growth mechanism for single walled carbon nanotubes

Charlier *et al.* [66] investigated the uncatalyzed edge growth of carbon nanotubes by MD simulations. They report that at experimental temperatures the open end of single walled nanotubes were observed to close spontaneously into a graphitic dome, suggesting that the nanotubes do not grow in the absence of transition metal catalyst. Formation of the graphitic dome is shown in Figure 2.8 [66].

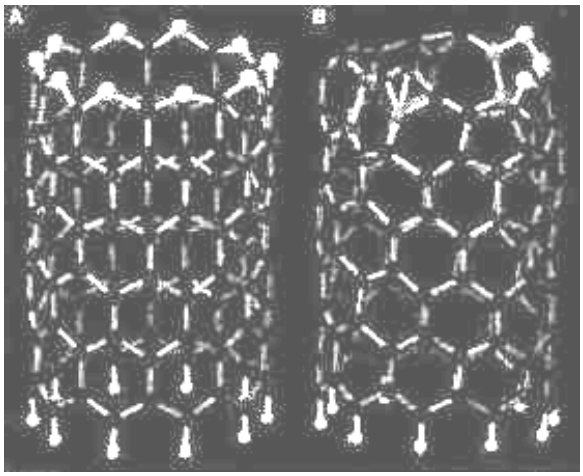

Figure 2.8 (a)Side view of the open-end starting configuration without a catalyst and with 10 two-coordinate carbon atoms at the top edge. (b) First pentagon is formed from one of the top hexagonal rings, resulting in inward bending [66].

The tip closure results in a substantial reduction on the localized density of electron states. This is the reason for the lower reactivity of closed nanotube tips than

open ended nanotubes. Finally they report that it is unlikely that single-walled nanotubes could grow by sustained incorporation of C atoms into the closed tip [67].

Additionally, Charlier *et al.* [68] in their later work report single-walled nanotubes not to grow in the absence of transition metal catalysts. However, they caution that the role played by the metal atoms to be controversial and inaccessible for observation to determine the growth. They plausibly suggest the metal atoms initially decorate the dangling bonds of an open fullerene cluster, preventing it from closing. When more carbon atoms collide with metal decorated open carbon cluster, they are inserted between the metal and the existing carbon atoms in the shell.

Kiang *et al.* [69] propose polyyne rings to serve as nuclei for the formation of single-wall tubes (see Figure 2.9) , and report the diameter to be related to the ring size. In this model the starting materials are monocyclic carbon rings acting as nanotube precursors and Co_mC_n species acting as catalysts, in the presence of cobalt catalyst. Co_mC_n plays the role of a catalyst by adding C_2 or other gas phase species into the growing tube. Though the composition and structure of the Co carbide cluster is undetermined, they bond to C_n species and/or to add the C_n carbon species to the growing tube. The helical angle of the single walled tube is determined by the ratio of cis to trans conformation during the growth initiation process as shown in the Figure 2.9.

Birkett *et al.* [70] report transition metals to have necessary high propensity for decorating the surface of fullerenes, there by adsorbing on the surface of C_{60}. This is reported to provide a template for the formation of single-walled nanotube. As carbon fragments or carbon species bind to the metal-clad fullerene, they self-assemble as a surrounding circular hexagonal chicken-wire-like fence. On formation of a belt, the

network propagates as a cylinder, either by accretion to the reactive edge or by ingestion into the closed sheet. In both cases, the metal coated fullerene acts as a growth template and once growth has been initiated, nanotube propagation occurs.

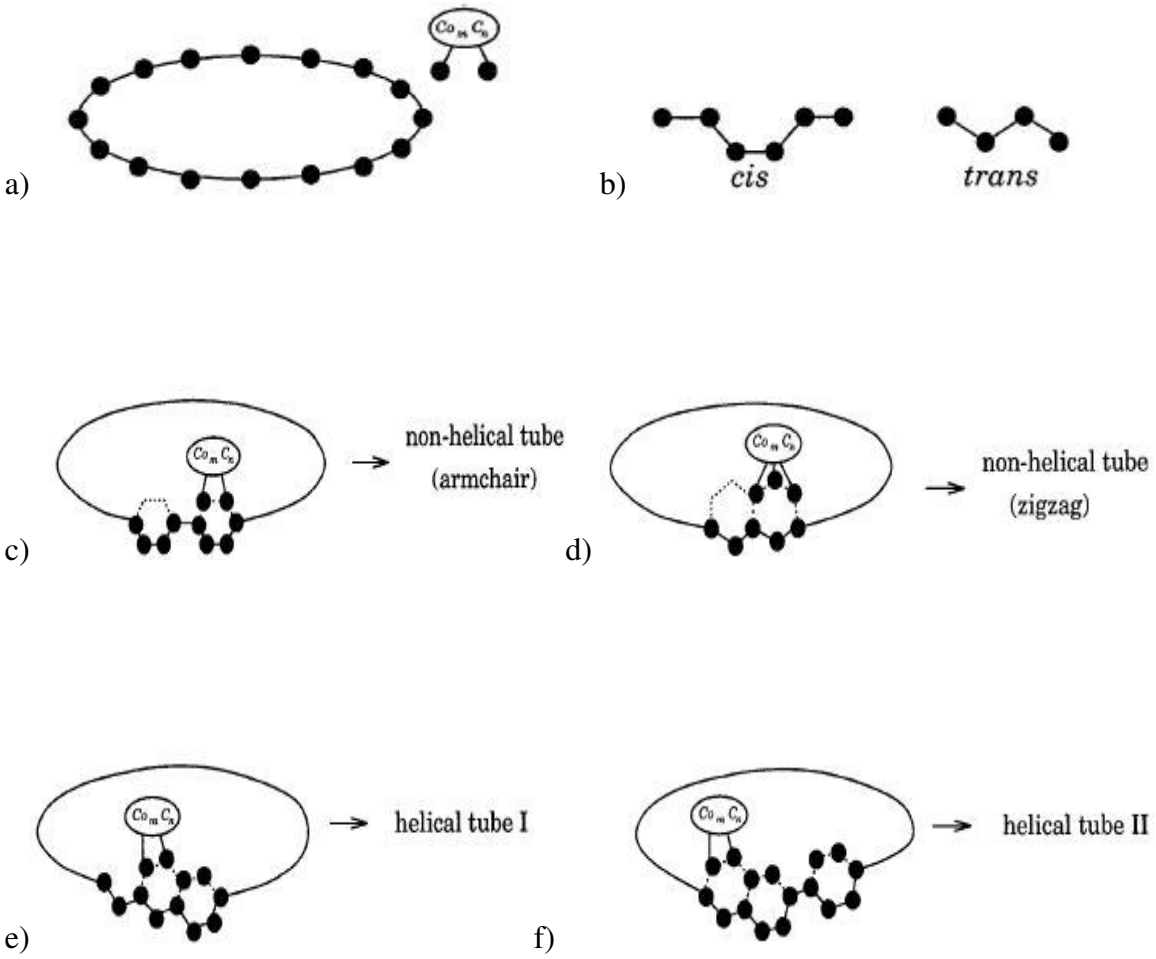

Figure 2.9 Diagrams illustrating the polyyne rings nucleus mechanism for growth of single-layer carbon nanotubes. [69]

Another explanation suggested that the carbon fragments accrete on one hemisphere of the $C_{60}Ni_mCo_n$ particle when nickel and cobalt were used as catalyst and further suggested that a dynamic surface-moderated carbon assembly process weaves the

carbon atoms into a tube. They also report that the particle has a role to play in both the initiation process as well as the secondary propagation step [70].

Thess *et al.* [71] hypothesize a scooter mechanism, where metal atoms sitting at the open end of the growing tube determines the uniform diameter of the tube. The metal atoms scoot around the open edge of the sheet, helping to anneal away any carbon structures that are not energetically favorable. Optimum diameter is reported to be determined by the competition between the strain energy due to curvature of the graphene sheet and the dangling bond energy of the open edge. A metal scooter atom as shown in Figure 2.11 promptly anneals local structure into hexagons (preventing formation of pentagons) lengthening the straight tube section and keeping the end completely open.

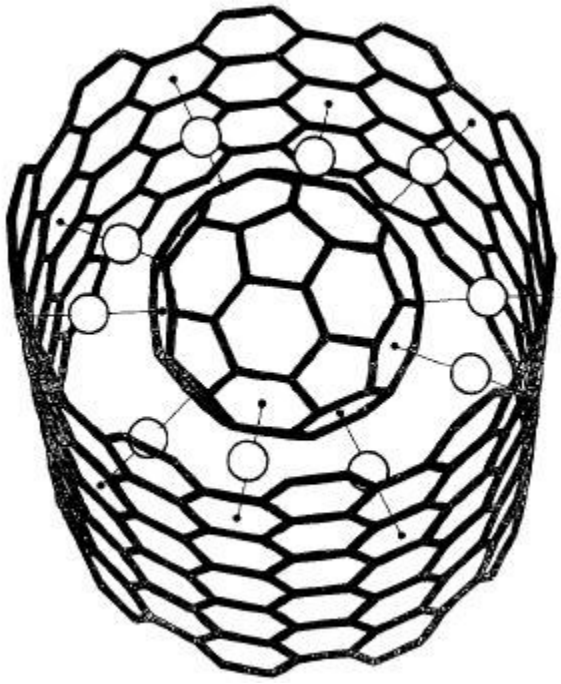

Figure 2.10 Representation of hexagonal rings linked to metal atoms. Ni and Co atoms adsorbed on the C_{60} surface are possible agents for the creation of single walled nanotubes of uniform diameter [70]

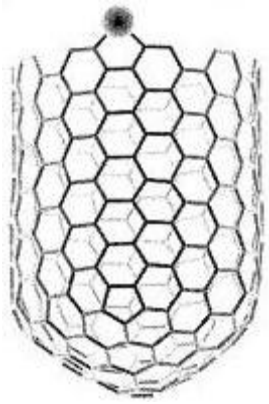

Figure 2.11 Nucleus of a SWNT with Ni atom chemisorbed onto the open edge [71].

A static *ab initio* study of the scooter model was investigated by Lee *et al.* [72]. They report the Co or Ni atom is strongly bound but still very mobile at the growing edge. The metal atom is reported to inhibit the formation of pentagons that would initiate dome closure. Additionally, the metal catalyst assists the incoming carbon atoms in the formation of carbon hexagons, increasing the tube length. In the absence of the catalyst at the tube edge, defects can no longer be annealed efficiently, thus initiating tube closure.

Further Lee *et al.* [72] proposes a catalytic growth mechanism for single walled carbon nanotubes based on an *ab initio* study. They suggest that highly mobile Ni catalyst atoms to catalyze the continuing assembly of hexagons from carbon feedstock diffusing along the nanotube wall. In a concerted exchange mechanism, Ni atoms anneal carbon pentagons that would initiate a dome closure of the nanotube. This is illustrated in Figure 2.12.

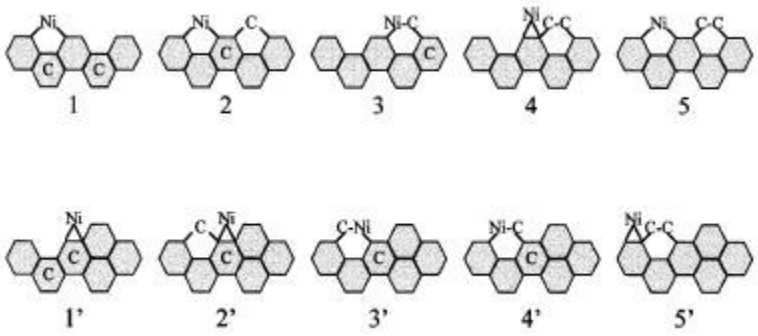

Figure 2.12 Schematic diagram of intermediate steps involved in the catalytic annealing of pentagon defects at the growing nanotube edge by a concerted exchange mechanism [72]

When two carbon atoms diffuse along the surface to the tube edge that contains a Ni atom, one of the carbon atoms forms a pentagon defect as shown in Figure 2.12 (2). Due to the high mobility of Ni atom at the edge, the catalyst reacts with the adsorbed carbon atom to form a hexagon as shown in 2.12 (3). This intermediate structure is less stable than a perfect carbon hexagon at the growing edge. The incoming carbon atom pushes out the Ni atom and forms the carbon hexagon. Ni atom may now continue its diffusion about the tube edge to assist in the catalytic annealing of other defects.

Although the scooter model and earlier models suggest an open ended growth, investigation based on MD simulations by Charlier *et al.* [66, 68] suggest that cobalt-carbon chemical bonds frequently break and reform providing a pathway for carbon incorporation, leading to a closed-end catalytic growth mechanism. They report that the model based on molecular dynamics simulations supports the growth by chemisorption from the vapor phase [35,46,50], also adopting the concepts of the Vapor-liquid- Solid (VLS) model [48].

However, in the VLS model growth occurs by precipitation from a super-saturated catalytic liquid droplet located at the tip of the filament into which carbon

atoms are preferentially absorbed from the vapor phase. From the supersaturated liquid, the solute continuously precipitates generally in the form of faceted cylinders or tubular structures [48]. The VLS model is a macroscopic model based on fluidic nature of the metal particle which dissolves carbon from vapor phase and precipitates dissolved carbon on the fiber walls.

Maiti *et al.* [73] investigated the growth of nanotubes by classical MD and kinetic MC simulations. They report that wide, helical tubes are grown by the net addition of hexagons at the step edges. This addition is reported to occur when several non hexagonal ring structures (pentagons, heptagons, and octagons) initially formed from atoms or small clusters, combine and annihilate to form hexagons.

Regardless of their initial energy, carbon atoms were always found to insert into the nearest ring, or form a pentagon at a step edge. Dimers and trimers showed no unique pattern of deposition; rather they insert all atoms into the same ring. An incident atom was found to insert into the nearest ring to form a larger ring. The insertion occurs irrespective of the initial energy of the adatom. If the atoms initially inserts into a hexagon away from a step edge, it forms a heptagon (octagon). Octagons were found to be energetically unstable and break up into smaller rings by means of a single bond switch as shown in Figure 2.13.

The initially formed heptagons and pentagons migrate and anneal into an essentially all-hexagonal structure, with the possible exception of a few isolated pentagons that get converted to hexagons by subsequent deposition.

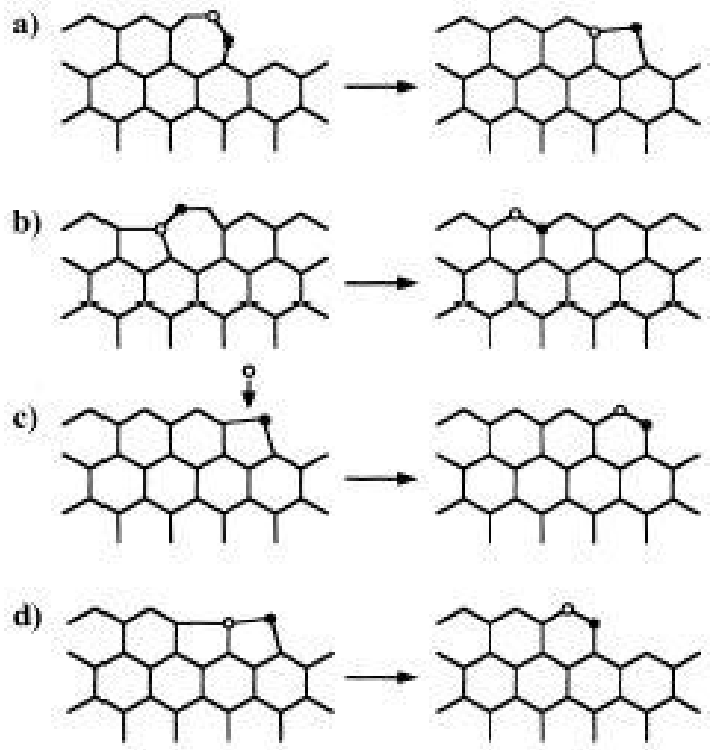

Figure 2.13 Various ways in which heptagons and pentagons "anneal" to result in a defect free growth. (a) a heptagon at a step edge breaks up into a hexagon and a pentagon; (b) a heptagon "annihilates" with a pentagon to form a hexagon pair; (c) a pentagon coverts to a hexagon by direct insertion of a deposited atom; (d) a pair of adjacent pentagons at a step edge "fuses" together into a single hexagon [73].

2.4.6 Root growth mechanism for single walled carbon nanotubes:

Classical molecular dynamics simulations by Maiti *et al.* [74] reveal a possible atomistic process by which single-walled carbon nanotubes grow out of metal-carbide particles by the root growth mechanism (see Figure 2.14) . According to the model the carbon atoms precipitate from the metal particle, migrate to the tube base, and are incorporated into the nanotube network, resulting in a defect free growth.

They report the addition of new hexagons at the tube base occurring through a sequence of processes involving a pair of "handles" formation on the opposite bonds of

heptagons as shown in Fig 2.15. a. These “handles” are formed by adatoms between a pair of nearest-neighboring carbon atoms.

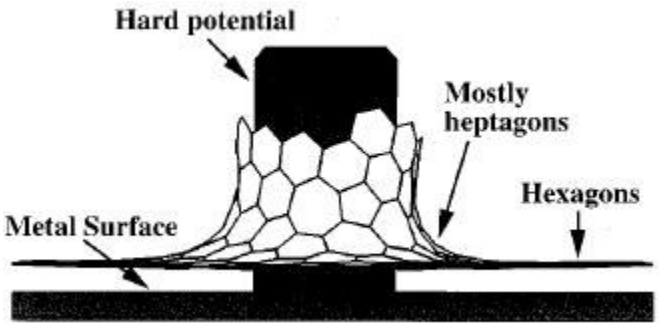

Figure 2.14 Snapshot from a MD simulation showing curving up and growth [74].

These handles act like interstitial point defects and impart tremendous kinetic flexibility to the structure by being able to migrate thermally. The migration mechanism involves a kick out by the handle atom of one of its two neighboring atoms as shown in Fig 2.15. b. The ejected atom forms a new handle, while the previous handle atom becomes one of its neighbors. On a flat graphene sheet, the handle will thermally migrate on the hexagonal network until it reaches the tube base.

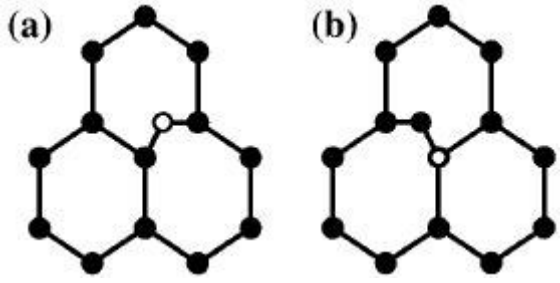

Figure 2.15. Atomistic mechanism of handle migration by kick-out mechanism

2.4.7 Molecular mechanism taking place in the extrusive-diffusive model

Vinciguerra *et al.* [62] report that diffusion inside the metal catalyst particle is not essential in case of SWNTs growth. The chemisorption processes underlie the catalytic process and hydrocarbons get rid of their hydrogen eventually breaking some of their C bonds and start assembling the carbon fragments on the metal catalyst to form a CNT. Additionally, the chemisorption of carbon fragments, such as C_2 fragment on a transitional metal surface, is favored due to the presence of π electrons that have the right symmetry to overlap with the 3d electrons. Consequently, a C_2 fragment has two possible positions on the surface of a transition metal, i.e. on top of the 3d metal atom or between two of them. Study of the structural properties of the Fe, Ni, and Co metal surfaces show that (1-1 0) planes of Fe and the (1 1 1) planes of Co and Ni to exhibit the symmetry and distances required to overlap with the lattice of a graphene sheet [62].

2.5 MACROSCOPIC GROWTH MECHANISMS

2.5.1 Extrusive-diffusive growth model

Vinciguerra *et al.* [62] report the growth of carbon nanotubes in the presence of two forces: (i) a viscous force, due to the surrounding gas, which opposes and slows down the growth of CNT, and (ii) an extrusive force that causes the growth. They propose a macroscopic growth mechanism based on the extrusive-diffusive growth model.

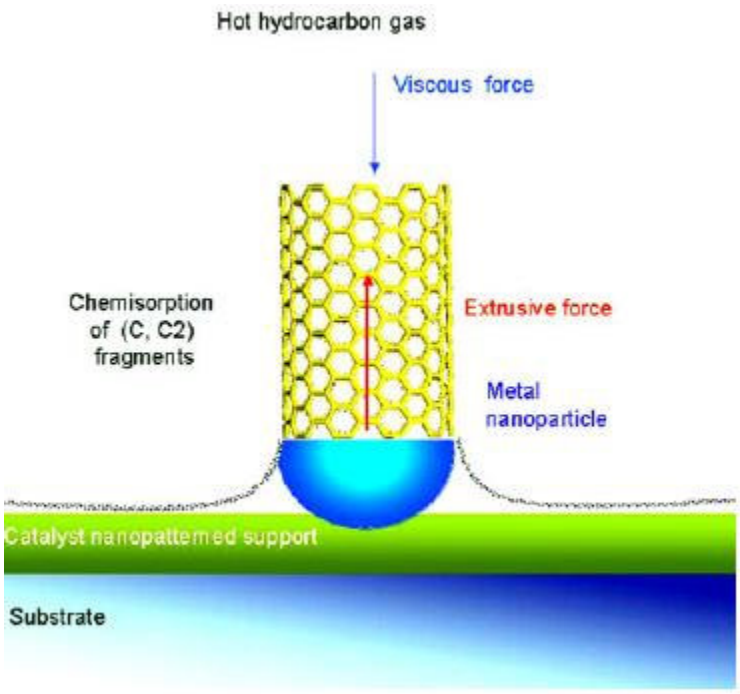

Figure 2.16 Sketch of growth process based on extrusion-diffusion model [62]

The proposed model is schematically depicted in Figure 2.16. Considering that the continuous feedstock of carbon atoms comes from a hot and dense gas surrounding the growing CNT, they argue that the CNT growth process occurs in a diffusive regime where surrounding hot gases provide a viscous force that slows down the CNT growth. They propose an empirical model where all the processes that oppose the growth are included as a single friction force. In order to explain the formation of CNT in the presence of this resistive force, they bring into play the presence of another force, which is responsible for the tube growth i.e., the extruding force.

They report a decrease in free energy in the assembling reaction that occurs at the interface of the catalyst and growing nanotubes to be the origin of the extruding force that drives and pushes off the CNTs from the surface. Further in a growing nanotube a continuous reaction occurs at the interface of the metal catalyst particle, and because of

the catalytic action of the metal particle, dehydrogenated carbon fragments are assembled to form a carbon nanotube.

2.5.2 Growth mechanism of CNT forest by chemical vapor deposition

Louchev *et al.* [63] propose a growth mechanism of carbon nanotubes forests by chemical vapor deposition. Based on their analysis of kinetics processes involved in carbon nanotube forest growth during chemical vapor deposition they suggest that (i) carbon species are unable to penetrate to the forest bottom whenever the mean free path in gas is much larger than the typical distance between nanotubes,(ii) instead, they collide with the nanotube surfaces, chemisorbing within the atoms of the top few μ-meters, diffusing along the surface, and feeding the growth at nanotube tips. They further estimate the typical mean free path of the C species in the gas to be 30-50 μm, which is much higher than the intertube distance within the forest, which was estimated to be 1 μm. They report that the forest bottom is reached only by a negligible number of species. On analyzing the diffusion process, they additionally report that the contribution of carbon dissolution and diffusion through the catalyst nanoparticle in feeding the growth of nanotube to be restricted to the initial stage of the nanotube's growth.

They also report that the post-nucleation stage nanotube growth to occur via the carbon incorporation into the nanotube tip by surface diffusion over the lateral surface including the stages of dehydrogenation of chemisorbed hydrocarbons independent of the nanoparticle location, which may be either the nanotube tip or base.

Louchev *et al.* [63] report that the diffusion process through the nanoparticle to be important for nucleation stage and also for selection of the nanotube growth mode as shown schematically in the Figure 2.17.

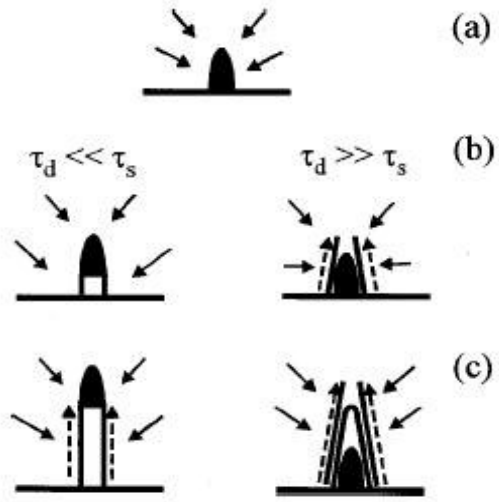

Figure 2.17. Sketch of the selection mechanism proposed by Louchev *et al.* [63] whether the nanoparticle is detached from the substrate and rides on nanotube tip, catalyzing growth and preventing nanotube closure (left-hand side) or remains on the substrate serving as a template for nanotube nucleation (right-hand side): (a) stage of nanoparticle saturation with carbon, (b) stage of NT nucleation, and (c) stage of post nucleation growth. Solid and dashed arrows indicate carbon flux from vapor and surface diffusion fluxes respectively.

The selection is defined by two characteristic times, dependent on $D_{b,}$ bulk diffusion coefficient of carbon species: (i) the diffusion time of order required for carbon species penetration to the nanoparticle base [63]:

$$\tau_d \approx R_P^2 / D_b ,$$

τ_d , is the diffusion time, and R_P is the nanoparticle radius

(ii) The surface saturation time of order corresponding to the increase of C species content to the saturation concentration, C^*, triggering carbon precipitation directly on upper surface of nanoparticle.

$$\tau_s \approx C^{*2} D_b / Q^2 .$$

τ_s, surface saturation time, Q is the total carbon flux at the particle surface

If $\tau_d >> \tau_{s,}$ the nanoparticle surface saturates with C species much faster than carbon penetrates its base. Therefore, carbon precipitates at the nanoparticle surface which provides a nanoscale template for NT nucleation.

In contrast, when $\tau_d << \tau_s$, carbon species penetrates to the base much faster than the nanoparticle surface reaching the saturation threshold, and carbon precipitates at the bottom, lifting the nanoparticle, and later on maintaining it on the nanotube tip. In this mode, the role of the nanoparticle remains important for inhibiting pentagon formation and preventing nanotube tip closure.

The selection mechanism for nanotube forest growth modes determines the final morphology of the nanotubes and their properties. If the nanoparticle is held on the nanotube tip it inhibits the formation of pentagons and consequent nanotube closure and allows the growth of straight wall nanotubes. A nanoparticle remaining at the nanotube base provides only an initial template with a nanoscale curvature for nanotube nucleation predefining the morphology of resulting nanotubes. Thus cylindrical nanoparticles are able to form nanotubes with a straight wall whereas on conical nanoparticles, conical nanotubes nuclei and tend to form bamboo-like nanotubes.

2.5.3 Mechanism for formation of helical tubes

To explain the growth of helical tubes Amelinckx *et al.* [76] introduce the concept of spatial velocity hodograph (geometric locus of the end points of the vectors describing the extrusion velocity or the growth velocity in the points along a curve) which ignores the atomic structure and considers the graphene sheet as continuum. They report the tip growth as well as base growth to be consistent with the assumption that growth occurs by the extrusion of carbon along the contact curve between the catalyst particle and the already growing tube. In the case of the growth of a straight tube, the longitudinal growth velocity, ν_1 or the speed of extrusion is the same all along the ring shaped area where carbon is deposited. However, the catalyst activity is often anisotropic and inhomogeneous depending on the exposed crystal facet of the particle and on its topography. Due to this, the spatial hodograph of the extrusion speed can be more complicated as illustrated in Figure 2.18 C.

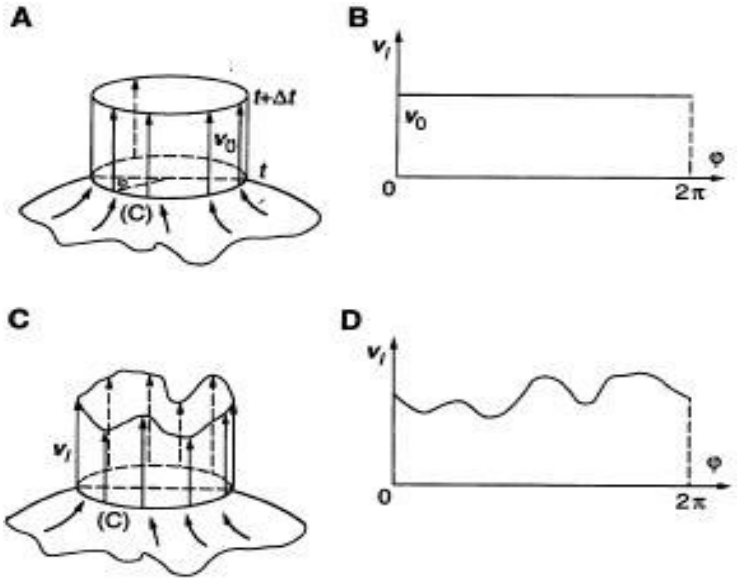

Figure 2.18 Hodograph of the extrusion velocities for the formation of straight tubules. The locus of active sites is a circle (c). (A) Spatial hodograph: The extrusion velocity is constant along (c). (B) Planar hodograph corresponding to (A); the surface area under the hodograph is proportional to the extruded material. (C) General spatial hodograph. (D) Planar hodograph corresponding to (C) [76].

At the points where excess carbon is generated the resulting compressive stress slows the carbon deposition rate, and in points where too little carbon is produced the resulting tensile stress tends to increase the deposition rate of carbon. This feedback process is thought to be responsible for the growth of a helix shaped tube. However, large stresses may induce the formation of pentagonal meshes in the graphite network to relieve part of the stresses. The occurrence of pentagon-heptagon pairs minimizes the long-range stresses.

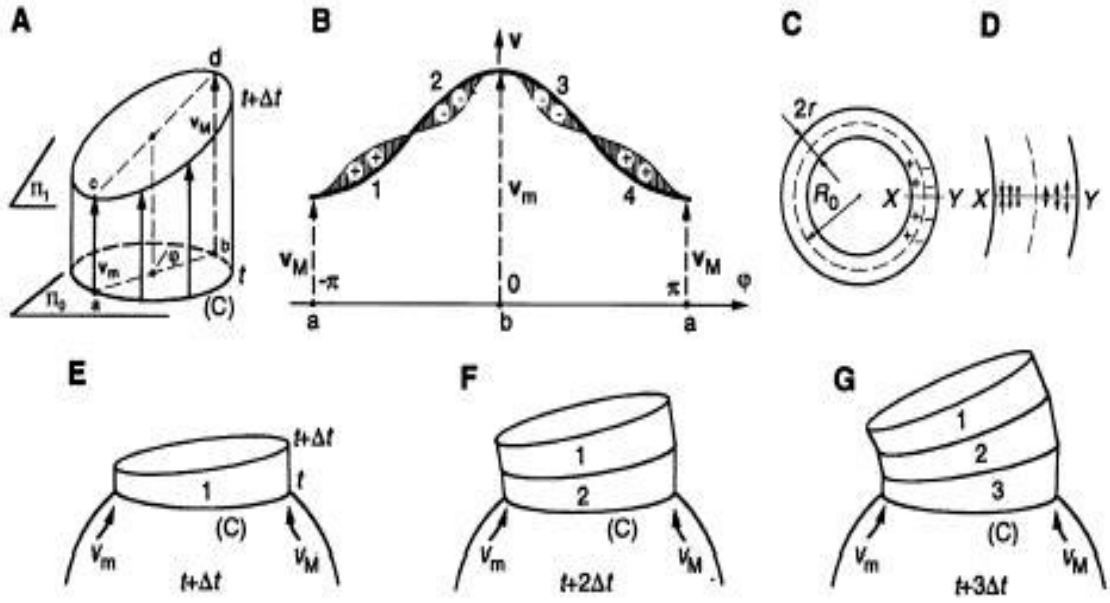

Figure 2.19 (A) Spatial hodograph of a bent tubule, (B) Planar hodograph of (A), (C) & (D) The outer rim is under tensile stress and the inner rim is under compressive stress. (E) to (G) Successive stages in the extrusion of carbon in formation of a bent tubule [76].

2.5.4 Bamboo growth

Saito [79] upon observing a carbon nanotube with a peculiar shape resembling a bamboo, proposed a growth model. Saito suggests an intermittent growth model whereby

layers of graphite would form on the catalyst surface until the accumulated stresses in the system propels the nanotube away from each other creating a fresh surface for subsequent nucleation.

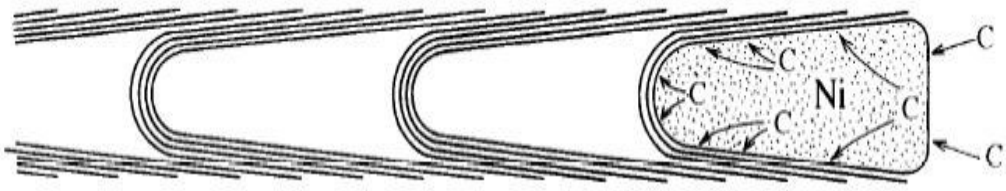

Figure 2.20 Growth model of a bamboo tube [79]

Cui *et al.* [78] suggest that continual growth and renucleation mechanism to take place in the growth of bamboo structured nanotubes. The distance between tips within a single tube is reported to be indicative of the time lag between renucleation events. They propose the renucleated tips to be continuous to the point where they terminate on the outer walls of the tube, forming a series of stacked cones.

Lin *et al.* [82] report the formation mechanism of the bamboo-like CNTs to be dependent on the following parameters: (1) presence of nitrogen or other heavy gases; (2) keeping an active and clean top surface of the catalyst particles; and (3) prolonging the carbon bulk diffusion of the catalysts. The presence of nitrogen is reported to be essential for establishing conditions (2) and (3).

2.5.5 Push-out growth mechanism

Zhong *et al.* [88] report a push-out growth mechanism for formation of polymerized nanobells structures similar to bamboo growth. After CH_4 is introduced, carbon atoms dissolve in metal particles and segregate as graphite at the surface of the

particle. When several tens of graphite layers are formed, the carbon shell just outside the catalyst particle will be pushed out suddenly as the stress in the layers accumulate to a critical value. Once this carbon shell is pushed outside, another carbon shell is formed outside the catalyst particle, and is again pushed out by forming nanobell or bamboo-like structure. This process continues and results in the formation of nanotubes containing nanobell or bamboo-like structure as shown in Figure 2.21. The stress accumulation in the carbon shell is reported to be the result of presence of nitrogen.

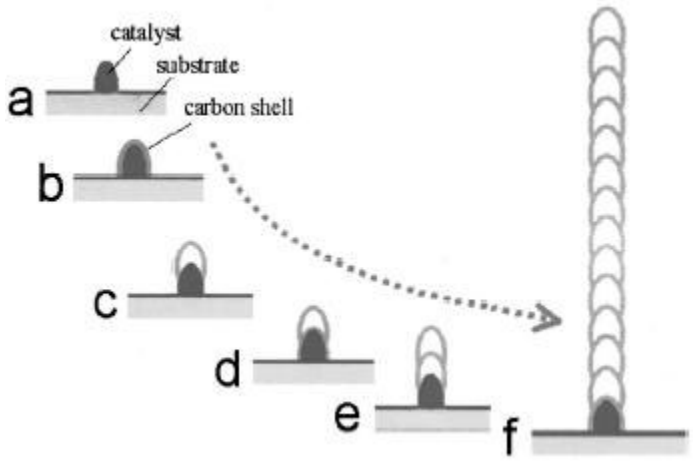

Figure 2.21 Push-out growth mechanism [88].

2.5.6 Tip growth mechanism

Amelinckx *et al.* [76] report a tip growth mechanism in growth of helical tubules as shown in Figure 2.22. Chen *et al.* [90] propose a tip growth model where growth of nanotubes takes place through the reaction sequences of deposition, adsorption, decomposition, diffusion, and growth of the carbon species.

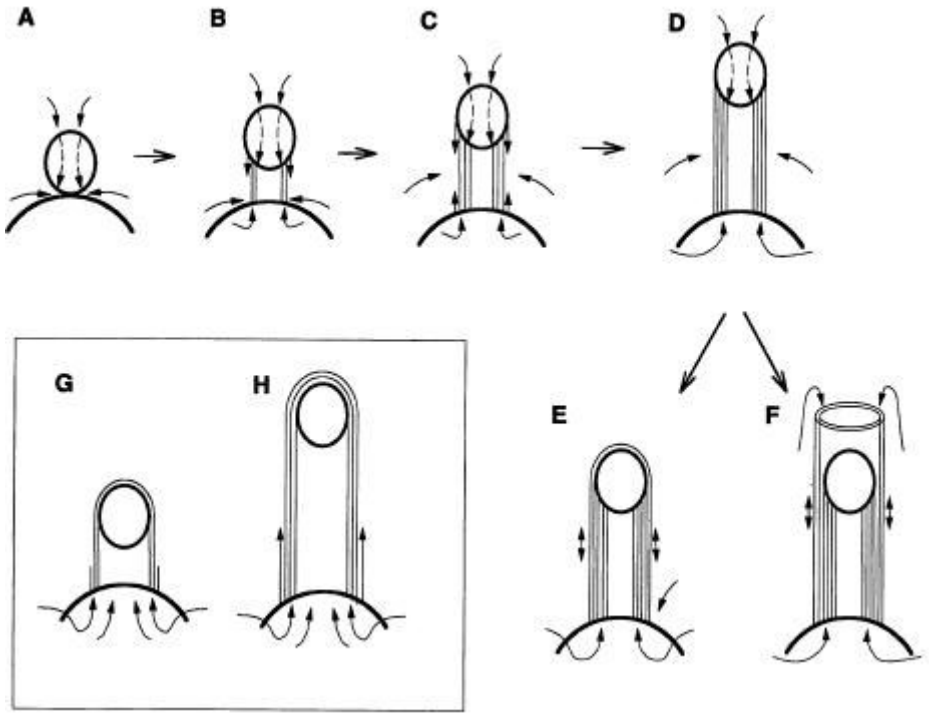

Figure 2.22 Tip growth of carbon nanotubes. **A.** Small catalyst particle resting on another catalyst particle which acts as support **B. & C.** The catalyst particle lifted away from the support by deposition of graphene sheets. **D.** Outer diameter of the tube becoming equal to the catalytic particle size. **E.** a layer of graphite covers the catalyst particle and inhibits further growth of tube. **F.** Additional growth of tubes further supported by the catalyst particle. **G. & H.** If the particle is covered by a graphite layer during the initial stage, further growth occurs by extrusion through the base, and diffusion occurs along the graphite surface [76].

In the tip growth models, 1) Carbon is dissociated from the hydrocarbon source gases, and gets deposited on the surface of catalyst particles, where physical adsorption of carbon atom takes place (Figure 2.23 A). 2) After carbon adsorption, a saturated carbon film is formed from the continuous decomposition of carbon source gas, and often encapsulated the metal catalyst (Figure 2.23 B). 3) The catalyst and substrate surfaces are saturated with carbon layers, and Fe catalyst pushed upward due to diffusion and osmotic pressure, depositing carbon into the graphite structure below the catalyst. 4) Carbon encapsulated metal catalyst particles quickly move upward by continuous osmotic

pressure and a core is thus formed as shown in Figure 2.23 C and D. The walls of the tubes are thus formed. 5) Continuous supply of carbon species results in the diffusion and growth of CNTs.

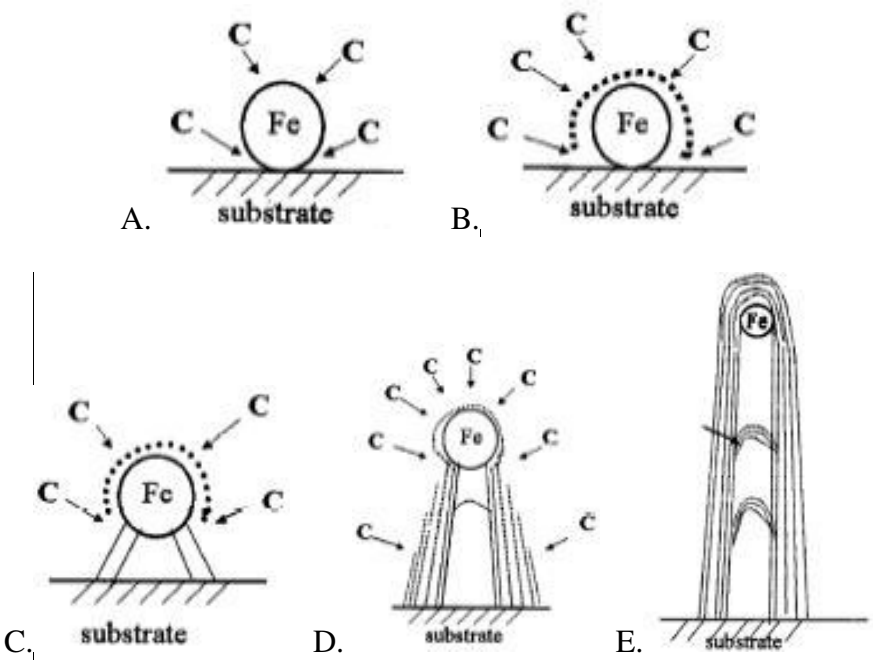

Figure 2.23 Growth model of multiwalled CNTs following tip growth model [90]

2.5.7 Multiwalled nanotubes growth

Kanzow *et al.* [91] report growth of multiwalled nanotubes to take place if the catalyst particles are big and also if the carbon supply is high. Also lack of enough energy in the system is reported to be the reason for growth of multiwalled nanotubes. Carbon containing gas molecules exothermally decompose on the surface of the catalyst particle resulting in the heating of the surface. When carbon is absorbed and diffuses toward the cooler region of the metal catalyst particle substrate, super saturation on the cooler side

leads to segregation of carbon atoms. These adsorbed carbon species move on the catalyst surface to combine and form a first graphitic layer. If there is not enough kinetic energy in the system, this layer does not bend to form a cap and continues to grow. If the carbon supply is high, the graphitic layer rapidly grows and subsequently more graphitic planes are generated causing the previous planes to bend. The bending of graphite planes stabilize the unsaturated sp^2 orbitals at the border of the graphene sheets by over lapping with the orbitals of the metal. This contact then serves as crystallization seed for the following segregation of carbon. Thus a cylindrical multiwall growth is initiated.

2.5.8 Single-wall carbon nanotube growth

Kanzow *et al.* [91] focus on the energetics of the oscillation of the graphitic plane to explain the growth of SWNTs. At high temperatures (<1200℃), carbon is adsorbed and precipitated on the catalyst metal particle. If the system contains sufficient kinetic energy, the graphite plane precipitated oscillates with respect to the metal surface in such a way that a small cap is formed. This cap formation is reported to be assisted by fluctuating bonds at high temperatures. Subsequent bending of the graphite plane stabilizes and results in overlapping of unsaturated sp^2 orbitals of graphene with the metal orbitals. This contact then serves as a crystallization seed for the segregation and growth of single walled nanotube.

A certain angle – minimum overlap angle –of the unsaturated sp^2 orbitals on the edges of the graphitic plane must be reached to obtain a significant stabilizing interaction with the metal orbitals [91]. If this condition is not reached, the plane will flatten out again and the graphitic cap will not be sufficiently stable to initiate the tube growth. But after a small tube formation, flattening out would require a huge amount of energy. The

key step is the bending of the planes and there are two forces that have to be overcome in order to bend the plane: 1. the surface tension of the sheet and 2. the work of adhesion between the graphitic sheet and the metal. However, the kinetic energy needed to bend the plane is proportional to temperature and size of the sheet.

2.5.9 Nucleation and growth of nanotubes in plasma enhanced CVD

In plasma enhanced CVD, nanotube growth on catalyst particles is reported to occur similar to a gas – solid interaction process such as thin film deposition on substrates. The growth proceeds according to the following steps and one or more of these steps may be rate controlling, which varies from case to case.

i. Diffusion of hydrocarbon precursors through a thin boundary layer to the substrate
ii. Adsorption of carbon species onto the surface.
iii. Surface reactions leading to film growth
iv. Desorption of product species and
v. Diffusion of species through the boundary layer into the bulk stream.

Additionally, Meyyappan *et al.* [95] report that a hydrocarbon, such as methane in a PECVD reactor when adsorbed onto the catalytic particle surface releases carbon upon decomposition, which then dissolves and diffuses into the catalyst particle. When a supersaturated state is reached, carbon precipitates in a crystalline tubular form. At this juncture, two different scenarios are possible. If the particle adheres to the substrate strongly enough, then the carbon precipitates from the top surface of the particle and the

filament or tube continues to grow with the particle anchored to the substrate. This is called the base growth model in a plasma enhanced CVD reactor.

The second case occurs when the particle attachment to the substrate is relatively weak. In this case carbon precipitation occurs at the bottom surface of the particle and the filament lifts the particle as it grows. As a result, the top end of the filament is filled with the catalyst particle. This method is called the tip growth model. These two models are illustrated in Figure 2.24.

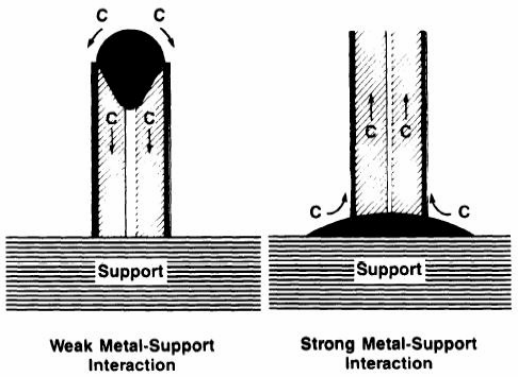

Figure 2.24 Tip and base growth mechanism [34]

2.5.10 Growth mechanism for vertically grown aligned tubes

Merkulov *et al.* [96] propose an alignment mechanism as shown in Figure 2.25.The electrostatic force *F* creates a uniform tensile stress across the entire particle/CNT interface, regardless of where the particle located (tip or base). As growth proceeds, CNTs may bend if there are spatial fluctuations in the carbon precipitation; this leads to nonuniform stresses at the particle/CNT interface. When the particle is at the top, the electrostatic force *F* produces a compressive force at the CNT/particle interface where a greater growth rate is seen as shown in Figure 2.25 c. On the side where less growth rate happens, a tensile stress is applied at the interface. This opposite behavior favors subsequent carbon precipitation at the interface with tensile stress and a smaller growth

rate. The net result is a stable, negative feedback that works to equalize the growth rate everywhere, and vertical orientation is maintained. When the catalyst particle is at its base, the stress at the interface with the higher growth rate is tensile; this acts to further increase the rate at the same location, resulting in bending of the structure. This is an unstable positive feedback system.

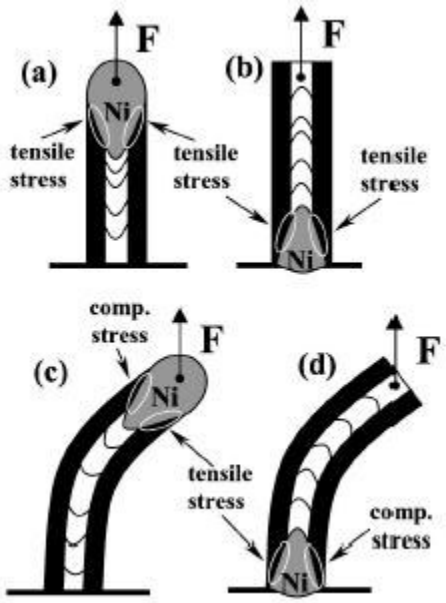

Figure 2.25. Alignment mechanism proposed by Merkulov *et al.* [96]

CHAPTER 3

PROBLEM STATEMENT

For microelectro mechanical systems (MEMS) applications, it is necessary to organize or grow carbon nanotubes to the desired structures whose linear dimensions are on the order of several micrometers while the dimensions of individual nanotubes are only a few tens of nanometers. Further growth of uniform, dense multiwalled carbon nanotubes (MWNTs) which are vertically aligned has been a challenging problem. Alignment of carbon nanotubes in a regular array and organized growth of nanotubes into a pattern has also been an equally challenging problem.

So, the objective of the present investigation is to obtain vertically aligned growth of carbon nanotubes on cobalt catalyst deposited on a silicon wafer surface using microwave assisted CVD technique. The following sub goals were identified to accomplish this:

1. Deposition of cobalt catalyst on a silicon wafer surface prior to CVD growth
2. Deposition of patterned catalyst film on to the wafer surface using Pulsed laser deposition (PLD) technique
3. Parametric studies to determine the process conditions suitable for vertically aligned growth of nanotubes

The important parameters of the microwave-assisted CVD for vertically aligned carbon nanotubes growth are the following:

1. Growth time
2. Plasma treatment time
3. Process gases
4. Flow rate of methane gas
5. Patterning of catalyst film
6. Pressure
7. Temperature

Some of the above parameters have been studied in the present investigation to obtain optimum conditions for growth of vertically aligned carbon nanotubes.

CHAPTER 4

EXPERIMENTAL APPROACH

4.1 INTRODUCTION

The major emphasis of this investigation was on growth of nanotubes and achieving aligned nanotubes in a patterned fashion using microwave assisted CVD apparatus. The plasma enhanced CVD plays a very important role in the aligned growth of nanotubes. The CVD apparatus employed in this investigation was originally used for the growth of diamond thinfilms on different substrate materials. However, some modifications of the substrate heater design and vacuum fittings were done prior to the synthesis of nanotubes. Since growth of carbon nanotubes needs a transition metal catalyst, a transition metal catalyst thin film was deposited before the growth of nanotubes in the CVD setup.

4.2 NEED FOR CATALYST DEPOSITION

A transition metal catalyst is needed to decompose the carbon precursor radicals under the experimental conditions to facilitate the growth of nanotubes on the silicon wafer surface. S0, the experimental procedure included a first step of catalyst deposition onto the substrate surface. Transition metal cobalt was used as a catalyst in this investigation and a pulsed laser deposition setup was used for depositing the cobalt catalyst on to the silicon wafer surface. Details of the pulse laser deposition setup are provided in the following section.

4.3 PULSE LASER DEPOSITION SETUP

Figure 4.1 is a schematic of the pulsed laser deposition setup used for the catalyst deposition on to the silicon wafer surface. Figure 4.2 is a photograph of the PLD experimental setup.

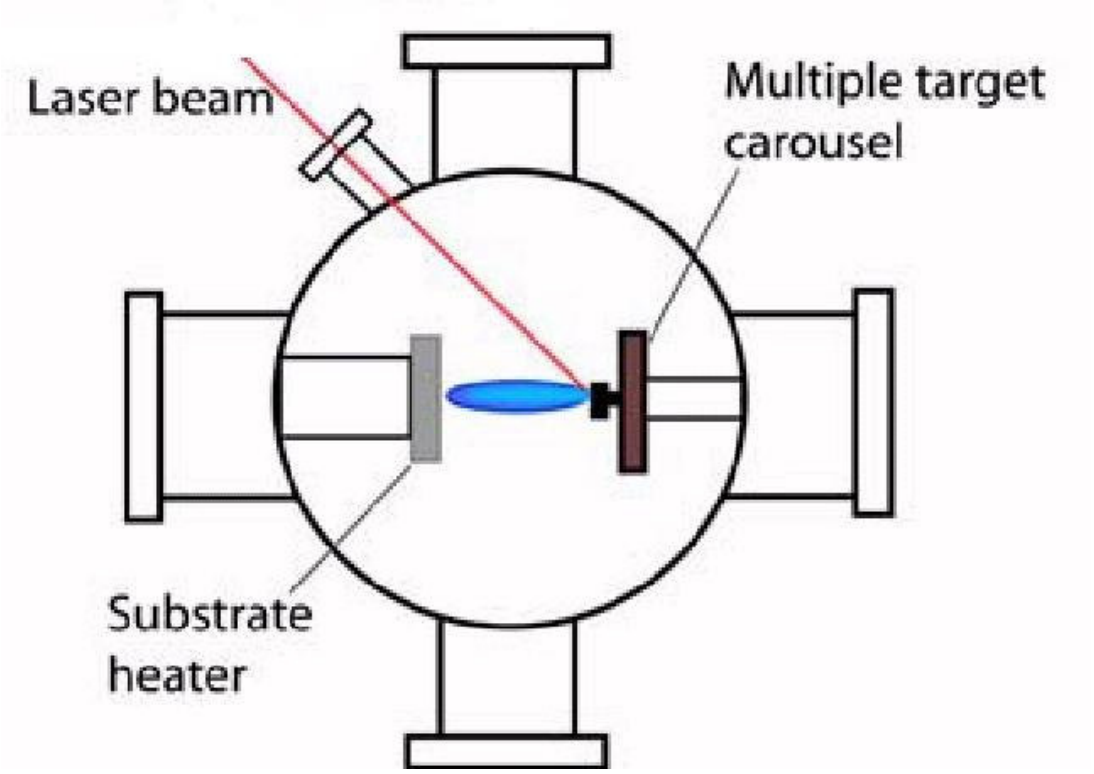

Figure 4.1 Schematic of the pulsed laser deposition setup

The apparatus consists of a vacuum chamber that houses the target holder and the substrate holder. The laser beam is focused by the optical system and then allowed into the chamber through a glass window. Means are provided to raster the beam over the surface of the target. The target and the substrate are placed co-axially such that the plume of ablated material from the target strikes the substrate. The substrate holder has

an integrated heater into it to facilitate heating of the substrate during the deposition process. A thermocouple is used to measure the temperature of the substrate. The target is rotated by a motor at a uniform rate to ensure that the laser beam ablated the target uniformly.

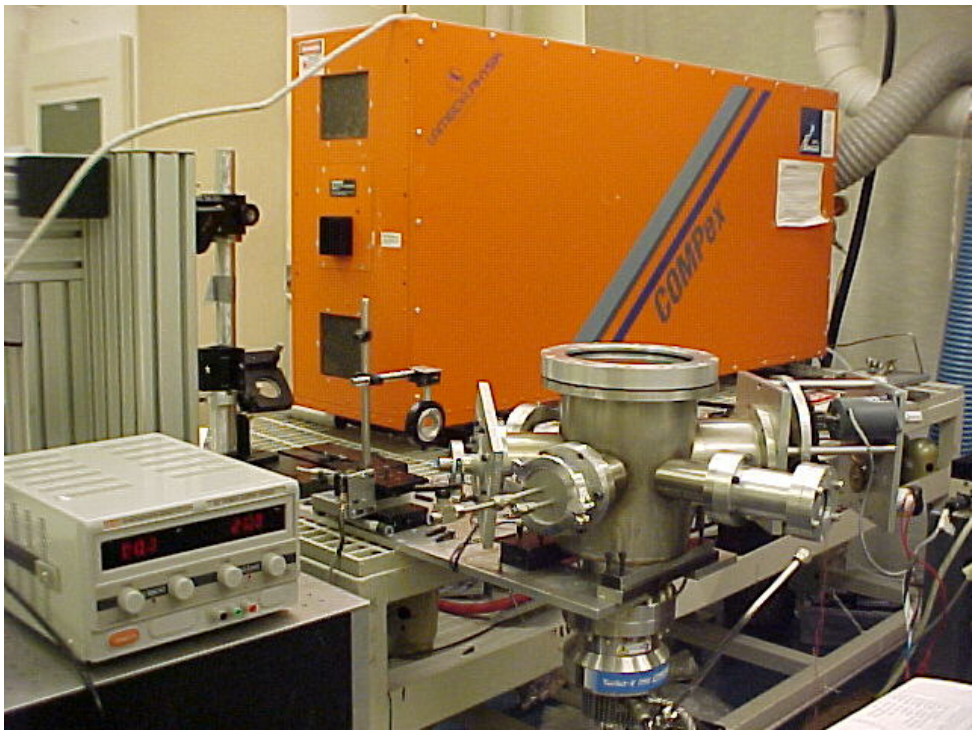

Figure 4.2 Photograph of KrF Excimer laser pulsed laser deposition (PLD) setup.

4.3.1 Excimer laser and Optics

The laser used in the PLD process is a Lambda Physik Compex (model 201) KrF pulsed Excimer laser (with an average power of 4W @ 10Hz, 30KV). The Excimer laser system is air-cooled and operates on a single phase power supply. The laser beam is delivered through a manually operated shutter type window. Between the output port of the laser and the input port of the deposition chamber, optical elements are placed in

order to focus the beam on to the target. The optical elements that couple the energy from the laser to the target are lenses, apertures, mirrors, beam splitters, and laser window. The lenses have a low loss, high energy anti-reflective coating on them, and the mirrors have a highly reflective dielectric coating for high durability and high damage threshold.

The optical system used consists of two fully reflecting mirrors placed such that the laser beam is reflected at right angles. This is necessary as the laser outlet and the chamber are at different heights and the beam has to be brought down to a lower elevation. The reflected beam is made to pass through a spherical lens to focus the beam on to a spot. The lens is UV coated to prevent any damage that could be caused by the laser beam passing through it. The optical system allows the delivery of the beam into the chamber through the front window of the chamber. The chamber is pumped down to 10^{-6} torr using a turbo molecular pump backed by a mechanical pump.

4.4 MICROWAVE ASSISTED PLASMA CVD –EXPERIMENTAL SETUP

Figure 4.3 is a schematic of the microwave assisted CVD reactor employed in the present study. The microwave CVD system used for the synthesis of nanotubes in this investigation uses a ASTEX S-1500, 1.5 KW microwave power generator operating at powers of 125 to 1500 watts at 2.45 GHz microwave frequency. Microwaves generated at the generator are coupled by the symmetric plasma coupler to produce a ball of plasma at, or slightly above, the substrate surface in vertically mounted, water cooled, double-wall stainless steel chamber. A motorized substrate stage is used to raise or lower the substrate to change the proximity of the substrate to the plasma, and a resistive heater is integrated into the substrate stage, which can be heated up to 1100^{o}C. The vacuum system, gas flow system, and temperature monitoring system is briefly discussed in the following section.

4.4.1 Vacuum system

Typically pressures in the range of a few torr to a few tens of torr are used in nanotubes growth. This is achieved by evacuating the chamber to a pressure of 2 X 10^{-2} torr using a mechanical pump (Alcatel Model 2008A) and by back filling the chamber with the process gases. The pressure inside the chamber is monitored continuously using a pressure transducer (MKS type 127) and controlled using a pressure controller (MKS type 250).

4.4.2 Gas flow system

The gases required for nanotubes growth, i.e., methane (CH_4), hydrogen (H_2) and nitrogen (N_2) are handled by mass flow meter (MKS type 247C) along with mass flow controllers (MKS Type 1159B). Stainless steel tubing with hand operated valves, and swagelok fittings are used for the gas flow piping. Typically, the gas flow is maintained at or around 100 SCCM. The gases were introduced into the chamber through a gas inlet port.

4.4.3 Other systems used

The substrate temperature is monitored using a Williamson dual-wavelength pyrometer. The dual wavelength pyrometer features a rotating chopper carrying four narrow-band pairs of spectral filters of different wavelengths and determines the temperature by computing the ratio of the radiant energies emitted by the target in these wavebands.

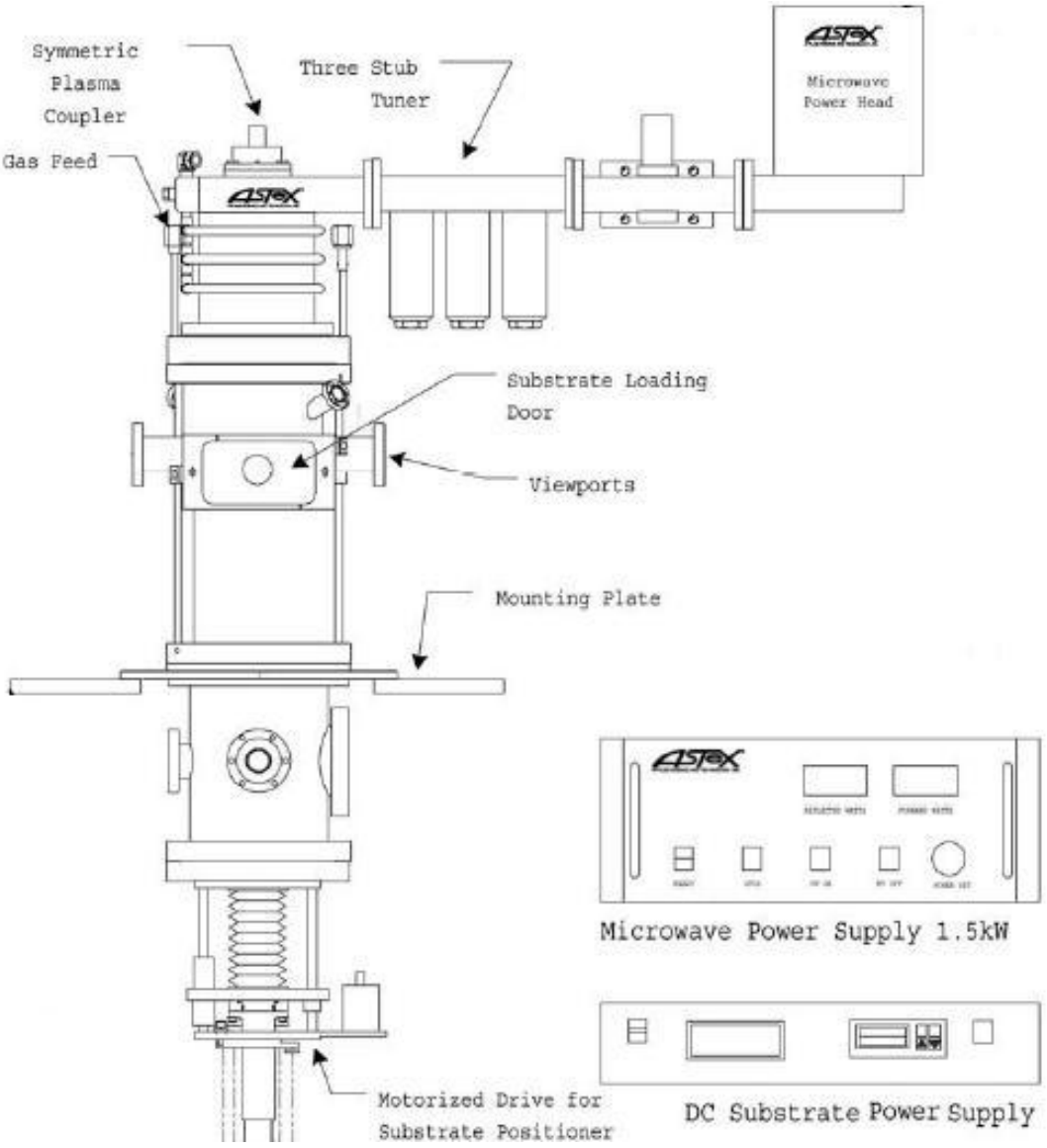

Figure 4.3 Schematic of Microwave CVD Experimental setup

Additionally Figure 4.4 and Figure 4.5 are photographs of the microwave CVD experimental setup. Figure 4.5 is a closer view showing the microwave generator and the chamber access door.

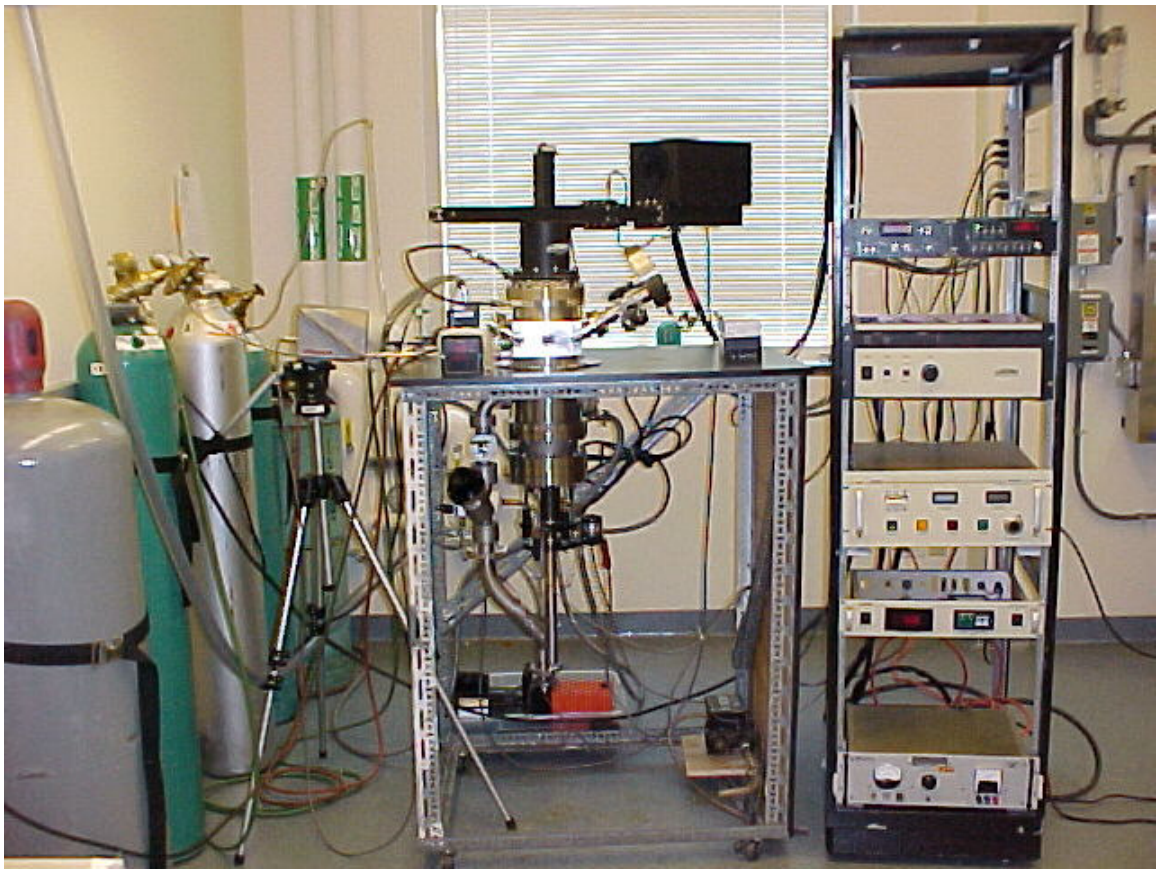

Figure 4.4 Photograph of Microwave assisted CVD reactor.

4.5 CHARACTERIZATION

Different characterization tools were used through out the length of the study. However, scanning electron microscopy was the main characterization technique employed. A JEOL JSM -6400 scanning Electron microscope (SEM) was used for this purpose. Additionally, a JEOL 100 CX II STEM was used to study the internal morphology of the tubes, and for TEM analysis samples were prepared by scraping a part of the grown nanotubes from the silicon wafer surface and dispersing them in alcohol. Few drops of the nanotubes dispersed in alcohol were dropped on to TEM grids for analysis. Further a SPEX-500 MicroRaman spectrometer was used for determining the characteristics of the nanotubes. And a MicroXam, optical interference microscope was

used to characterize and image patterned catalyst thinfilms. AFM characterization was performed using a Digital instruments Dimension 3100 series scanning probe microscope.

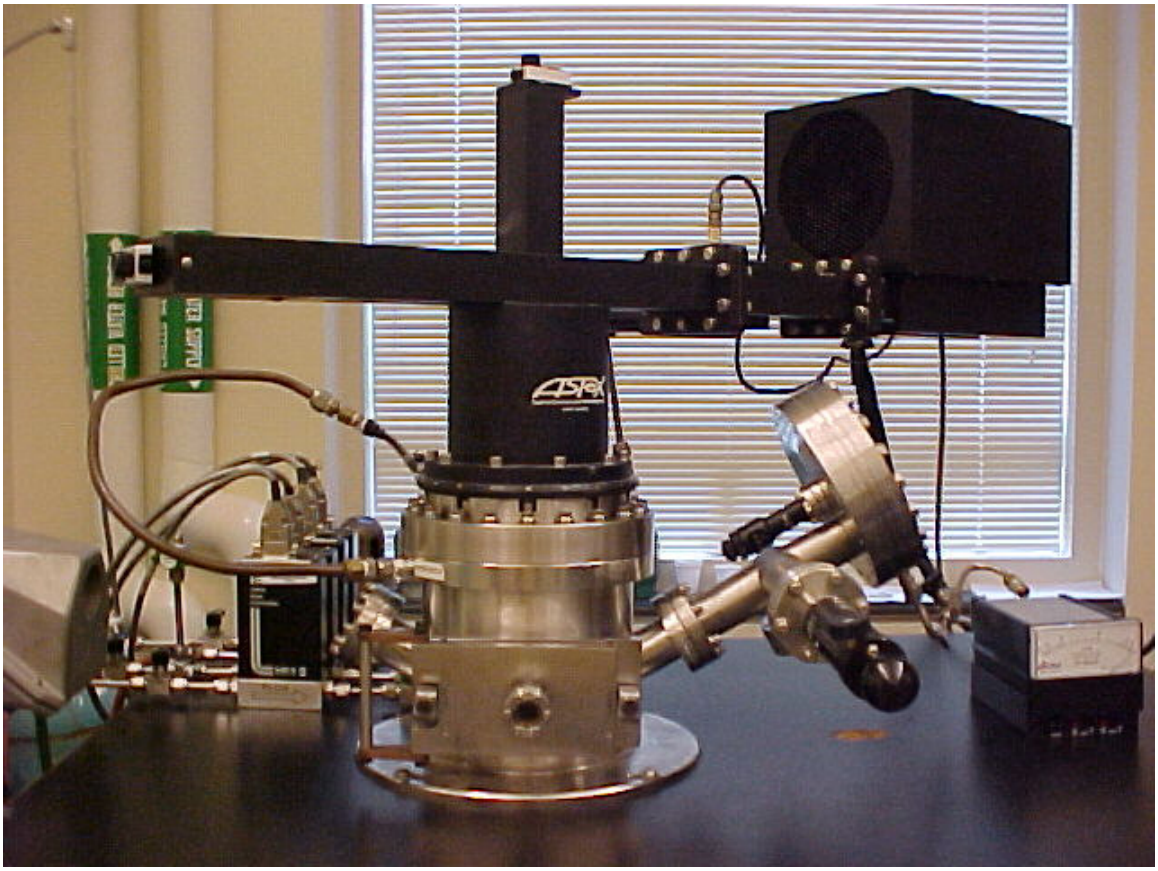

Figure 4.5 Closer view of the microwave CVD reactor.

CHAPTER 5

METHODOLOGY FOR GROWING NANOTUBES

5.1 INTRODUCTION

The present study is concerned with obtaining vertically aligned growth of nanotubes. Since growth of nanotubes necessitates catalyst particles, a thin film of cobalt metal catalyst is deposited using the PLD setup described in the previous chapter. Once the catalyst is deposited on to the wafer surface, it was transferred to the CVD reactor for growth of nanotubes. The steps involved are categorized under catalyst deposition and CVD growth procedure in the following sections of the chapter.

5.2 CATALYST DEPOSITION AND PROCEDURE

The PLD setup employed deposits a continuous thin film on to the silicon wafer substrate. Various steps involved in the deposition procedure is listed in steps in the following:

1. Silicon wafer samples are broken into small pieces of wafers sized about 1" X 1" for conveniently positioning inside the PLD deposition chamber.
2. Broken pieces of the samples are ultrasonicated in acetone for 10 minutes prior to loading inside the deposition chamber.
3. The samples are placed inside the deposition chamber and the chamber was evacuated to 10^{-2} torr.

4. The Excimer laser is turned on to strike the target surface.
5. KrF- Excimer laser of 248nm wavelength is used and the pulse repetition rate of the laser is kept at 10 Hz.
6. The laser exposure time is varied from 15 seconds to 45 seconds to control the thickness of the catalyst film deposited.
7. The sample is removed from PLD chamber for further processing in CVD.

5.3 CVD PROCEDURE

Once the catalyst is deposited, the samples are removed from the PLD chamber and transferred to the CVD chamber, the following procedure is followed:

1. The substrate is inserted into the CVD reaction chamber and placed on the graphite plate of the substrate stage.
2. Turn on the vacuum pump and evacuate the system to a pressure of $< 10^{-2}$ torr. Set the desired pressure and flow rate. Typically, pressures used are in the range of 10 – 15 torr and a total flow of 100 sccm of the process gases (hydrogen, nitrogen, and methane) are used for the growth of nanotubes.
3. Flush the chamber with hydrogen at a pressure of ~10 torr, and turn on the water supply.
4. Switch the microwave power and initiate hydrogen plasma, microwave power is maintained ~ 500 watts.
5. Once the plasma is initiated, the chamber pressure is quickly increased to 15 torr along with the introduction of nitrogen gas.

6. Hydrogen and nitrogen plasma is maintained for 5 minutes for the plasma pretreatment of the sample.
7. Methane gas is pumped in.
8. Reflected power of the microwaves is tuned using the wave guide.
9. Optical pyrometer is used to measure the temperature of the substrate.
10. Continue the growth of nanotubes for the required time.
11. After the growth is complete, shut off methane and hydrogen and the microwave generator.
12. After cooling in nitrogen for 5 minutes, switch off all the gas flows and water supply and vent the system before removing the sample for further characterization.

CHAPTER 6

RESULTS

6.1 INTRODUCTION

Experiments on the growth of carbon nanotubes on a cobalt catalyst deposited silicon wafer substrates were conducted under different process conditions. Process conditions were varied to study their effect on the growth of nanotubes, but were chiefly focused towards obtaining the growth of aligned nanotubes. The key process parameters investigated include plasma treatment time, growth time, process gases, and flow rates of methane gas. Additionally, the effect of patterning the catalyst film and growth of aligned nanotubes on patterned catalyst surfaces is also investigated. Since this study was performed concurrently with investigation of nanotubes growth on iron and iron oxide catalysts by a team of three members, changes in process parameters were quickly adopted based on results of current study and also based on the results obtained from other two catalysts mentioned [109, 110]. This was done in an effort to quickly narrow down the parameters favorable for the growth of aligned nanotubes.

In addition to the detailed investigation presented here, more investigation towards the effect of the flow rates of methane, effect of chamber pressure and the effect of other process parameters on the growth and morphology of nanotubes is reported else where in the thesis work by other two team members along with whom this study was accomplished [109, 110].

Once the tests were conducted, the nanotubes grown on silicon wafer substrates were characterized using a scanning electron microscope. Additionally, transmission electron microscope (TEM) characterization of grown nanotubes was also performed for studying the morphology of individual nanotubes. Furthermore, characterization of nanotubes by atomic force microscopy was performed to estimate the nanotubes diameters and μ Raman spectrometer characterization was performed to determine if tubes are multiwalled or single walled type.

6.2 EFFECT OF GROWTH TIME

Table 6.1 lists the process parameters used in the study of the effect of growth time on growth morphology of nanotubes. Figures 6.2, to 6.6 are micrographs of the nanotubes grown on silicon wafer samples after CVD growth times of 30 seconds, 3, 5, 10, and 15 minutes, respectively. It can be seen from Figure 6.1, (photograph of silicon substrate taken after CVD growth) that area of black deposition, increases progressively as the growth time is increased.

It can be observed from the Figures 6.1 A and Figure 6.2 that at 30 seconds growth time, no growth of nanotubes occurs. Whereas at 3 minutes growth time, a black film is deposited on the wafer as shown in Figure 6.1 B, and the corresponding SEM micrograph shown in Figure 6.3 shows dense nucleation without appreciable growth of tubes. After 5 minutes growth time, we can see that the there is a dense growth of tubes as shown in Figure 6.4. After 10 minutes, the growth density increases and it can also be seen that the tubes are appreciably longer than the 5 minutes sample as shown in the SEM micrograph in Figure 6.5. After 15 minutes growth time, the nanotubes become

dramatically thicker than the previous samples. This can be clearly seen in the SEM micrograph of the 15 min CVD grown sample as shown in Figure 6.6.

Table 6.1 Process parameters employed to study the effect of growth time

Catalyst Deposition time, s		30
Plasma pretreatment time, min		5
Growth time, min		30 s, 3, 5, 10, 15 and 30
Process gases and flow rates, sccm	H_2	40
	N_2	50
	CH_4	10
Microwave power, watts		500
Chamber pressure, torr		15
Substrate temperature, ^oC		750 to 850

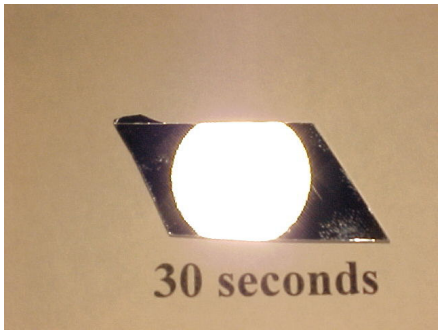

A. 30 seconds growth time

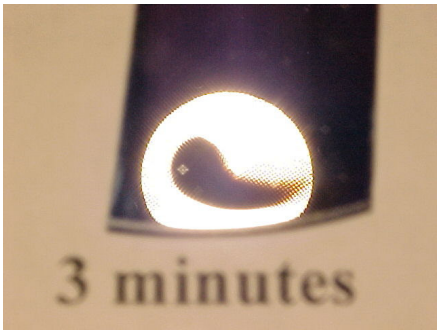

B. 3 minutes growth time

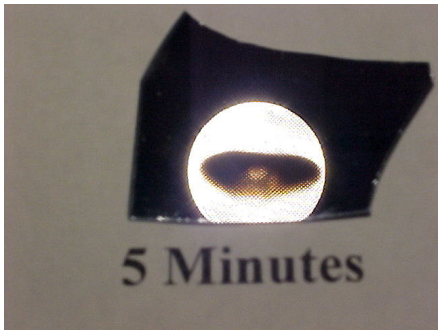

C. 5 minutes growth time

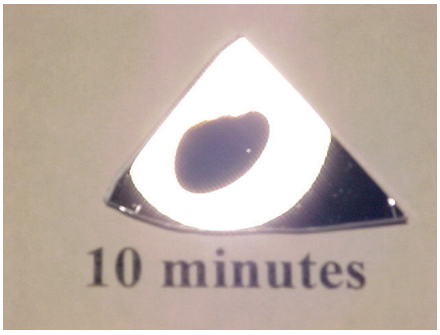

D. 10 minutes growth time

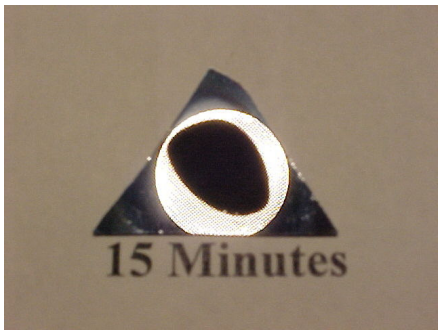

E. 15 minutes growth time

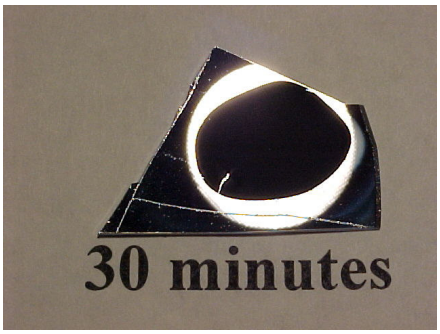

F. 30 minutes growth time

Figure 6.1 Photograph of silicon wafer substrates after CVD growth. Silicon substrates are subjected to different growth times, and as a result growth area (seen as black deposition) increases progressively with increase in growth time.

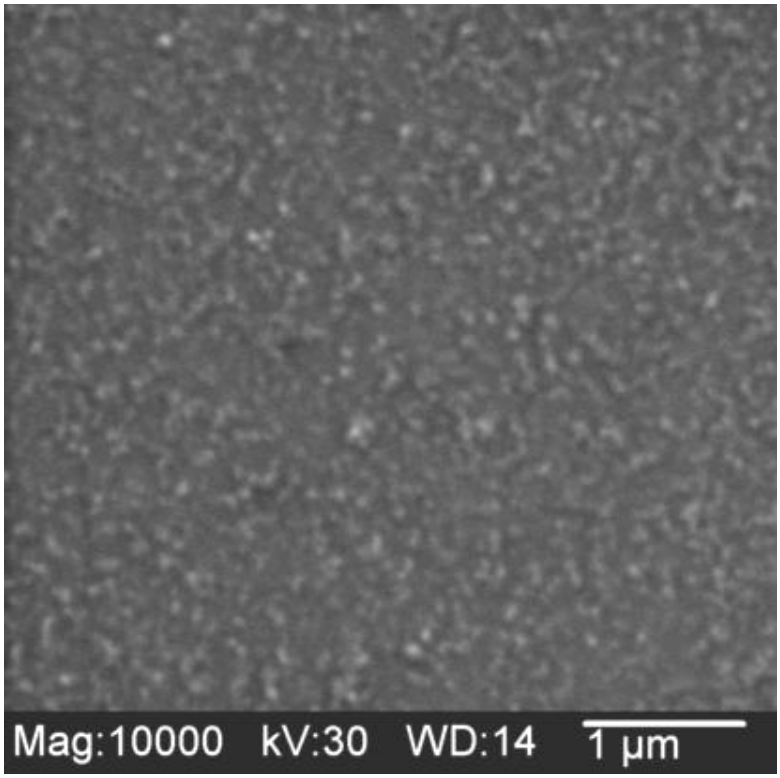

Figure 6.2 SEM micrograph showing no nanotubes growth (30 sec growth time)

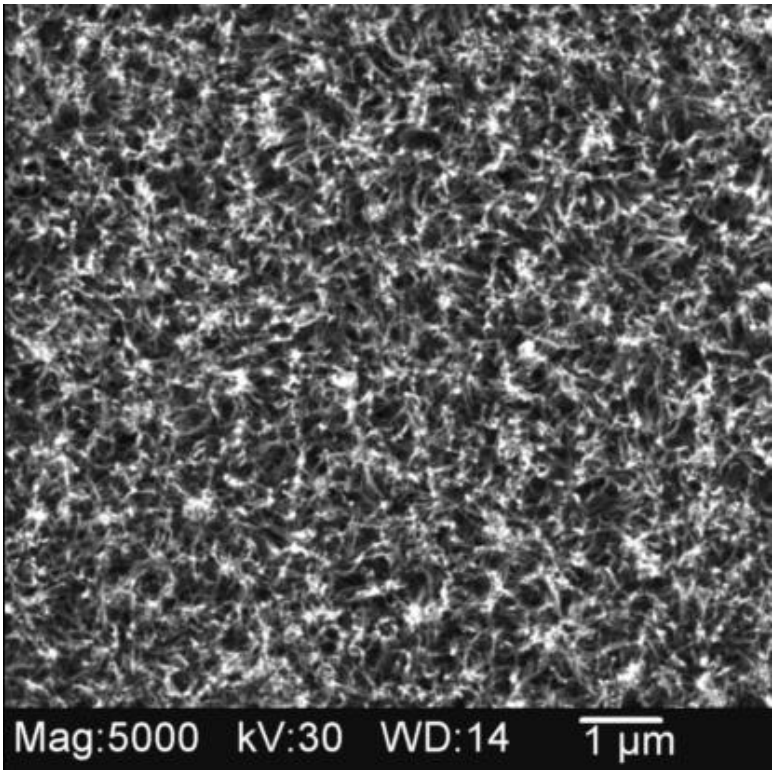

Figure 6.3 SEM micrograph showing nucleation of nanotubes (3 min growth time)

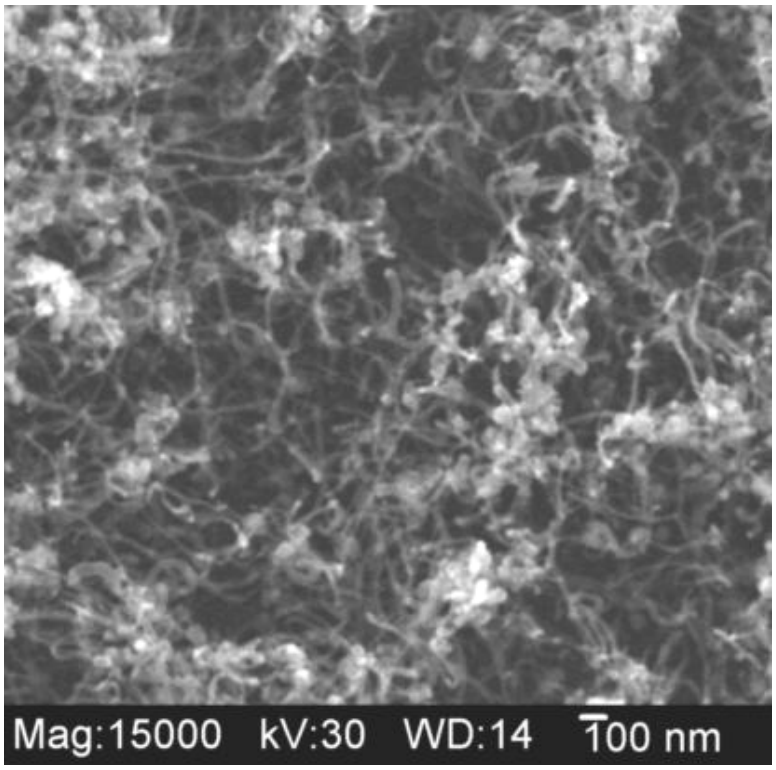

Figure 6.4 SEM micrograph showing growth of nanotubes (5 min growth time)

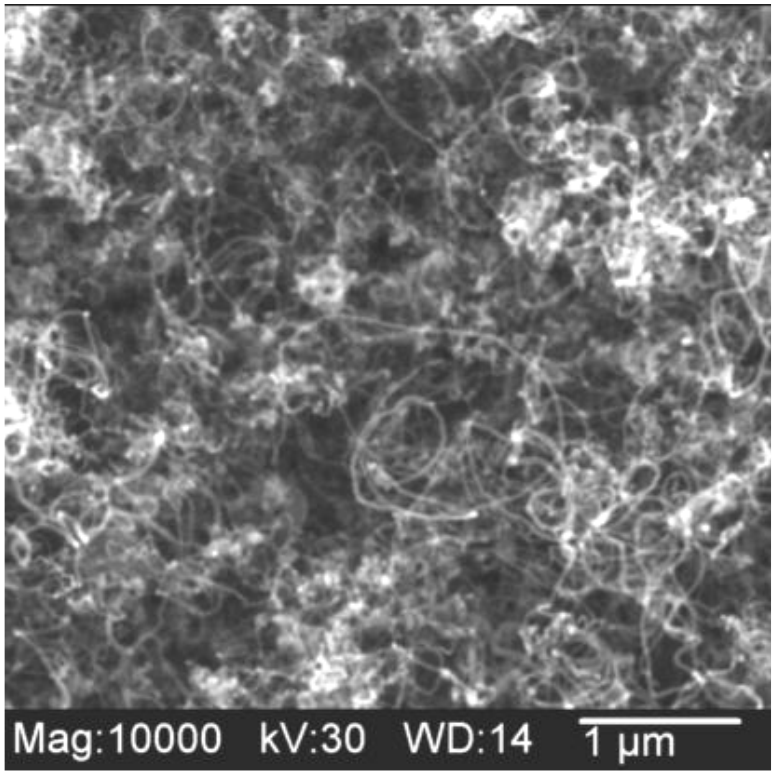

Figure 6.5 SEM micrograph showing longer tubes (10 min growth)

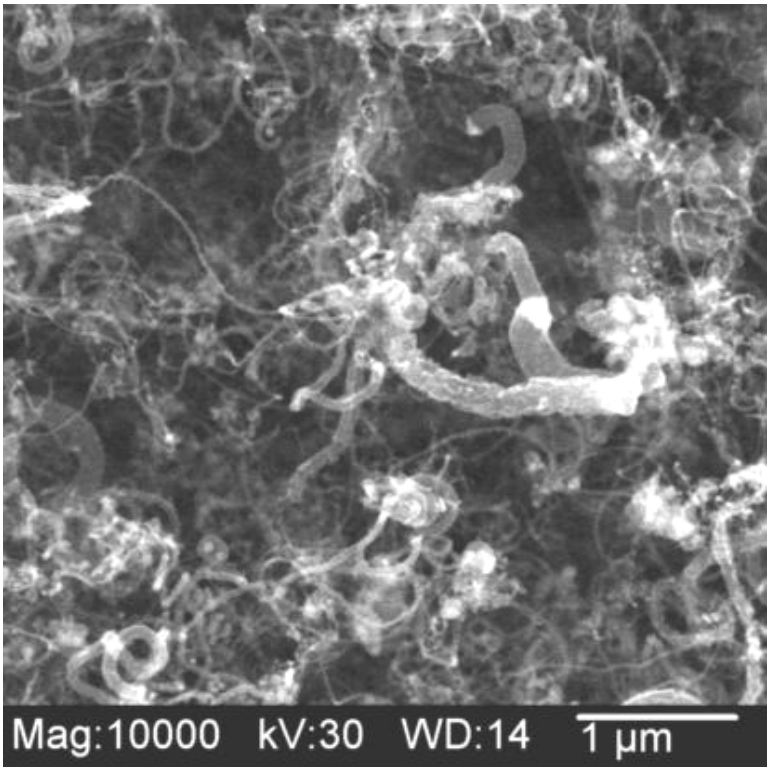

Figure 6.6 SEM micrograph showing thicker nanotubes (15 min growth time)

Based on the observation of SEM micrographs in Figures 6.4 and 6.5, 5-10 minutes of CVD growth time appears to be the optimum growth time to form nanotubes with good amount of growth density and relatively uniform tubes.

6.3 EFFECT OF PLASMA TREATMENT TIME

Experiments were conducted at 0, 1, 3, 10 and 15 minute's plasma pretreatment time. The other experimental conditions employed were maintained constant and are listed in Table 6.2

Table 6.2 Process parameters used to study the effect of plasma treatment

Catalyst Deposition time, s		30
Plasma pretreatment time, min		0, 1, 3, 5, 10 and 15
Growth time, min		10
Process gases and flow rates, sccm	H_2	40
	N_2	50
	CH_4	10
Microwave power, watts		500
Chamber pressure, torr		15
Substrate temperature, ^oC		750 to 850

The SEM micrographs of nanotubes grown under these conditions are shown in Figures 6.7, to 6.12 respectively. It can be seen that there is a clear difference in the growth morphology of the nanotubes as the plasma treatment time is increased from 0 to 15 minutes. The SEM micrographs of nanotubes were taken in the vicinity of an open region, or pin holes observed in the black deposition after the CVD growth. In the absence of pin holes or open regions, a scratch mark was deliberately made on the black deposition using sharp tweezers to reveal the growth morphology of the tubes.

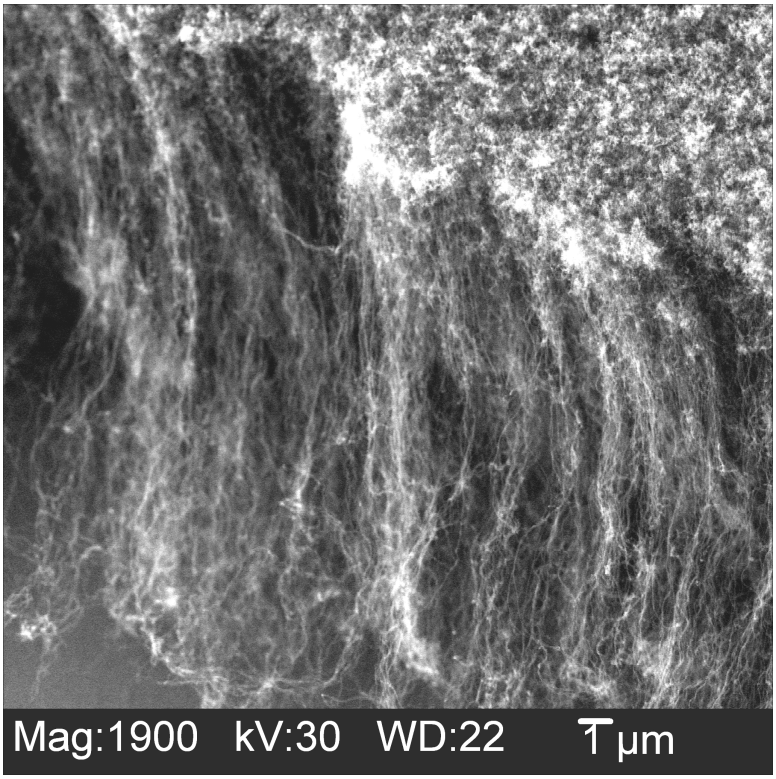

Figure 6.7 SEM micrograph of nanotubes growth under no pretreatment condition

It can be seen from Figures 6.7 and 6.8 that nanotubes are not well defined in the case of 0 and 1 minute pretreatment experiments. However in both cases the growth appears to be very dense, with cluster like white spots observed on the top surface of the growth layer.

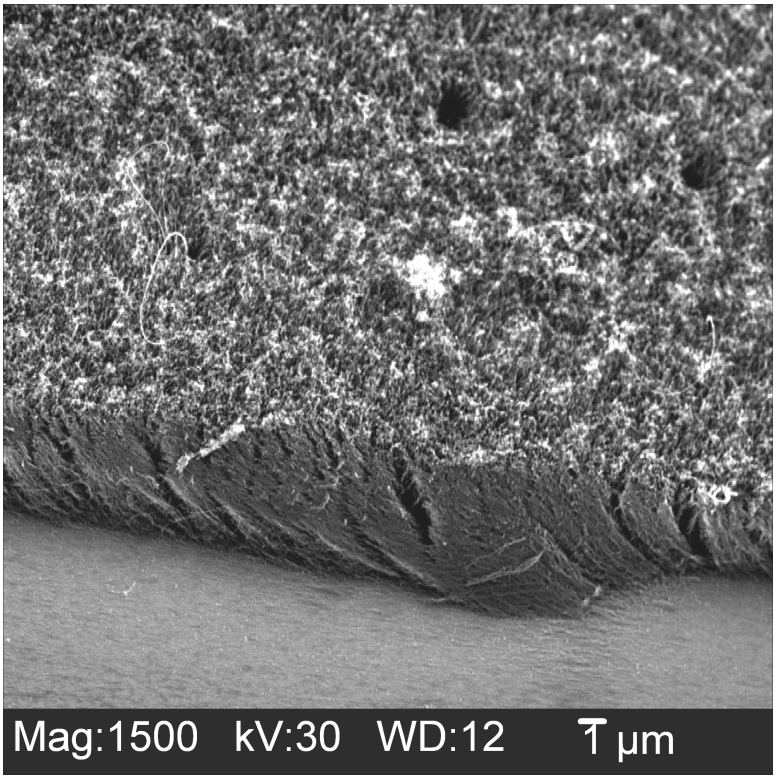

Figure 6.8 SEM micrograph of silicon substrate (1 min plasma treatment)

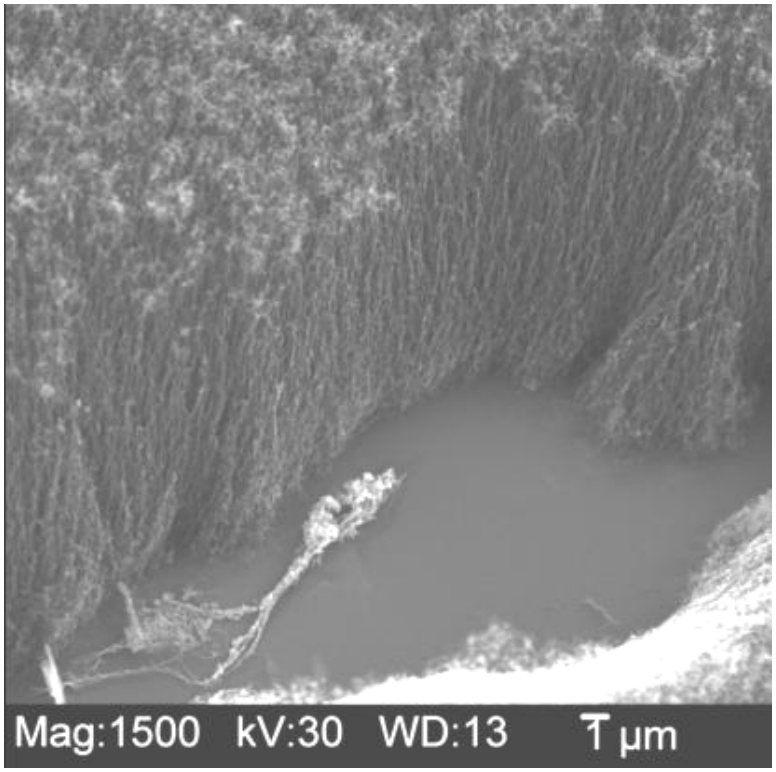

Figure 6.9 Clearly defined nanotube growth (3 min plasma treatment)

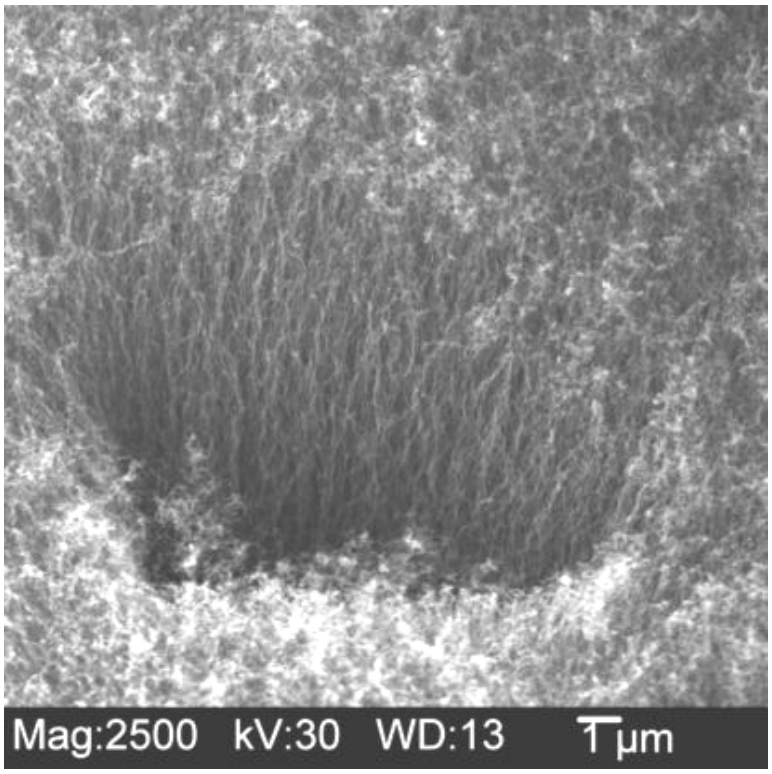

Figure 6.10 SEM micrograph of nanotubes grown (5 min plasma treatment time)

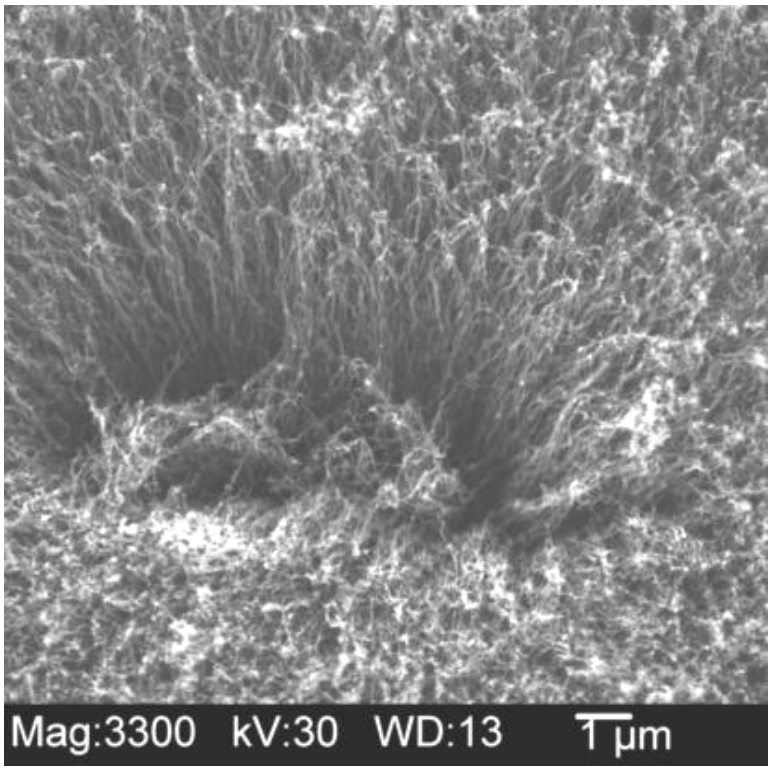

Figure 6.11 SEM micrograph of nanotubes (10 min plasma treatment)

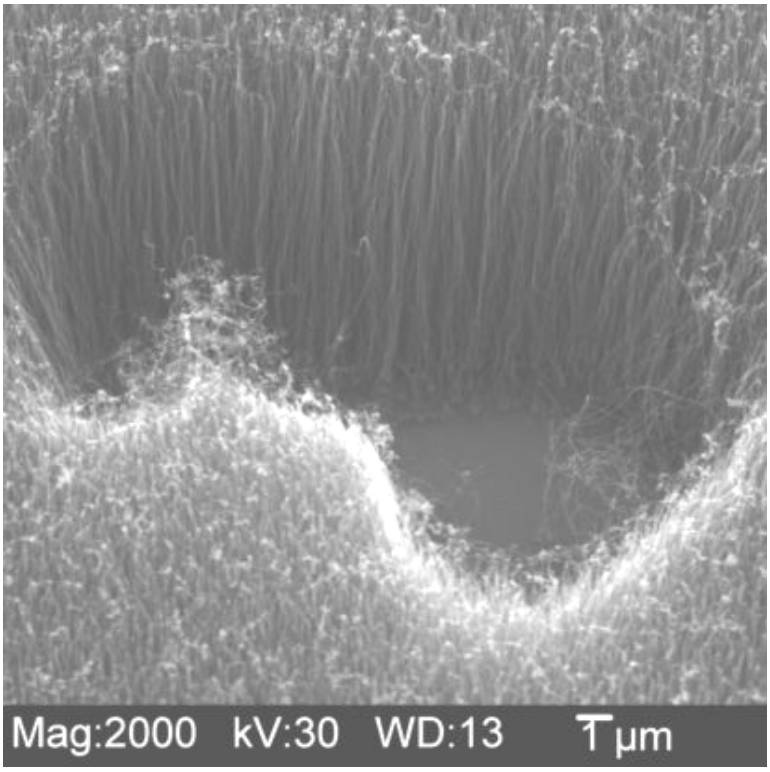

Figure 6.12 SEM micrograph of nanotubes (15min plasma treatment)

Comparing Figures 6.8 and 6.9, it can be seen that clearly defined nanotubes are observed when nanotubes are grown with pretreatment condition than with less or no pretreatment. It can also be seen from Figures 6.9 and 6.10, that growth morphology of nanotubes is similar in the case of 3 and 5 minutes pretreatment time. It can be seen that the nanotubes grown from sample subjected to 15 minutes pretreatment time resulted in vertically grown tubes which are less curly compared to previous samples subjected to 3, 5 and 10 minutes pretreatment. This is can be observed from Figure 6.12. Additionally the growth of tubes with 15 minutes pretreatment seems to be less dense compared to samples shown in Figures 6.9 and 6.10. Further, nanotubes are found to grow much straighter with 15 minutes pretreatment time than the samples with no pretreatment or less pretreatment time.

6.2.1 Wrinkle formation under no pretreatment condition

In addition to the initial observations, another interesting phenomenon was observed when nanotubes are grown under no plasma treatment condition. As mentioned earlier, a scratch mark is deliberately made by sharp tweezers before SEM characterization. When scratch marks of samples with no pretreatment were compared with scratches on samples subjected to pretreatment condition, it can be seen that there is a dramatic difference in the morphology of the growth shown in Figures 6.13 and 6.14, respectively.

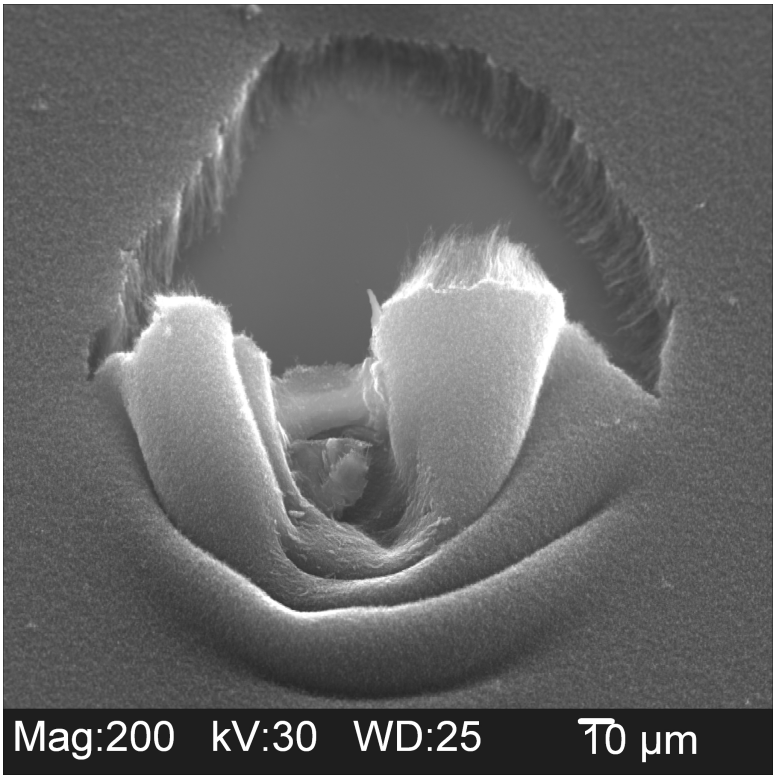

Figure 6.13 Formation of wrinkles and folds when nanotubes are scratched (observed on a silicon substrate after CVD growth under no plasma pretreatment condition)

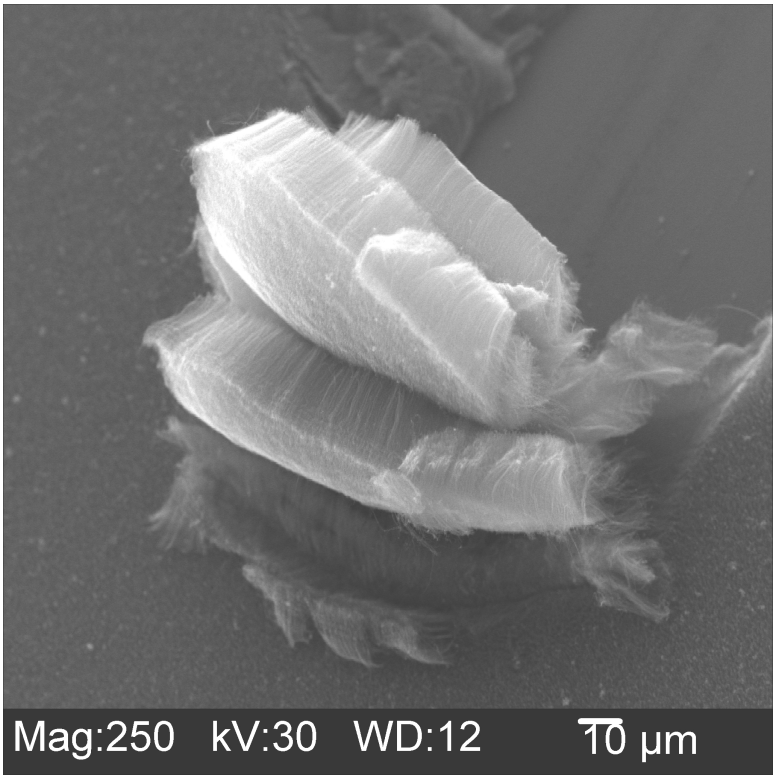

Figure 6.14 Scratch mark showing no wrinkle formation on silicon wafer substrate after CVD growth (plasma pretreated)

It is can be seen from Figure 6.13 that the black deposition with nanotubes obtained after the CVD growth acted similar to a continuous flexible sheet or a fabric. Based on this behavior, the black deposition on the wafer surface with nanotubes can be considered as a carpet forming wrinkles when scratched. This is very much evident from the fact that the black deposition with nanotubes wrinkled and formed folds when scratched rather than breaking. Further this phenomenon was observed only on the nanotubes grown with no plasma treatment condition during their growth. When nanotubes grown with plasma treatment condition during their growth was scratched in a similar fashion, it resulted in no wrinkle formation and the difference in the morphology of the scratch and the nanotubes can be seen as shown in Figure 6.14.

Figure 6.15 shows another scratch mark made on the same sample with no plasma treatment. This further confirms the phenomenon of wrinkle and crease formation in the no pretreatment condition sample when scratched. In contrast, Figure 6.16 shows the less dense morphology of the tube growth, of the sample subjected to 15 minutes pretreatment conditions. Another interesting observation in this particular sample (no pretreatment sample) is the fact that there is tube growth even under no pretreatment condition. Figure 6.17 is a SEM micrograph showing growth of nanotubes under no plasma treatment condition.

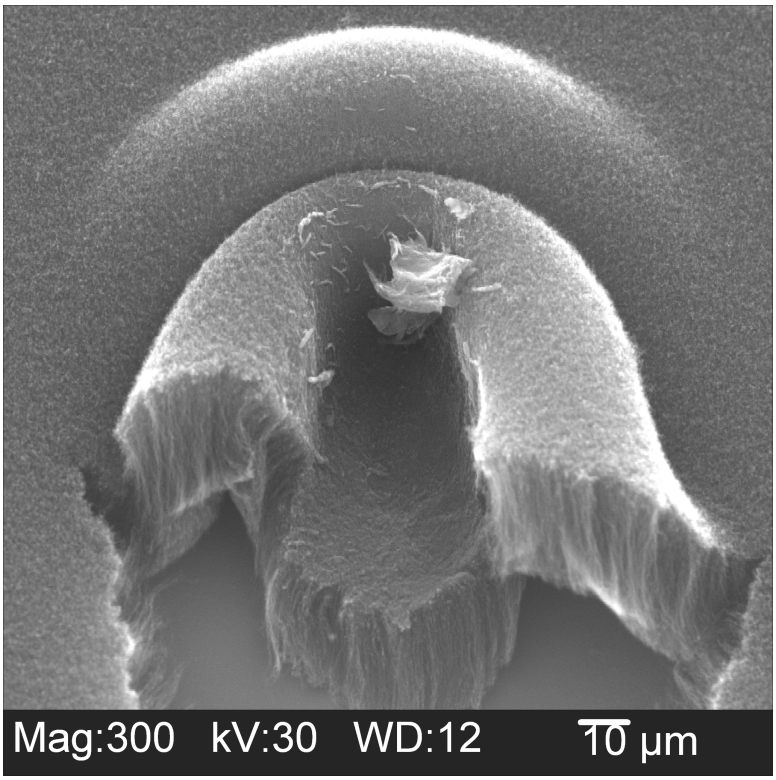

Figure 6.15 Scratch mark showing the wrinkle and crease formation (no pretreatment condition)

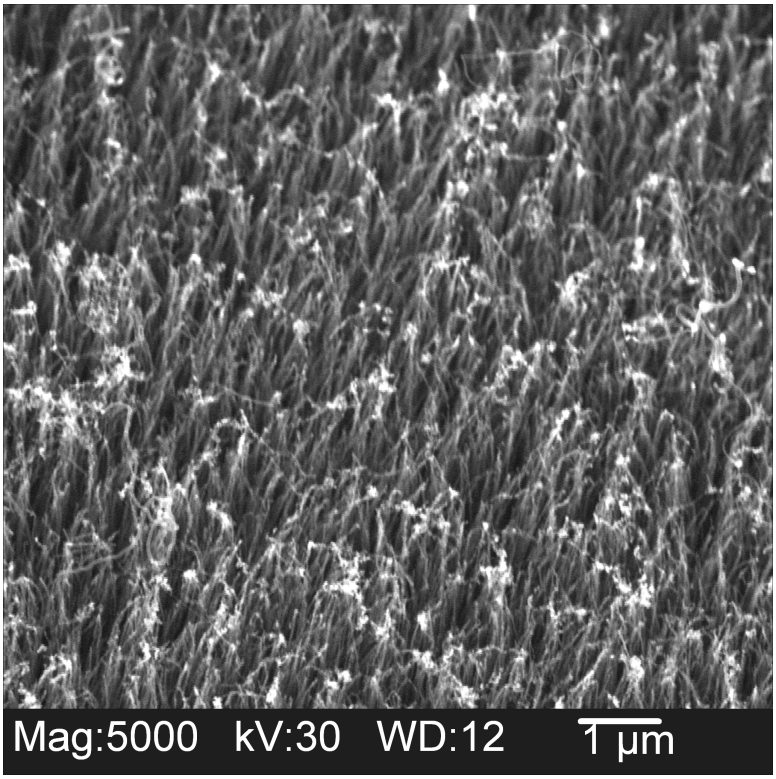

Figure 6.16 Less dense tube formation (growth with 15 min pretreatment condition)

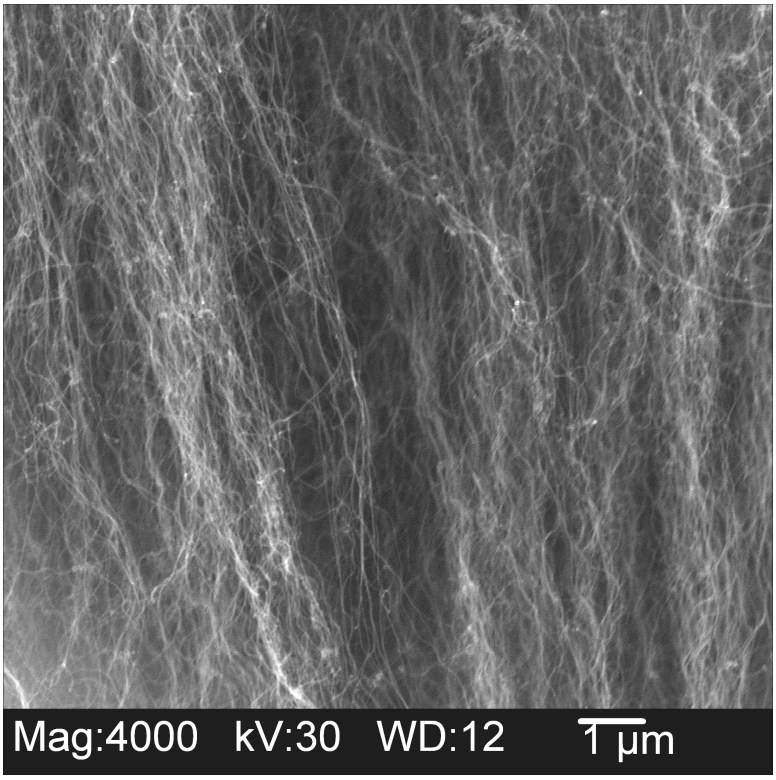

Figure 6.17 Nanotubes growth observed even under no pretreatment condition

6.4 EFFECT OF PROCESS GASES

A series of experiments was conducted in the absence of either one of the process gases, hydrogen or nitrogen, and in cases when all the process gases are used, the flow rates of methane was modified. Table 6.3 lists the process parameters of the experiments conducted. In the first experiment, when nitrogen gas was not used as one of the process gases, no deposition was observed at the end of the CVD growth. But a black deposition indicating growth of nanotubes was observed on the catalyst coated wafer surface, even in the absence of hydrogen gas. Further experiments were conducted with varying flow rates of hydrogen, nitrogen and methane. Since there was no black deposition or any growth of tubes observed in the absence of nitrogen, nitrogen gas was always included as one of the process gases through out the experimentation.

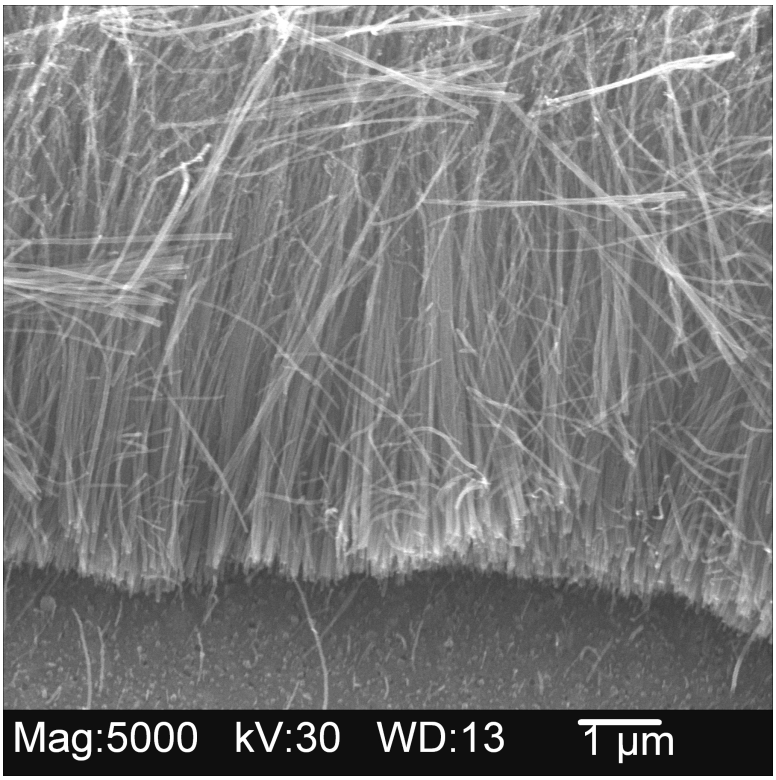

Figure 6.18 vertically aligned growth of tubes obtained in the absence of hydrogen

Table 6.3 Process parameters employed in the study and effect of flow rates of gases

Sample	Hydrogen flow rate (sccm)	Nitrogen flow rate (sccm)	Methane flow rate (sccm)	Pretreatment time (min)	Growth time (min)	Comments
1	50	0	10	5	30	No growth
2	0	36	10	5	30	Vertical tube growth
3	50	36	10	5	30	Curly tube growth
4	40	50	15	5	10	Carpet growth
5	50	36	10	5	10	Growth observed

Figure 6.18 is a SEM micrograph showing nanotubes grown in the absence of hydrogen as one of the process gases. Since no growth of nanotubes was obtained in the absence of nitrogen, micrographs of silicon substrates experimented with conditions listed for sample 1 in the Table 6.3 are not provided. However, nanotubes growth were obtained when hydrogen and nitrogen were used as process gases along with methane. Figure 6.19 is a SEM micrograph showing nanotubes grown on sample 3. From comparing Figures 6.19 and 6.18, the difference in growth morphology can be seen. Figure 6.20 is a high magnification SEM micrograph of nanotubes grown in the presence of nitrogen and methane as process gases (no hydrogen). It can be seen, that nanotubes

are straighter and apparently fewer defects when compared to Figure 6.21. Figure 6.21 shows nanotubes which are grown curly when hydrogen is included in the process gases.

Figure 6.22 is a SEM micrograph of nanotubes grown with only nitrogen as the process gas along with methane. It can be seen that the upper ends of the tubes have amorphous particles attached to the tubes. Where as nanotubes grown with hydrogen as one of the process gas did not show any amorphous particles attached to the tubes. This is shown in Figure 6.23.

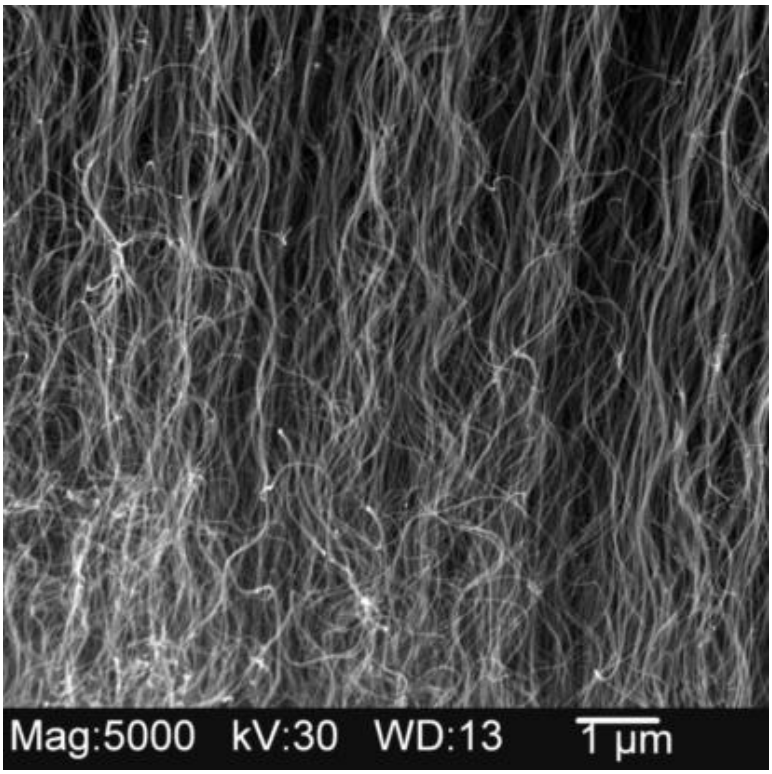

Figure 6.19 Curly tubes formed in the presence of hydrogen and nitrogen process gases

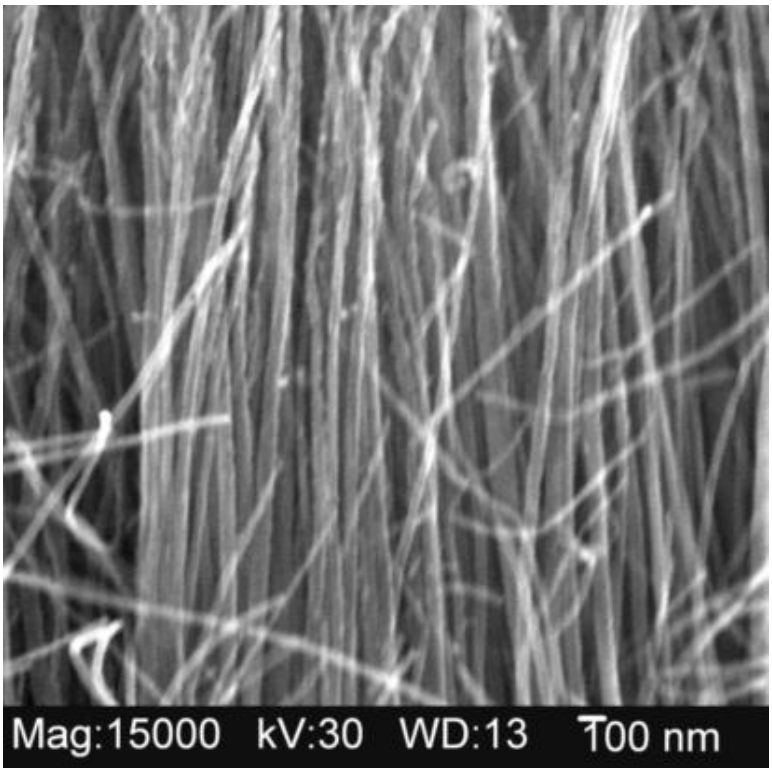

Figure 6.20 SEM micrograph of straight and aligned tubes in the absence of hydrogen

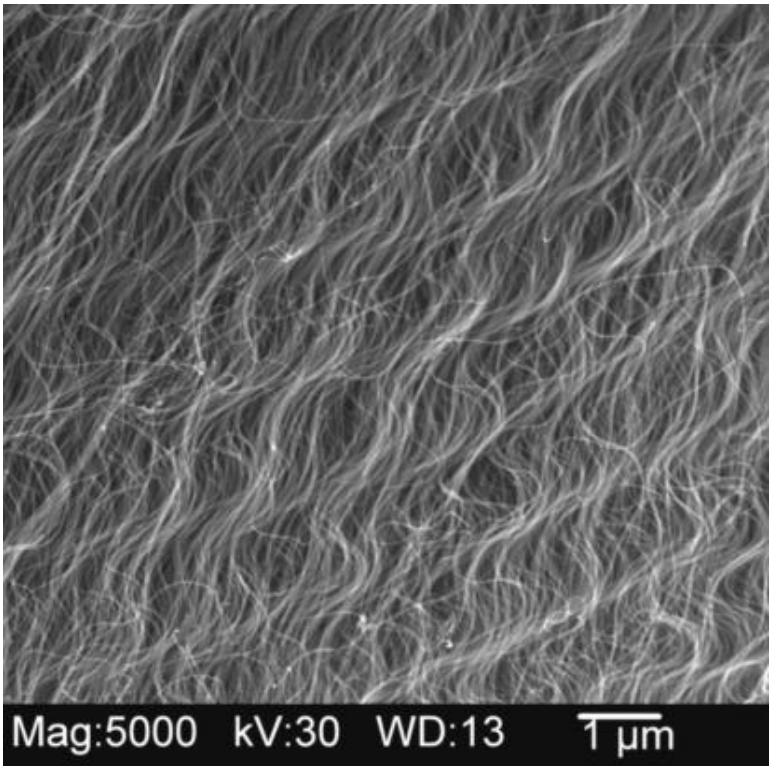

Figure 6.21 SEM micrograph of curly tubes in presence of H_2 and N_2

Figures 6.24 and 6.25 are SEM micrographs of nanotubes grown with experimental conditions given under sample 4 and sample 5 respectively on table 6.3. As shown in Figure 6.24 when the nanotubes are grown in a methane flow rate of 15 sccm , it results in the formation of carpets of tubes, which are very dense and thick. Figure 6.25 shows thinner tubes formed when nanotubes are grown with reduced flow rate of ~ 10 sccm.

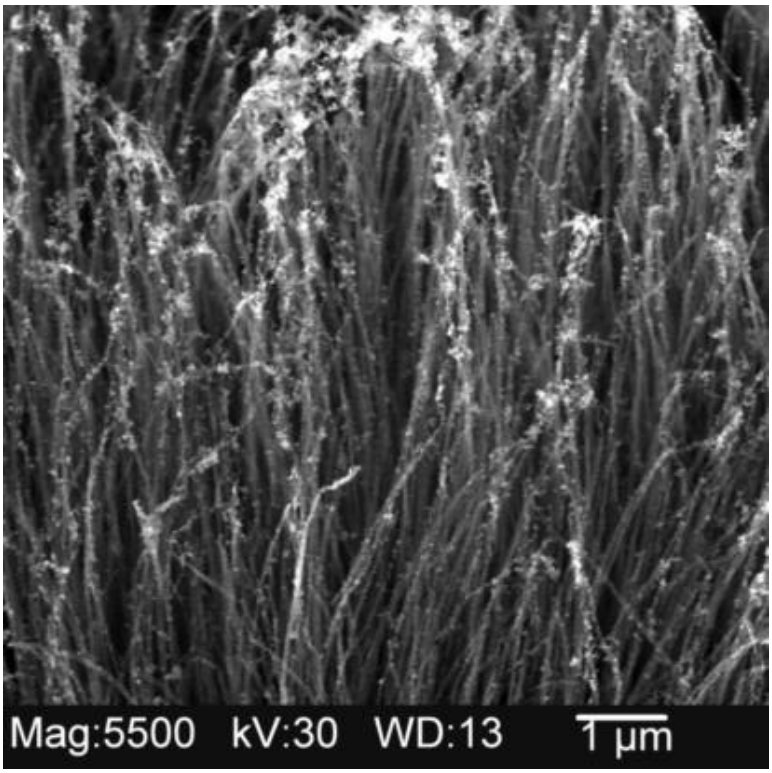

Figure 6.22 SEM micrograph showing amorphous particles on the surface of tubes

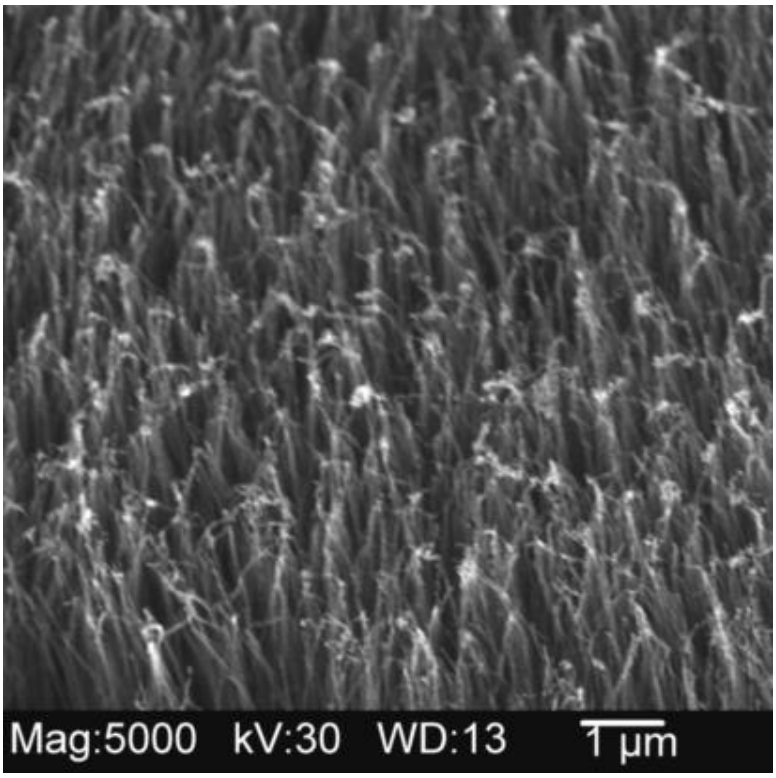

Figure 6.23 Tubes grown under H_2 showing no amorphous particles.

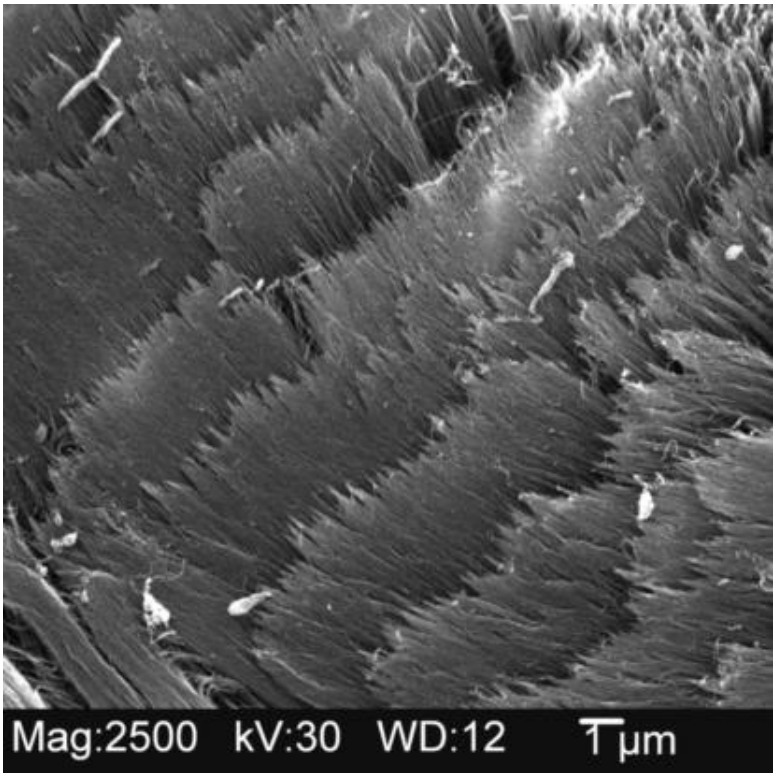

Figure 6.24 SEM micrograph showing carpet growth at 15 sccm methane

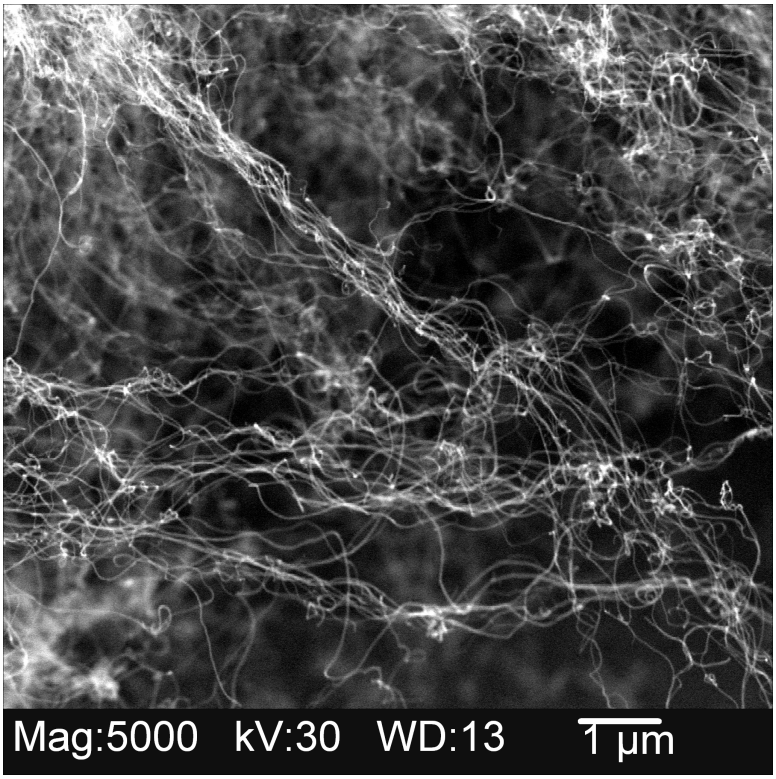

Figure 6.25 SEM micrograph of thin tube formation at 10 sccm methane flow

When the flow rate of methane gas was varied, higher methane flow rate resulted in a dense growth of carbon nanotubes. Very often the growth of nanotubes under 15 sccm of methane flow rate resulted in carpet-like growth of nanotubes as shown in Figure 6.24. Further, methane flow rates were varied from 5 sccm to 20 sccm, in steps of 5 sccm at a time, and the results indicate that the growth of tubes were observed only when the methane flow rates were maintained at 10 sccm and 15 sccm. Figure 6.25 is a SEM micrograph of nanotubes grown with a relatively less flow rate of methane around 8 – 10 sccm. It can be seen from the picture that the tubes are relatively thinner and the growth is less dense unlike the samples subjected to higher methane flow rates.

6.5 EFFECT OF PATTERNED CATALYST AND FLOW RATES OF GASES

To study the effect of patterned catalyst film towards growth of aligned nanotubes, experiments were conducted on silicon wafer substrates with patterned cobalt catalyst coating obtained by use of a template during PLD deposition. The parameters used in these experiments are listed in Table 6.4.

Since the aim of this investigation was to grow nanotubes which are aligned and patterned, several experiments were conducted by varying experimental conditions starting from varying the catalyst film thickness and varying one parameter at a time. Experimental conditions which would support the growth of aligned nanotubes were narrowed down from the experimentations conducted and reported in the earlier sections. Further, cues and modifications to the parameters were picked up from the concurrent investigation on the aligned growth of nanotubes on iron catalyst along with the current study by other members of the research team. These parameters can be obtained from their theses [109, 110].

It can be observed from Table 6.4, the catalyst thickness can be varied by varying the catalyst deposition time, and the growth time, the process gases and their flow rates were varied to support the growth of aligned and patterned tubes.

Table 6.4 Process parameters employed in the study of patterned growth

Sample No:	N-1	H-1	H-2	A-1	C-1	T-1
Catalyst deposition time, sec	30	30	30	30	45	45
Pretreatment time, min	5	5	5	5	5	5
Growth time, min	10	10	15	10	10	10
Process gases and flow rates	H_2 and N_2 @ 40 and 50 sccm	Nitrogen only @ 50 sccm	Nitrogen only @ 50 sccm	Nitrogen only @ 50 sccm	Nitrogen only @ 50 sccm	H_2 and N_2 @ 40 and 50 sccm
Methane flow rate, sccm	5	20	15	10	10	15
Microwave power, watts	500	500	500	500	500	500
Chamber pressure, torr	15	15	15	15	15	15
Result	No growth	Patterned growth	Patterned growth not defined	Patterned Growth but individual tubes curly	Patterned growth but individual tubes are short	Patterned growth and individual tubes aligned

Figure 6.26 is a picture of a wafer surface before the catalyst deposition and Figure 6.27 shows the wafer surface after catalyst deposition. Figure 6.28 is a SEM micrograph showing the result of experiment on sample N-1, where no deposition or growth of tubes was observed on the catalyst patterned region.

Catalyst thickness and the flow rate of methane gas were varied in the consecutive experiments, and black deposition was observed after the CVD growth. Figure 6.29 is the SEM micrograph of sample H-1 after CVD growth. It can be seen that nanotubes have been grown on hexagonally patterned regions. However, the patterned region is not very clearly defined. Figures 6.30 and 6.31 are higher magnification SEM micrographs of samples H-1 and H-2, respectively. It can be seen that the first sample (N-1) does not have any tube growth but the second sample (H-1) reveals tube growth.

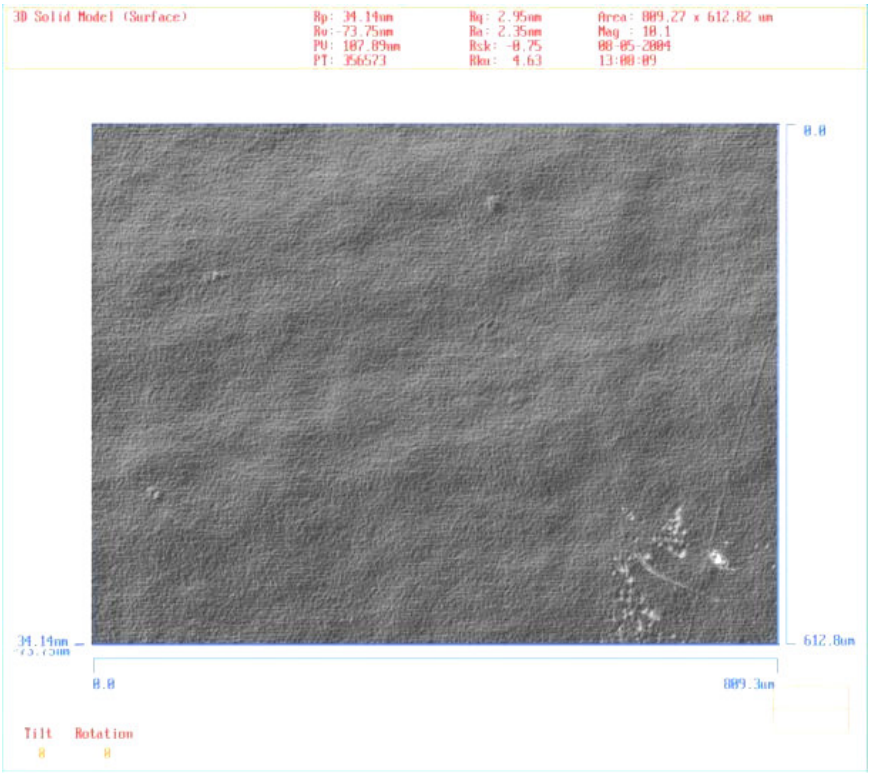

Figure 6.26 MicroXam picture of the silicon wafer surface before catalyst deposition

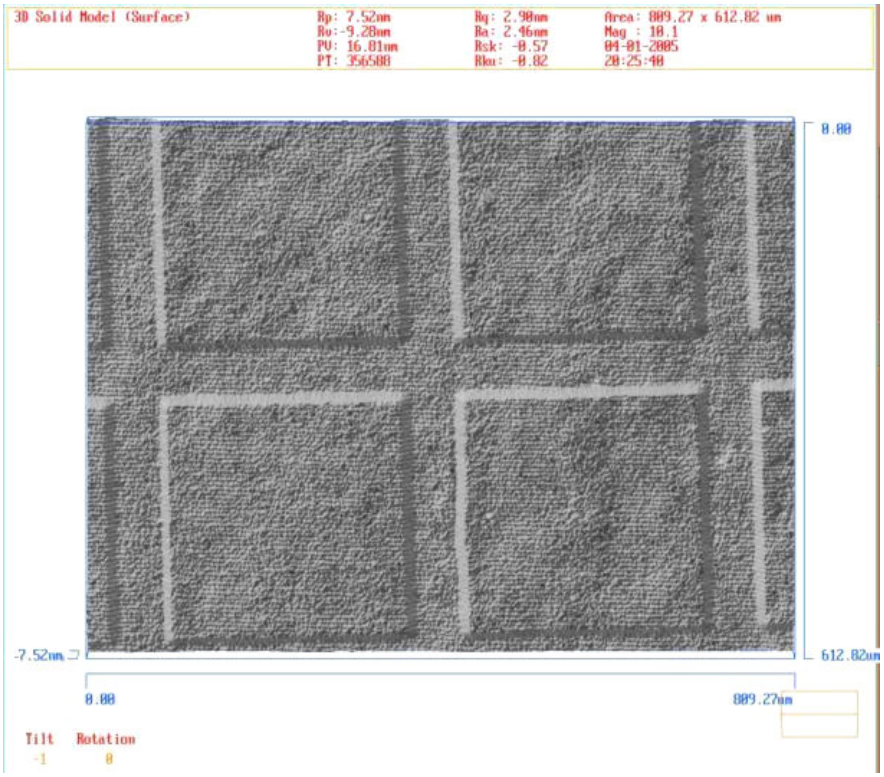

Figure 6.27 MicroXam picture of patterned catalyst layer deposition

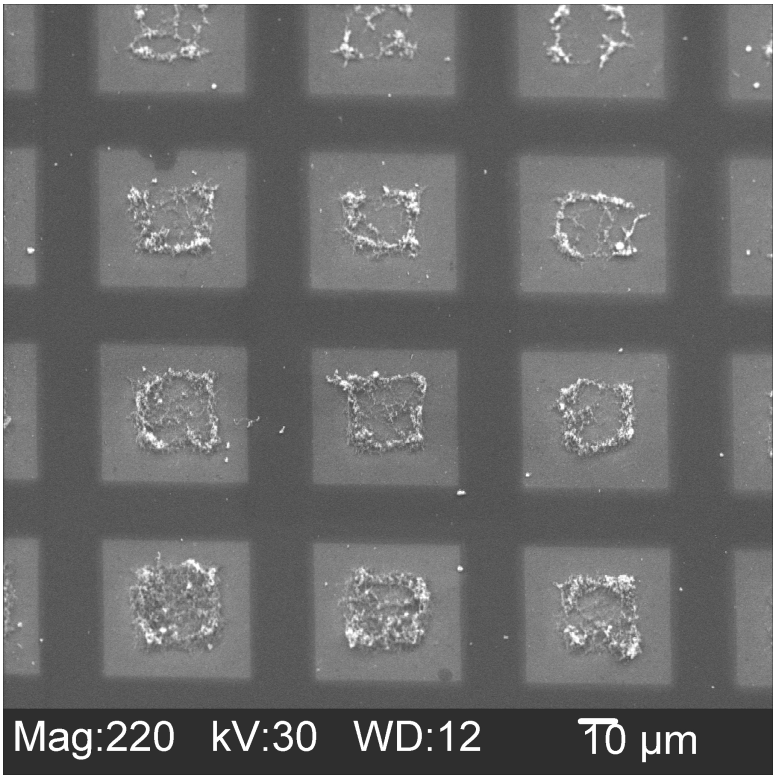

Figure 6.28 SEM micrograph showing no growth (5 sccm of methane)

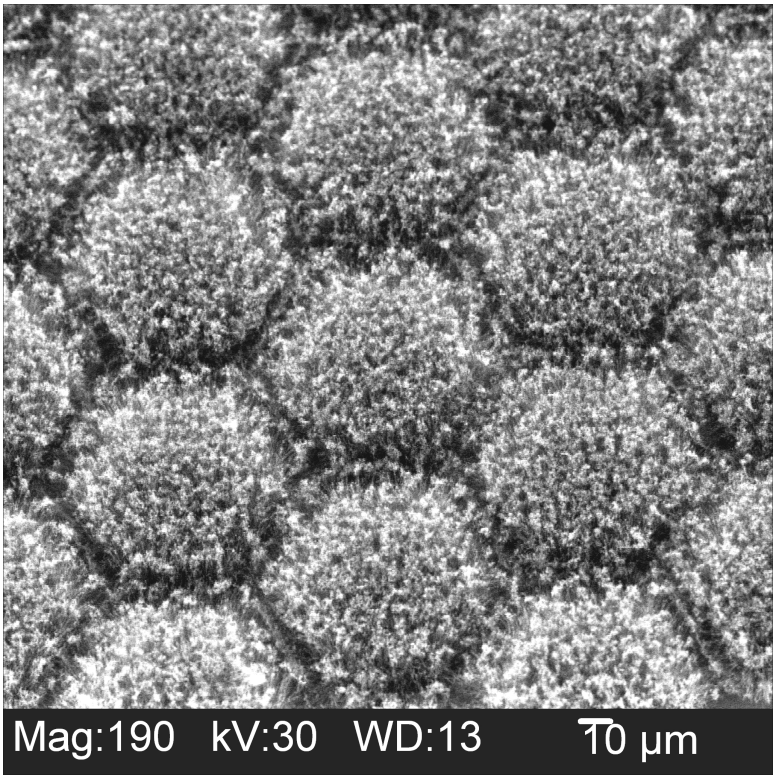

Figure 6.29 SEM micrograph showing thick growth (20 sccm of methane)

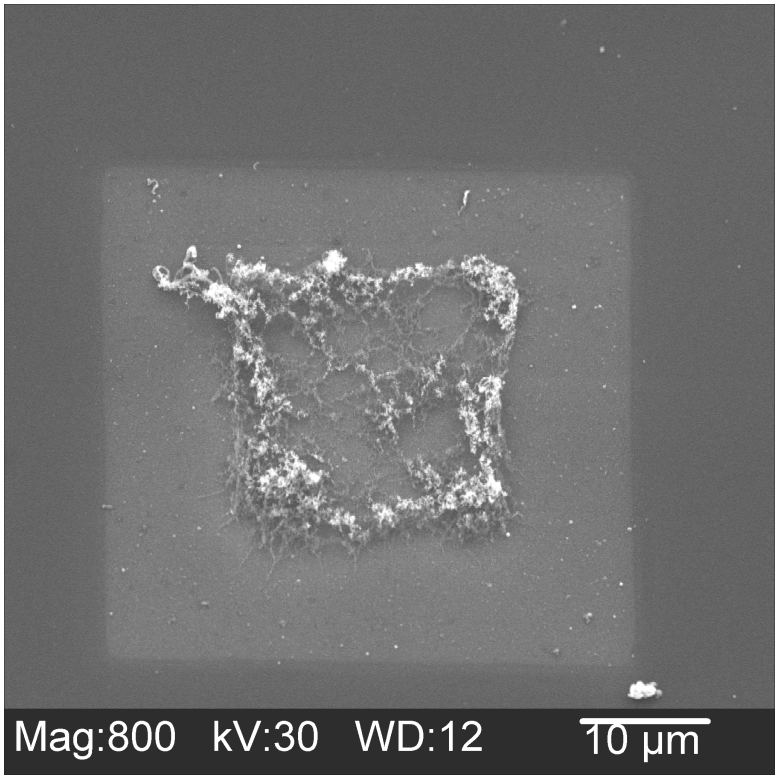

Figure 6.30 SEM micrograph showing no tube growth, sample N-1

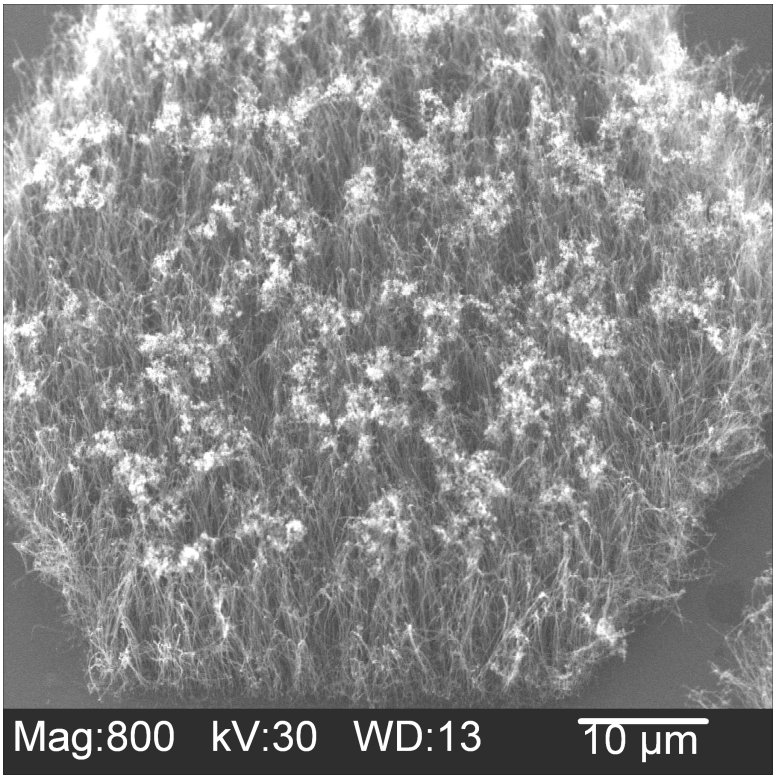

Figure 6.31 SEM micrograph of nanotubes (10 sccm of methane flow rate)

Once growth of carbon nanotubes on the patterned region was observed, experimental conditions were varied as shown in the Table 6.4 in an effort towards the growth of aligned tubes. Since the growth of nanotubes in sample H-1 was very dense, and in order to obtain growth as a clearly defined pattern, the methane flow rate was reduced to 10 SCCM in the next experiment on sample H-2. Figure 6.32 is a SEM micrograph of the well defined growth seen on a hexagonally patterned catalyst film.

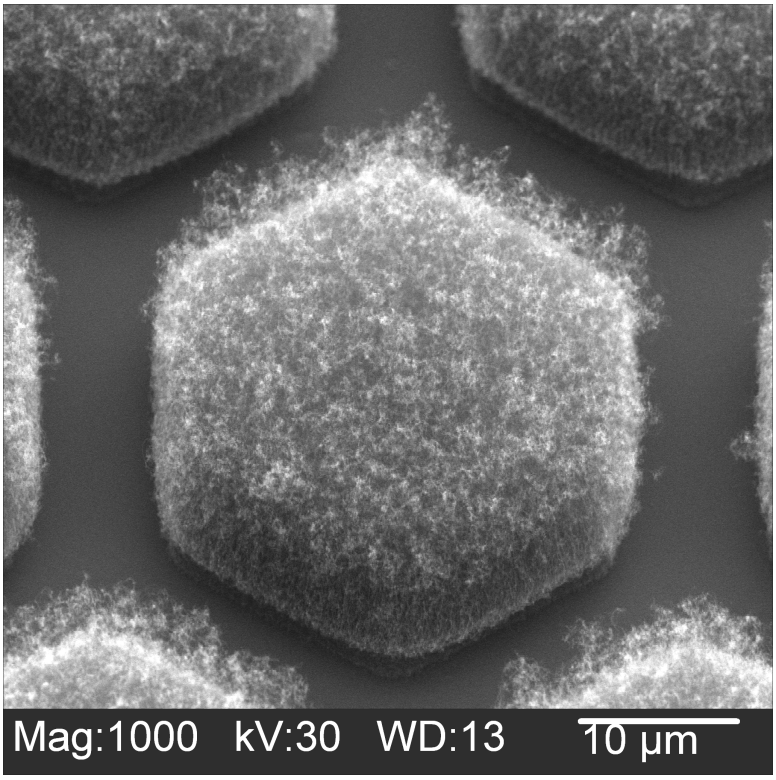

Figure 6.32 SEM micrograph revealing clearly defined growth on patterned region

Additionally, Figures 6.33 and 6.34 highlight the difference in the growth influenced by the effect of methane flow rate. Figure 6.33 is a SEM micrograph of sample H-1 where a higher flow rate of methane was used, and Figure 6.34 is a SEM micrograph of sample H-2 with less methane flow rate.

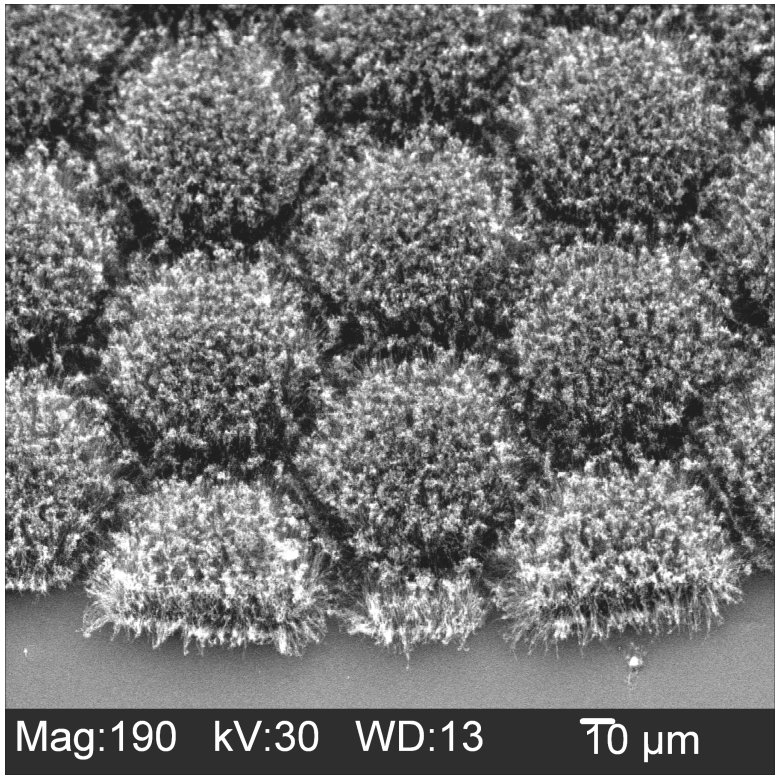

Figure 6.33 SEM micrograph of H-1 sample

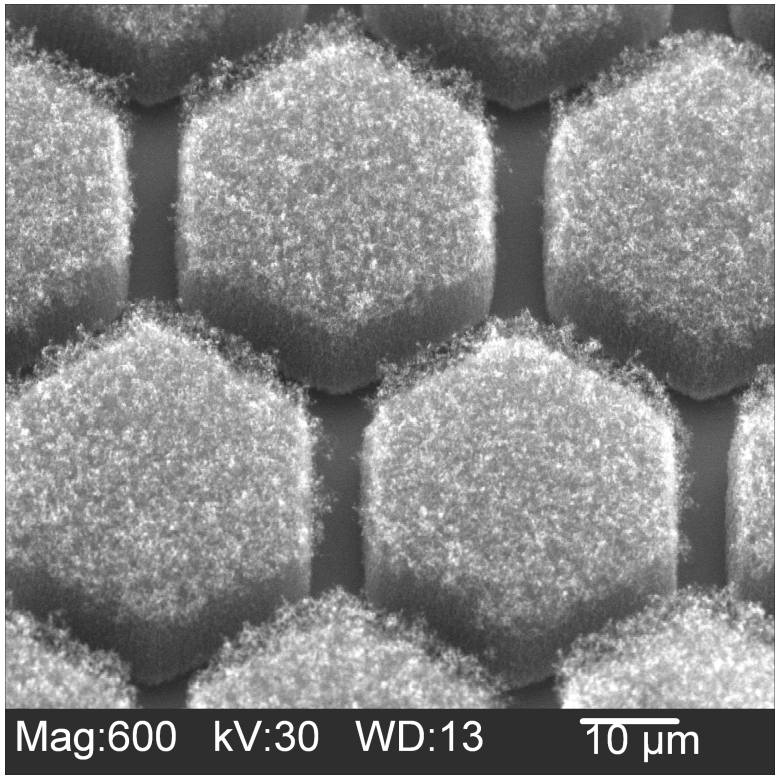

Figure 6.34 SEM micrograph of H-2 sample

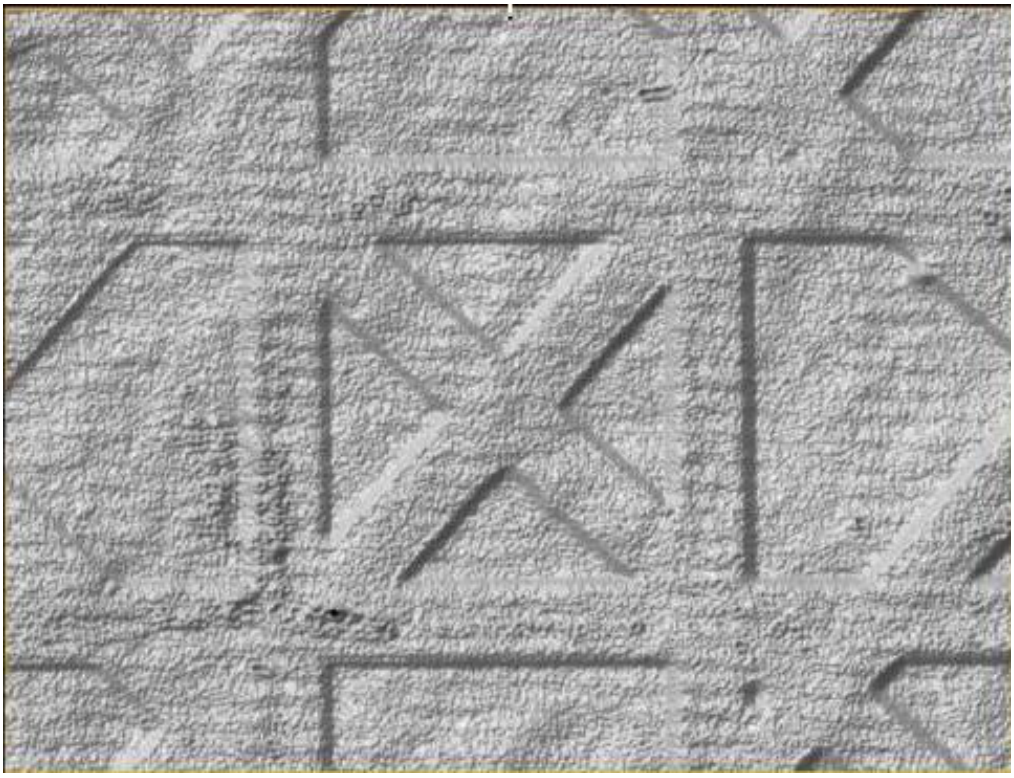

Figure 6.35 MicroXam picture revealing the catalyst pattern

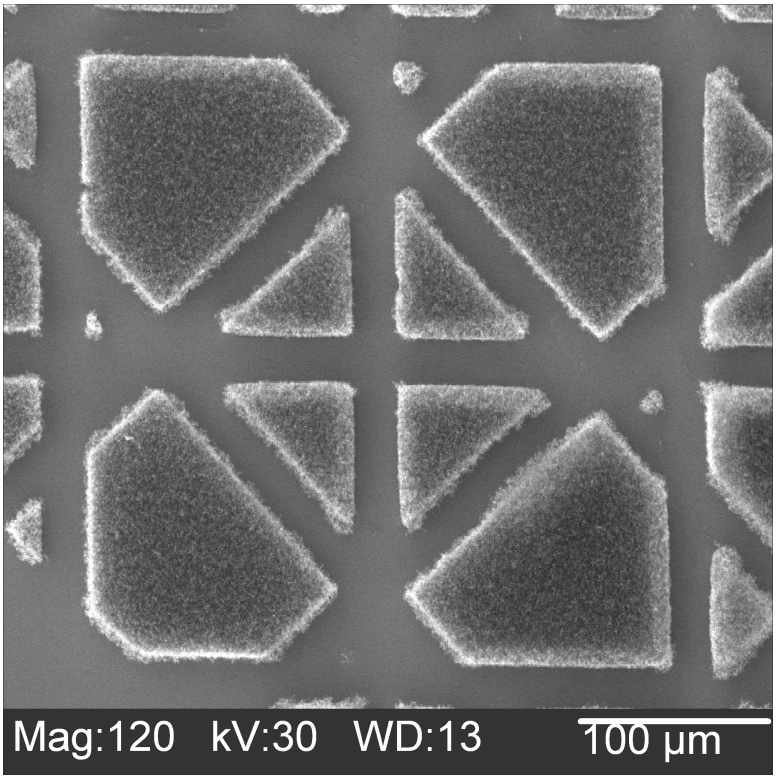

Figure 6.36 SEM micrograph of growth on the patterned region

It can be seen that flow rate of methane is plays a crucial role in obtaining patterned growth of tubes on the catalyst layer. Once the role of flow rate of methane is determined, templates with different geometrical patterns can be used for patterning the catalyst film. Figure 6.35 is a MicroXam picture showing the patterned catalyst film, and Figure 6.36 is a SEM micrograph after CVD growth on that particular region. Figures 6.37 is a SEM micrograph of sample with a methane flow rate of 10 sccm with 15 min growth time, and Figure 6.38 is a SEM micrograph of sample subjected to 15 sccm of methane and 10 minutes growth time. It can be seen that a longer growth time of 15 minutes was not a favorable condition. It can also be seen that shorter growth time with higher methane was also not a favorable condition.

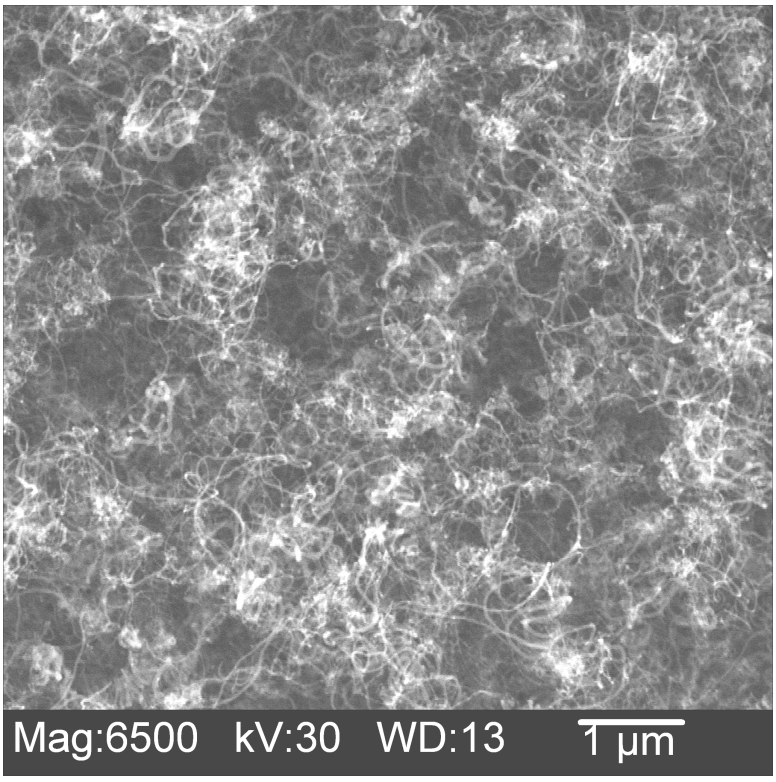

Figure 6.37 Coiled tubes grown due to higher methane flow rate

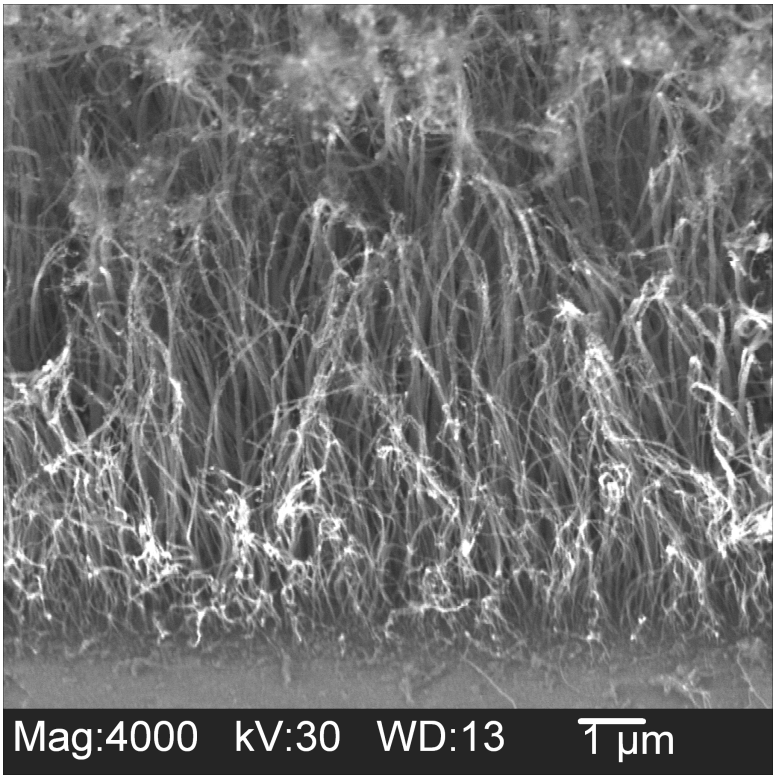

Figure 6.38 Shorter tubes due to reduced growth time with higher flow of methane

6.6 GROWTH OF ALIGNED TUBES IN PATTERNED REGION

Based on the results from samples N-1, H-1, H-2, A-1, and C-1, nanotubes growth was carried out on sample T-1 with the catalyst deposited for 45 seconds using PLD. In this case (see table 6.4), nanotubes were allowed to grow for 10 minutes after a 5 min pretreatment period. The methane flow rate was controlled at ~ 15 sccm and hydrogen and nitrogen were used as the other process gases at flow rates of 40 and 50 sccm respectively. These parameters were narrowed down after careful analysis of the earlier results involving growth of nanotubes on patterned region as well as on the non-patterned catalyst film. It can be seen from Figure 6.39 that aligned nanotubes are grown and the nanotubes are found to have a height of ~ 15 to 20 µm.

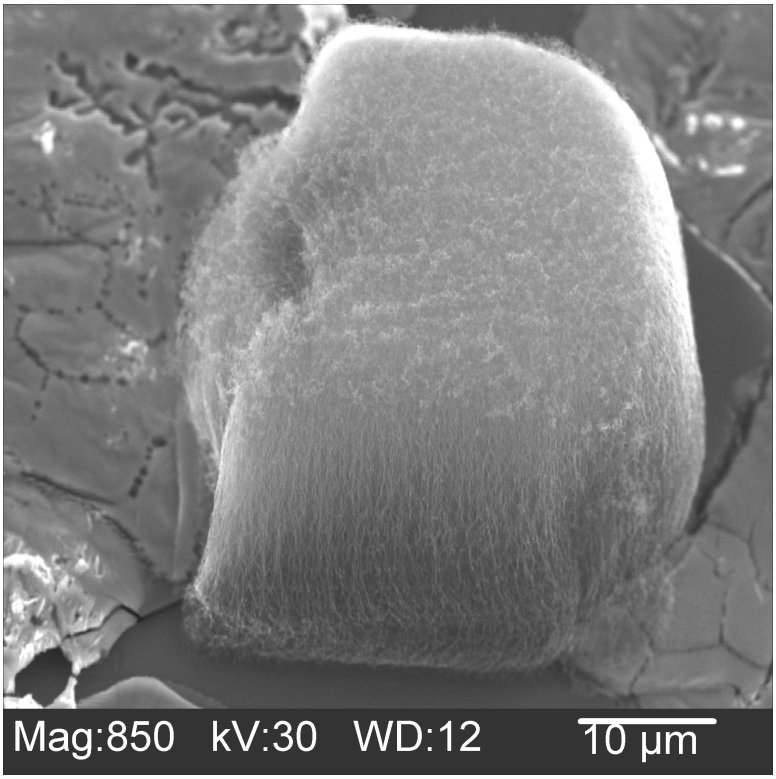

Figure 6.39 Growth of aligned nanotubes.

It is evident from Figure 6.39, that growth of aligned tubes was finally achieved successfully. It can be seen, that tubes are not coiled or curly and they do not form clusters or localized bundles or intertwined tubes. In Figure 6.39, aligned growth of tubes are shown where the template was left on the sample during growth. However, on the very same sample where the template was removed, we see formation of highly aligned patterned growth of nanotubes. This can be seen in Figures 6.40 and 6.41. These are the final results of this investigation, and the SEM micrographs clearly show the culmination of efforts towards the formation of faithfully aligned nanotubes within a patterned region. Figure 6.41 is a micrograph which clearly details the growth of the nanotubes on the patterned catalyst. Even at this magnification it is evident that the individual blocks of growth have perfectly well defined boundaries.

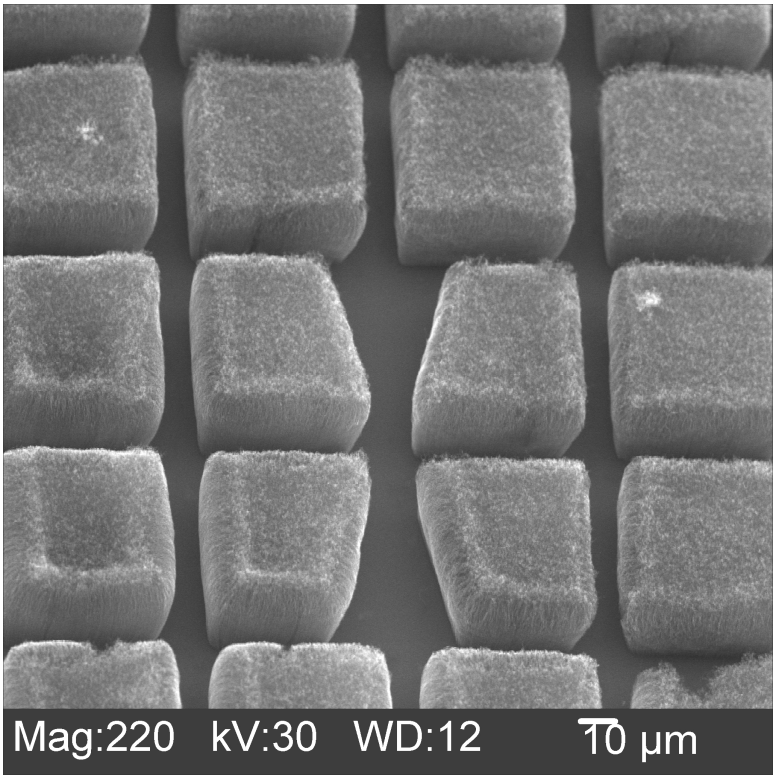

Figure 6.40 patterned carbon nanotubes grown in a regular array

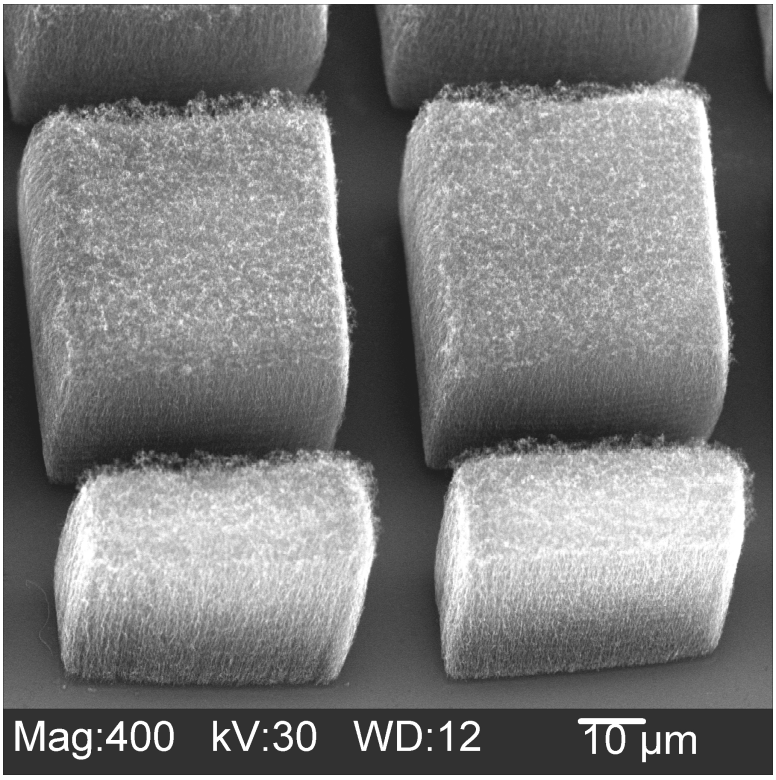

Figure 6.41 SEM micrograph showing faithful aligned, patterned growth of CNT

6.7 TEM CHARACTERIZATION

TEM characterization was performed to study the internal and external morphology of nanotubes. Sample preparation for TEM analysis involved scrapping of nanotubes from the silicon wafer substrate and dispersing the nanotubes in methanol. Ultrasonication of nanotubes dispersed in methanol solution was carried out for 10 ~ 15 minutes before they were transferred on to a TEM grid for analysis. Figure 6.42 is a TEM micrograph showing nanotubes of different diameters. Figure 6.43 is a TEM micrograph showing that nanotubes are closed at one end. Figure 6.45 is a TEM micrograph showing a catalytic particle within the nanotube. The TEM micrographs facilitate in locating the catalyst particles and knowing the location of the catalyst particle in the nanotube and can shed light on the growth mechanism involved in nanotube synthesis.

Figure 6.42 TEM micrograph showing multiwall nanotubes of different diameters

Figure 6.43 TEM micrograph showing a nanotube closed at one end.

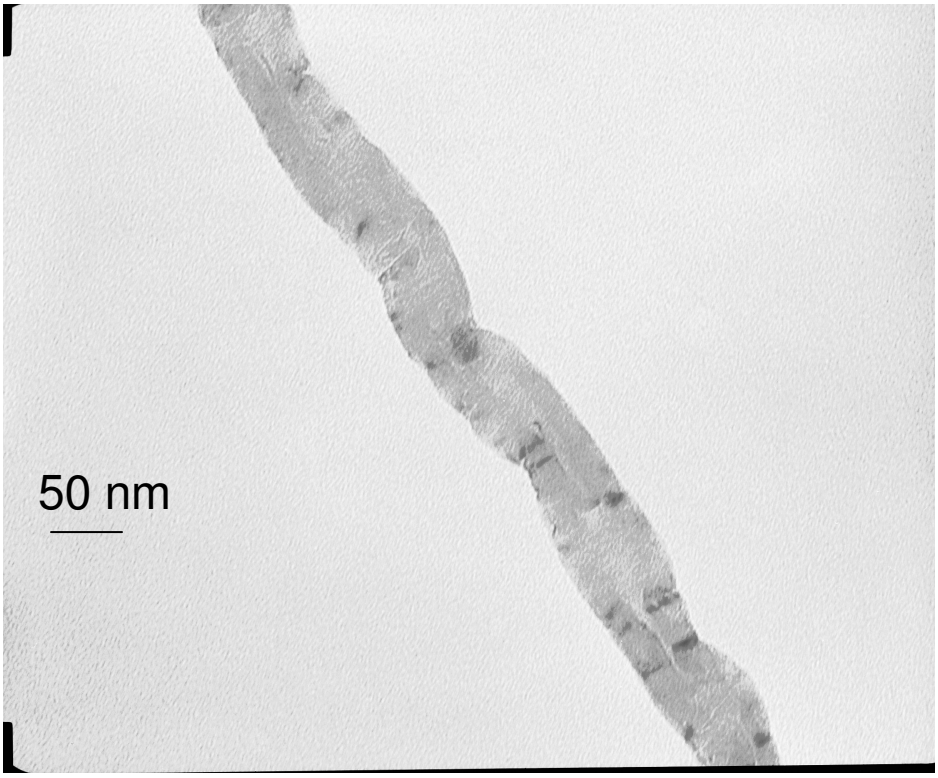

Figure 6.44 TEM micrograph of a single multiwall nanotube

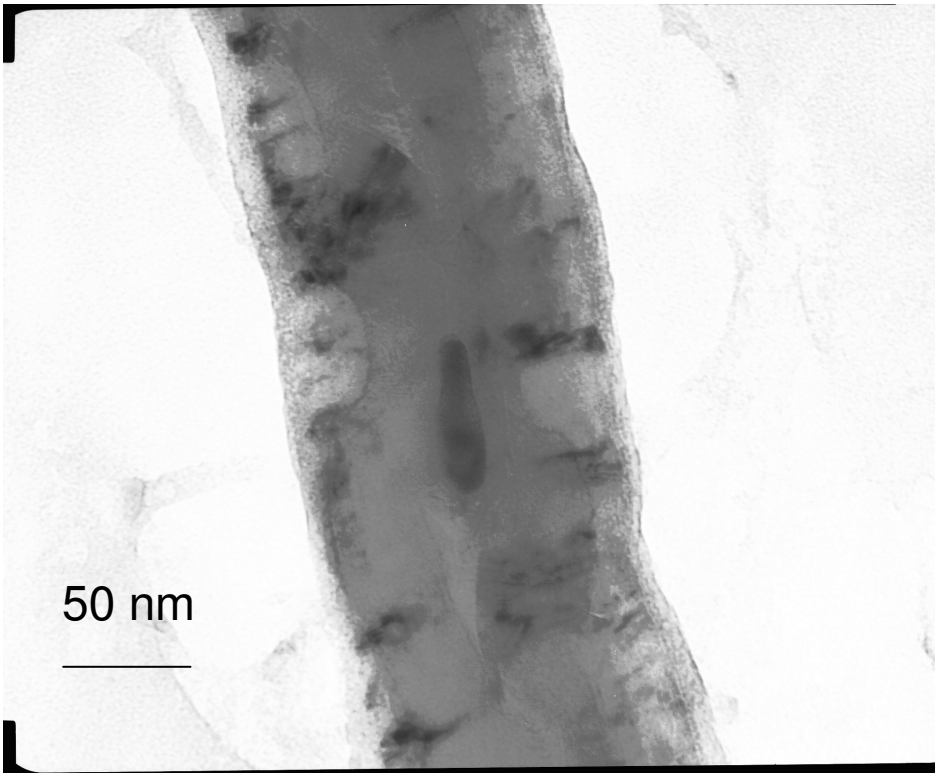

Figure 6.45 TEM micrograph showing catalyst particle inside a nanotube.

6.8 RAMAN SPECTROSCOPY CHARACTERIZATION

Figure 6.46 shows the Raman spectra of silicon wafer substrate showing the D peak ~ 1350 and the G peak ~ 1380. Additionally the second overtone of the D peak is also identified at 2700, which is also a characteristic of the nanotubes as shown in Figure 6.47

6.9 ATOMIC FORCE MICROSCOPY- CHARACTERIZATION

The sample preparation for AFM characterization of nanotubes is similar to the procedure followed for characterization of nanotubes under TEM. Nanotubes are scrapped from the silicon wafer substrate and dispersed in methanol and ultrasonicated

for 10 ~ 15 minutes. After ultrasonication, a few drops of nanotubes dispersed methanol is dropped on to a microscope cover glass. The microscope cover glass was examined in an AFM. Figure 6.48 is an AFM micrograph showing numerous nanotubes spread on the microscope cover glass surface. Figure 6.49 is an AFM micrograph showing a single nanotube and the diameter of the nanotube can be visually estimated to be ~ 100 to 125 nm.

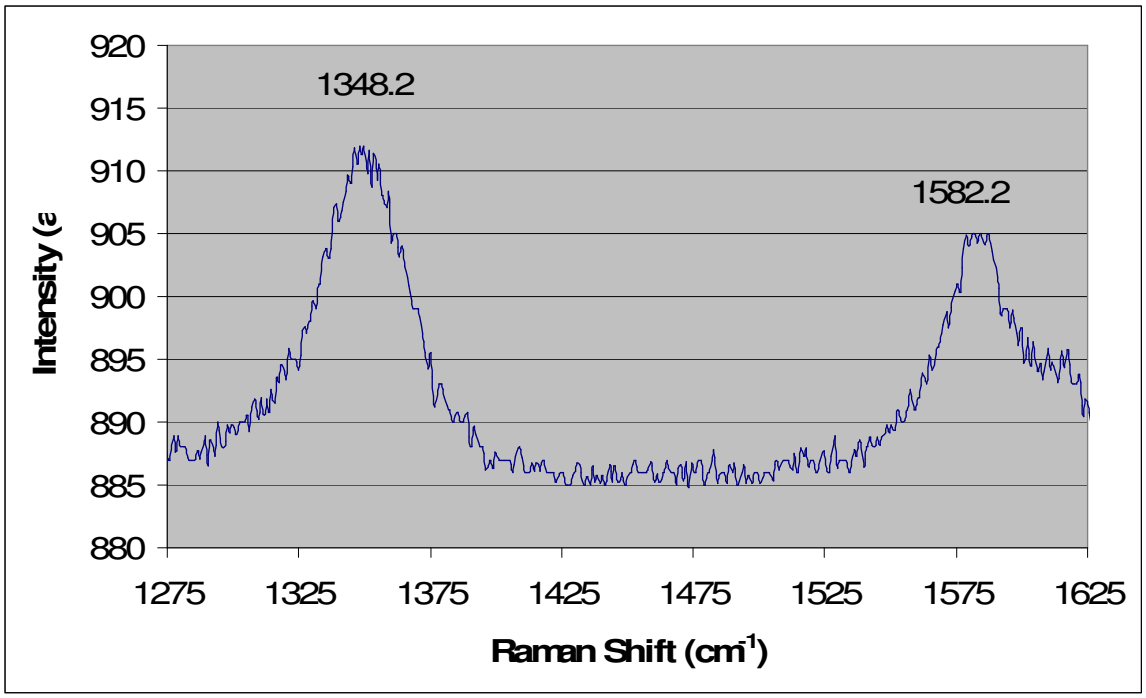

Figure 6.46 Raman spectra showing 'D' and 'G' peaks, at 1350 and 1580, respectively

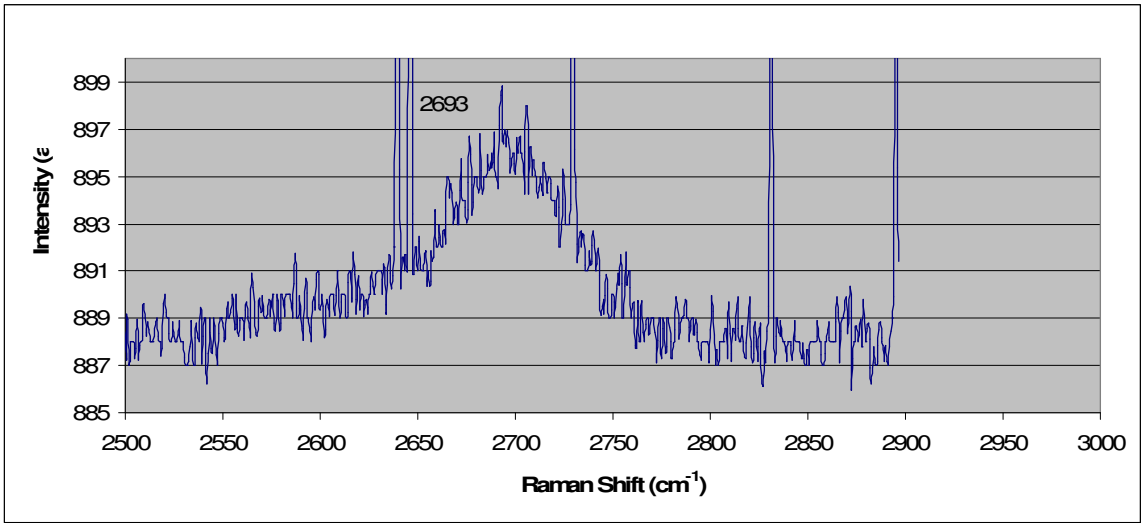

Figure 6.47 Raman Spectra showing second overtone of 'D' peak at 2700 wave number.

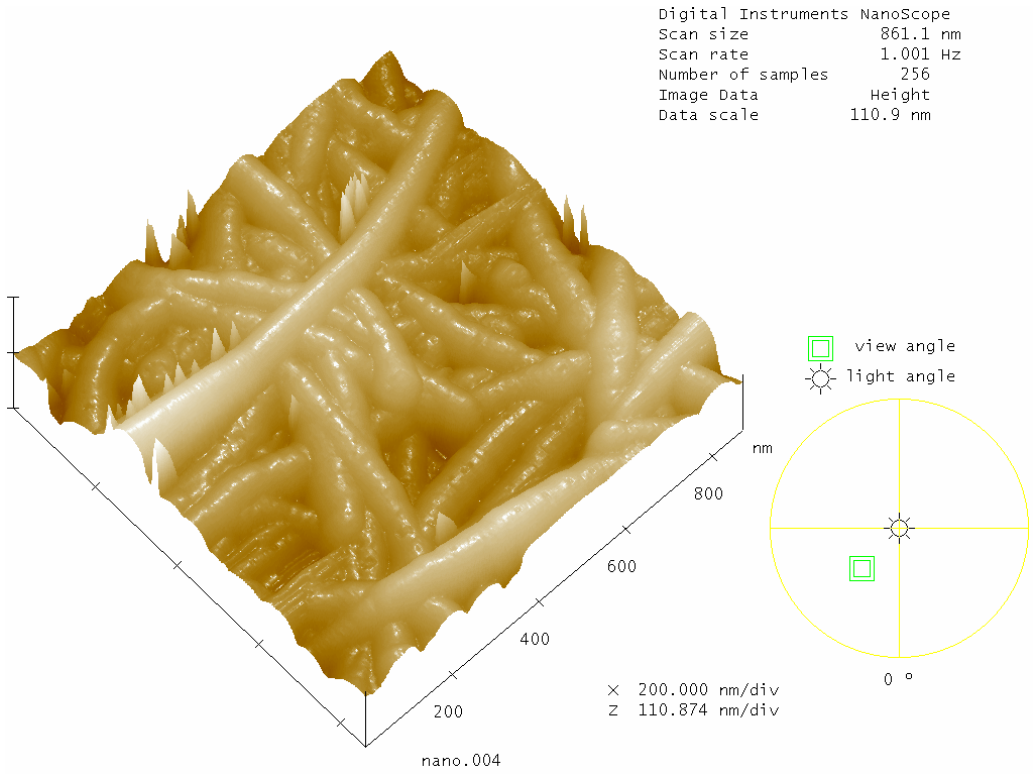

6.48 AFM micrograph of numerous nanotubes.

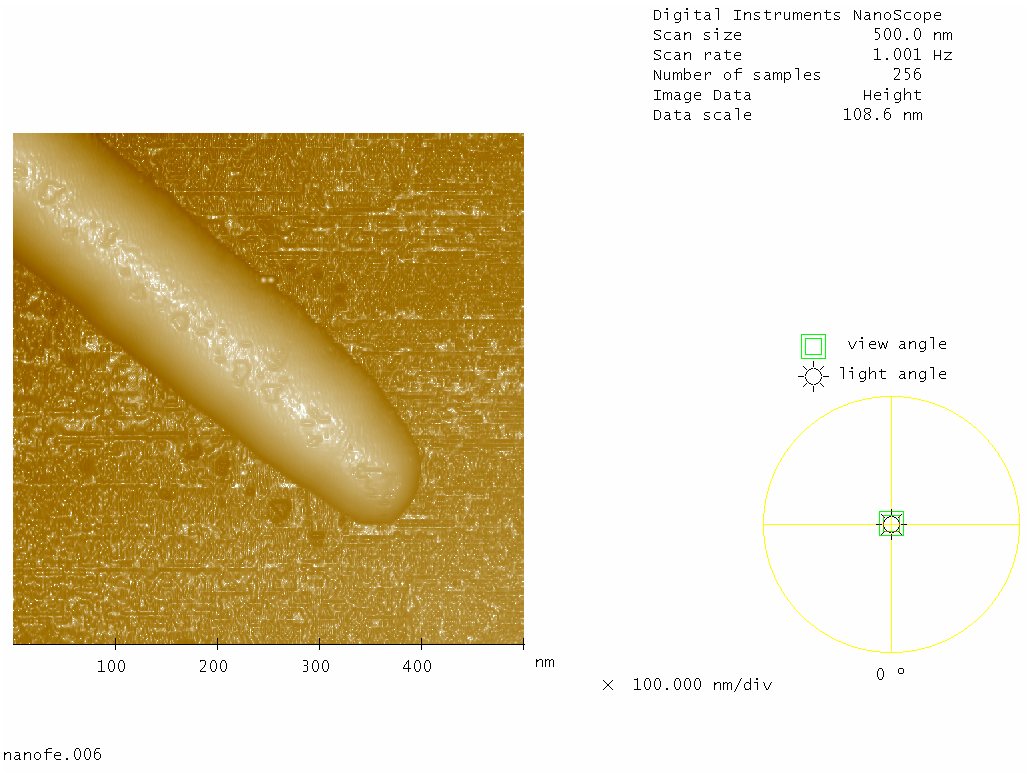

Figure 6.49 AFM micrograph of a single nanotube.

CHAPTER 7

DISCUSSIONS

7.1 EFFECT OF GROWTH TIME

It can be seen from Figures 6.2 to 6.6 that growth time has a major influence on the growth of nanotubes. At shorter growth time of ~ 30 seconds, no growth occurs because this is really shorter time for nanotubes to nucleate and grow. On the other hand, 15 minutes growth time resulted in the formation of unusually thicker nanotubes with large diameters as shown in Figure 6.6. The formation of thicker tubes after 15 minutes growth time suggest a growth time of 5 ~ 10 minutes to be the optimum condition. Growth of thicker tubes is explained by the fact that nanotubes continue to grow laterally after a certain amount of time as originally proposed by Iijima [65].

As long as the growing nanotube ends are open, carbon deposition along the open ends results in the growth of tubes. But after a certain amount of time, the nanotube ends are closed which renders the growing end of the nanotube inactive to incoming carbon species. Once the growth of the nanotube stops, growth takes place laterally around the walls of the existing nanotubes as suggested by Iijima [65]. Thus, a growth time of 5 ~ 10 minutes is found to be optimum for growth of tubes of fairly uniform diameter.

7.2 EFFECT OF PLASMA PRETREATMENT TIME

Plasma pretreatment time is one of the important parameters that controls the nucleation and growth density of nanotubes. Since a continuous film of catalyst deposited by PLD needs to be broken down to form individual catalyst particles, the catalyst deposited silicon wafer sample is subjected to plasma pretreatment prior to CVD synthesis of nanotubes.

It can be seen from Figures 6.7 to 6.12 that growth density of nanotubes vary significantly as the plasma treatment time is varied from 0 to 15 minutes respectively; For longer plasma treatment times, the growth density is observed to be less than that for samples subjected to shorter plasma treatment time. This is probably due to the fact that longer plasma treatment results in re-melting of individual catalyst particles and agglomeration of these melted catalytic particles, which results in the formation of larger sized particles. This step of agglomeration clearly reduces the particle density, eventually reducing the growth density of nanotubes. This could be the reason why the sample subjected to 15 minutes pretreatment time is less dense compared to samples subjected to shorter plasma treatment times.

Additionally, the formation of continuous sheet of nanotubes as shown in Figures 6.13 and 6.15 can also be explained as a result of no plasma treatment condition in that particular sample. Since the sample is not subjected to plasma treatment, the catalyst film may not have been broken into individual particles. Due to the absence of clearly defined catalyst particles, deposition of carbon species results in growth of nanotubes which do not have clearly defined structures. This is further confirmed by Figure 6.7 corresponding to the sample with no plasma treatment.

7.3 EFFECT OF PROCESS GASES

Nanotubes grow when nitrogen and methane are used as process gases, but nanotubes growth fails when hydrogen and methane are used as process gases. This can be explained by the fact that nitrogen plasma is reported to have higher bombardment energy than hydrogen plasma. Owing to higher bombardment energy, nitrogen plasma is also reported to keep the catalyst surface active for a longer time favoring the growth of nanotubes.

It can be seen from Figure 6.22 that nanotubes grown in the presence of nitrogen and methane gases result in the formation of nanotubes along with considerable number of impurities, such as amorphous particles (see Figure 6.22). However, nanotubes grown in the presence of hydrogen, nitrogen and methane showed no signs of amorphous particles clinging to the tubes (see Figure 6.23). The absence of amorphous particles in the second sample can be explained by the fact that the presence of atomic hydrogen is reported to be responsible for etching away all non-nanotube phases deposited as suggested by Kuttel *et al.* [80]. Also, the presence of atomic hydrogen is reported to be responsible for a delicate balance of deposition and etching away of nanotubes in the synthesis of nanotubes.

Further, it can be seen from Figures 6.19 and 6.20 that nanotubes grown under nitrogen and methane plasma are found to be straighter, whereas nanotubes grown in the presence of hydrogen resulted in growth of nanotubes curly and wavy. Since straight tubes are formed in the presence of nitrogen, nitrogen is found to be an essential parameter towards the growth of vertically aligned tubes. Since hydrogen has tendency to

etch away amorphous impurities, a mixture of nitrogen and hydrogen is always used as a process gas along with methane in the growth of nanotubes.

7.4 EFFECT OF METHANE FLOW RATE

In the present investigation, patterned growth of nanotubes were obtained when methane flow rate was maintained ~ 10 to 15 sccm. However, when samples with patterned catalyst region were subjected to varying flow rates of methane, the growth morphology was found to vary drastically depending on the flow rate of methane. It can be seen from Figures 6.28 and 6.30, that no nanotubes growth occurs when the methane flow rate is reduced to 5 sccm. When the methane flow rate was increased to 20 sccm in sample H-1, there was no definitive growth on patterned region. (see Figure 6.29). It can be seen from Figures 6.38 that a methane flow rate of 10 sccm resulted in poor growth of nanotubes on the patterned region. However, samples subjected to 15 sccm of methane flow rate resulted in patterned growth of nanotubes. This can be seen by comparing Figures 6.33 and 6.34, corresponding to samples subjected to 20 and 15 sccm respectively.

7.5 GROWTH OF ALIGNED CARBON NANOTUBES ON CATALYST PATTERNED SAMPLES

Finally growth of aligned carbon nanotubes on patterned region is obtained as shown in Figures 6.40 and 6.41. Figure 6.39 shows vertically aligned carbon nanotubes with a patterned growth. The process conditions used for the growth of vertically aligned tubes are listed in Table 7.1.

Table 7.1 Process parameters used for the aligned growth of nanotubes

Growth condition	Plasma treatment parameters	CVD growth parameters
Time period, min	5	10
Process gases	H_2 and N_2	H_2 ,N_2 and CH_4
Flow rates of gases, sccm	40 and 50	40, 50 and 15
Chamber pressure, torr	15	15
Microwave power, watts	500	500
Temperature, ^{c}C	785	885

CHAPTER 8

CONCLUSIONS AND FUTURE WORK

8.1 CONCLUSIONS

1. In this experimental study, growth of carbon nanotubes (CNT) is obtained on a cobalt catalyst deposited on a silicon wafer surface using plasma enhanced microwave assisted CVD technique.
2. When carbon nanotubes are grown for different growth times, the nanotubes exhibit significant difference in growth morphology depending on the growth time. Unusually thicker tubes are formed for 15 minutes growth time. Growth time of 10 minutes is found to be an optimum for growth of nanotubes with relatively uniform diameter.
3. When cobalt catalyst deposited silicon wafer samples were subjected to plasma treatment prior to the growth step, samples subjected to 5 ~ 15 minutes plasma treatment showed clearly defined growth of nanotubes compared to samples which were not pretreated prior to their growth.
4. Growth density of nanotubes is found to be less when samples are plasma pretreated for longer times before the growth.
5. When nitrogen and methane were used as process gases, significant growth of carbon nanotubes was observed. However, there was no growth of nanotubes when

hydrogen and methane was used as process gases. So, nitrogen is always needed and is included as one of the important process gases.

6. When nitrogen and methane were the only process gases used, it resulted in the growth of nanotubes with considerable non-nanotubes impurities, such as amorphous carbonaceous particles sticking to the ends of the nanotubes. But no amorphous particles are observed when hydrogen gas was included in the process gases along with nitrogen and methane.
7. Nanotubes are found to grow straighter when nitrogen and methane are used as the process gases. Wavy or curly nanotubes are grown when hydrogen gas is mixed as one of the process gases along with nitrogen and methane.
8. Higher flow rates of methane ~ 20 sccm resulted in passivation of the catalyst surface thereby resulting in no growth of nanotubes. A low flow rate of methane (~ 5 sccm) was found to result in no growth. Typically, carbon nanotubes are grown with methane flow rates varying from 10 ~ 15 sccm. However, the exact flow rate of methane gas needs to be varied and adjusted depending on the catalyst film thickness.
9. When the cobalt catalyst film is patterned on the silicon wafer surface, patterned growth of carbon nanotubes is successfully obtained.
10. In this investigation, vertically aligned growth of nanotubes on patterned catalyst region is finally obtained.
11. TEM characterization of nanotubes show that nanotubes have closed ends and catalyst particles are observed on upper sections of the tubes suggesting that the nanotubes do not follow a base growth mechanism but a tip growth mechanism.

12. μRaman characterization shows CNTs exhibit the characteristic D and G peaks at 1350 and 1580 wave numbers suggesting that nanotubes grown are multiwalled.
13. AFM characterization and TEM characterization enables estimation of the tube diameters. Tube diameters were found to be in the range of 50 ~ 100 nm.

8.2 FUTURE WORK

Major effort in this investigation has been towards the growth of vertically aligned carbon nanotubes on patterned catalyst surfaces. Experimental conditions were varied to study their effect on the growth of nanotubes. The results of these experiments were quickly analyzed to identify conditions favorable for the growth of vertically aligned nanotubes. With this done, future work recommended includes the following:

1) Efforts towards synthesis of SWNTs can be studied using the existing experimental setup. Since growth of SWNTs is favored by the presence of bimetal catalyst such as, iron and cobalt, or cobalt and nickel, multiple layers of catalyst thin film can be formed and studied towards SWNTs growth.
2) Aligned nanotubes can be studied for application such as reinforcement of composites.
3) To exploit the high thermal conductivity of nanotubes, patterned blocks of nanotubes can be studied for applications such as heat sinks for molecular devices.
4) Patterned growth of nanotubes can be investigated on different substrate surfaces, such as glass, and plastics.

REFERENCES

[1] Iijima, S., "Helical microtubules of carbon," Nature **354** (1991) 56 – 58.

[2] Kroto, H.W., Heath, J.R., O'Brien, S.C., Curl, R.F., and R.E. Smalley, "C60: Buckminsterfullerene," Nature **318** (1985) 162-163.

[3] Treacy, M.M., Ebbesen, T.W., and J.M. Gibson, "Exceptionally high young's modulus observed for individual carbon nanotubes," Nature **381** (1996) 680 – 687.

[4] Wong, E.W., Sheehan, P.E., and C.M. Lieber, "Nanobeam mechanics: elasticity, strength, and toughness of nanorods and nanotubes," Science **277** (1997) 1971- 1975.

[5] Hone, J., Whitney, M., and A. Zettle, "Thermal conductivity of single walled carbon nanotubes," Synthetic Metals **103** (1999) 2498 – 2499.

[6] Che, J., Cagin, T., and W. A. Goddard III, "Thermal conductivity of carbon nanotubes," Nanotechnology **11** (2000) 65-69.

[7] Berber, S., Kwon, Y.K., and D. Tomanek, "Unusually high thermal conductivity of carbon nanotubes," Physics Review Letters **84** (2000) 4613 – 4616.

[8] Frank, S., Poncharal, P., Wang, Z.L., and W.A. De Heer, "Carbon nanotube quantum resistors," Science **280** (1998) 1744- 1746.

[9] P.Cavert, "A recipe for strength," Nature **399** (1999) 210 – 211.

[10] Saito, Y., Hamaguchi, K., Hata, K., Uchida, K., Tasaka, Y., Ikazaki, F., Yumura, M., Kasuya, A., and Y. Nishina, "Conical beams from open nanotubes," Nature **389** (1997) 554 – 555.

[11] Baughman, R.H., Zakhidov, A.A., and W.A. De Heer, "Carbon nanotubes- the route towards applications," Science **297** (2002) 787 – 792.

[12] Collins, P.G, and Ph. Avouris, "Nanotubes for electronics," Scientific American **12** (2000) 62 – 69.

[13] Hoenlein, W., Kreupl, F., Duesberg, G.S., Graham, A.P., Liebau, M., Seidel, R., and E. Unger, "Carbon nanotubes for microelectronics: status and future prospects," Materials Science and Engineering C **23** (2003) 663 – 669.

[14] Ajayan, P.M., and O. Z. Zhou, "Application of carbon nanotubes," in Carbon nanotubes Synthesis, structure, properties, and Application (edited by M.S. Dresselhaus, G. Dresselhaus, and Ph. Avouris (Eds.) Vol **80** (2001) Springer- Verlag P 391.

[15] Dresselhaus, M.S., "Nanotube antennas," Nature **432** (2004) 959 -960.

[16] Regan, B.C., Aloni, S., Ritchie, R.O., Dahmen, U., and A. Zetti, "Carbon nanotubes as nanoscale mass conveyors," Nature **428** (2004) 924 – 927.

[17] Srivastava, A., Srivastava, O.N., Talapatra, S., Vajtai, R., and P.M. Ajayan, "Carbon nanotube filters," Nature Materials **3** (2004) 610 – 614.

[18] Sazonova, V., Yaish, Y., Ustunel, H., Roundy, D., Arias, T.A., and P.L.McEuen, "A tunable carbon nanotube electromechanical oscillator," Nature **431** (2004) 284 – 287.

[19] Graham, A.P., Duesberg, G.S., Hoenline, W., Kruepl, F., Liebau, M., et al. "How do carbon nanotubes fit into the semiconductor roadmap?," Applied Physics A **80** (2005) 1141 – 1151.

[20] Thostenson, E.T., Ren, Z., and T.W. Chou, "Advances in the science and technology of carbon nanotubes and their composites: a review," Composites Science and Technology **61** (2001) 1899 – 1912.

[21] Hamada, N., Sawada, S, and A. Oshiyama, "New one-dimensional conductors: Graphitic microtubules," Physical Review Letters **68** (1992) 1579 – 1589.

[22] Dresselhaus M.S., Dresselhaus, G., and Ph. Avouris, (Eds.) " Carbon nanotubes" Springer- Berlin (2001).

[23] Guo, T., Nikolev, P., Thess, A., Colbert, D.T., and R.E. Smalley, "Catalytic growth of single-walled nanotubes by laser vaporization," Chemical Physics Letters **243** (1995) 49 – 54.

[24] Dai, H., Rinzler, A.G., Nikolaev, P., Thess, A., Colbert, D.T., and R.E. Smalley, "Single walled nanotubes produced by metal catalyzed disproportionation of carbon monoxide," Chemical Physics Letters **260** (1996) 471 – 475.

[25] Kong, J., Soh, H.T., Cassell, A.M., Quate, C.F., and H.Dai, " Synthesis of individual single-walled carbon nanotubes on patterned silicon wafers," Nature **395** (1998) 878 – 881.

[26] Dai, H., "Nanotube growth and characterization," in Carbon nanotubes Synthesis, structure, properties, and Application (edited by M.S. Dresselhaus, G. Dresselhaus, and Ph. Avouris (Eds.) Vol **80** (2001) Springer- Verlag P29.

[27] Hashimoto, A., Suenaga, K., Gloter, A., Urita, K., and S.Iijima, " Direct evidence for atomic defects in graphene layers," Nature **430** (2004) 870 – 873.

[28] Ajayan, P.M., "How does a nanofiber grow," Nature **427** (2004) 402-403.

[29] Hughes, T.V., and C.R.Chambers, " Manufacture of carbon filaments," U.S. Patent No. 405,480 dated June. 18, 1889.

[30] Davis, W.R., Slawson, R.J., and G.R. Rigby, "An unusual form of carbon," Nature **171** (1953) 756.

[31] Baker, R.T.K., Barber, M.A., Harris, P.S., Feates, F.S., and R.J. Waite, "Nucleation and growth of carbon deposits from the Nickel catalyzed decomposition of acetylene," Journal of Catalysis **26** (1972) 51-62.

[32] Baker, R.T.K., and P.S.Harris, "Controlled atmosphere electron microscopy," Journal of Physics E **5** (1970) 793.

[33] Baker, R.T.K., Harris, P.S., Thomas, R.B., and R.J.Waite, "Formation of filamentous carbon from Iron, Cobalt and Chromium catalyzed decomposition," Journal of Catalysis **30** (1973) 86.

[34] Baker, R.T.K., "Catalytic growth of carbon filaments," Carbon **27** (1989) 315-323.

[35] Baker, R.T.K., and P.S.Harris, "Formation of filamentous carbon," In Chemistry and physics of carbon (edited by P.L. Walker, Jr. and P.A. Thrower) Vol **14** (1978) Dekker, New York P 83.

[36] Hofer, L.J.E., Sterling, E., and J.T. McCartney, "Structure of the carbon deposited from carbon monoxide on Iron, cobalt and nickel," J.Phys. Chem **59** (1955)1153.

[37] Walker, Jr., P.L., Rakszawski, J.F., and G.R. Imperial, "Carbon formation from carbon monoxide-hydrogen mixtures over Iron catalysts. I. Properties of carbon formed," Journal Phys. Chem. **63** (1959) 133.

[38] Kato, T., Jeong, G.H., Hirata, T., and R. Hatakeyama, "Structure control of carbon nanotubes using radio-frequency plasma enhanced chemical vapor deposition," Thin Solid Films **457** (2004) 2 – 6.

[39] Fryer, J.R., and Z. Paal," Low temperature formation of fibrous carbon on platinum black," Carbon **11** (1973) 665.

[40] Nishiyama, Y., and Y.Tamai, "Carbon formation on copper-nickel alloys from benzene," Journal of catalysis **33** (1974) 98.

[41] Rostrup-Nielson, J.R., and D.L. Trimm, "Mechanisms of carbon formation on nickel containing catalysts," Journal of Catalysis **48** (1977) 155.

[42] Yang, R.T., and K.L. Yang, "Evidence for temperature-driven carbon diffusion mechanism of coke deposition on catalysts," Journal of Catalysis. **93** (1985) 182.

[43] Rostrup-Nielson, J.R., "sulfur passivated nickel catalysts for carbon free steam reforming of methane," Journal of Catalysis. **85** (1984) 31.

[44] Audier, M., Coulon, M., and Oberlin, A., "Relative crystallographic orientation of carbon and metal in a filamentous catalytic carbon," Carbon **18** (1980) 73.

[45] Audier, M., Oberlin, A., and M. Coulon, "Crystallographic orientations of catalytic particles in filamentous carbon; case of simple conical particles," Journal of Crystal Growth **55** (1981) 549.

[46] Oberlin, A., Endo, M., and T. Koyama, "filamentous growth of carbon through benzene decomposition," Journal of Crystal Growth **32** (1976) 335-349.

[47] Baird, T., Fryer, J.R., and B. Grant, " Carbon formation on iron and nickel foils by hydrocarbon pyrolysis- reactions at 700^{o}C," Carbon **12** (1974) 591 -602.

[48] Wagner, R.S., and W.C. Ellis, "The Vapor-Liquid-Solid Mechanism of crystal growth and its application to silicon," Transactions of the Metallurgical Society of AIME, **233** (1965) 1053 – 1064.

[49] Mojica, J.F., and L.L. Levenson, "Bulk-To-Surface precipitation and surface diffusion on carbon on polycrystalline nickel," Surface Science **59** (1976) 447-460.

[50] Tibbetts, G. Gary., "Why are carbon filaments tubular," Journal of Crystal Growth **66** (1984) 632-638.

[51] Gilmer, G.H., "Computer models of crystal growth," Science **208** (1980) 355 – 363.

[52] Bradley, J.R., Chen, Y.L., and H.W. Sturner, " The structure of carbon filaments and associated catalytic particles formed during pyrolysis of natural gas in steel tubes," Carbon **23** (1985) 715 – 722.

[53] Sacco, A., Thacker, P., Chang, T.N., and A.T.S. Chiang, " The initiation and growth of filamentous carbon from α-iron in H_2,CH_4, H_2O, CO_2, and CO gas mixtures," Journal of Catalysis **85** (1984) 224 - 236.

[54] Ozturk, B., Fearing, V.L., Ruth, jr., J.A., and G. Simkovich, Metals transactions, **13A** (1982) 1871.

[55] Dresselhaus, M.S., and M. Endo, "Relation of carbon nanotubes to other carbon materials," in Carbon nanotubes Synthesis, structure, properties, and Application (edited by M.S. Dresselhaus, G. Dresselhaus, and Ph. Avouris (Eds.) Vol **80** (2001) Springer-Berlin 21.

[56] Harris, P.J.F., "Carbon nanotubes and related structures," Cambridge University press (1999) 10.

[57] Tibbetts, G.G., Devour, M.G., and E.J. Rodda, "An adsorption-diffusion isotherm and its applications to the growth of carbon filaments on iron catalyst particles," Carbon **25** (1987) 367-375.

[58] Dresselhaus, M.S., and Morinobu Endo, " Relation of carbon nanotubes to other carbon materials," in Carbon nanotubes Synthesis, structure, properties, and Application (edited by) M.S. Dresselhaus, G. Dresselhaus, and Ph. Avouris (Eds.) Vol **80** (2001) Springer- Berlin 12.

[59] Ajayan, P.M., and T.W. Ebbesen, "Nanometer-size tubes of carbon," Rep. Prog. Phys. **60** (1997) 1025- 1062.

[60] Endo, M., and H.W. Kroto, "Formation of carbon nanofibers," J. Phys. Chem. **96** (1992) 6941-6944.

[61] Saito, Riichiro., Fujita, Mitsutaka., Dresselhaus, G., and M.S. Dresselhaus, " Electronic structure and growth mechanism of carbon tubules," Materials Science and Engineering B **19** (1993) 185-191.

[62] Vinciguerra, V., Buonocore, F, Panzera, G., and Luigi Occhipinti, "Growth mechanisms in chemical vapor deposition," Nanotechnology **14** (2003) 655-660.

[63] Louchev, O.A., Sato, Y., and Hisao Kanda, "Growth mechanisms of carbon nanotube forests by chemical vapor deposition," Appl. Phys. Lett. **80** (2002) 2752-2754.

[64] R.E. Smalley, "From dopyballs to nanowires", Materials Science and Engineering B **19** (1993) 1-7.

[65] Iijima, S., "Growth of carbon nanotubes," Materials Science and Engineering B **19** (1993) 172-180.

[66] Charlier, J-C., De Vita, A., Blasé, X., and R. Car, "Microscopic growth mechanisms for carbon nanotubes," Science **275** (1997) 646 -649.

[67] Charlier, J-C., Blasé, X., De Vita, A., and R. Car, "Microscopic growth mechanisms for carbon and boron-nitride nanotubes", Appl. Phys. A 68 (1999) 267-273.

[68] Charlier, J-C., and S. Iijima, "Relation of carbon nanotubes to other carbon materials," in Carbon nanotubes Synthesis, structure, properties, and Application (edited by M.S. Dresselhaus, G. Dresselhaus, and Ph. Avouris (Eds.) Vol **80**, P67. Springer-Berlin 2001.

[69] Kiang, C.H., and W.A. Goddard, "Polyyne ring nucleus growth model for single-layer carbon nanotubes," Phys. Rev. Lett. **76** (1996) 2515- 2518.

[70] Birkett, P.R., Cheetham, A.J., Eggen, B.R., Hare, J.P., Kroto, H.W., and D.R.M. Walton, " Transition metal surface decorated fullerenes as possible catalytic agents for the creation of single walled nanotubes of uniform diameter," Chem. Phys. Lett. **281** (1997) 111-114.

[71] Thess, A., Lee, R., Nikolaev, P., Dai, H., Petit, P., Robert, J., Xu, C., Lee, Y.H., Kim, S.G., Colbert, D.T., Scuseria, G., Tomanek, D., Fischer, J.E., and R.E. Smalley, "Crystalline ropes of metallic carbon nanotubes," Science **273** (1996) 483-487.

[72] Lee, Y.H., Kim, S.G., and D. Tomanek, "Catalytic growth of single-wall carbon nanotubes: An *Ab Initio* study," Phys. Rev. Lett. **78** (1997) 2393- 2396.

[73] Maiti, A., Brabec, C.J., Roland, C., and J. Bernholc, "Theory of carbon nanotube growth", Phys. Rev B. **52** (1995) 14850-14858.

[74] Maiti, A., Brabec, C.J., and J. Bernholc, "Kinetics of metal-catalyzed growth of single-walled carbon nanotubes," Phys. Rev B. **55** (1997) R6097-R6100.

[75] Guo, T., Nikolaev, P., Rinzler, A.G., Tomanek, D., Colbert, D.T., and Richard E. Smalley, "Self-assembly of tubular fullerenes," J. Phys. Chem. **99** (1995) 10694-10697.

[76] Amelinckx, s., Zhang, X.B., Bernaerts, D., Zhang, X.F., Ivanov, V., and J.B. Nagy, "A formation mechanism for catalytically grown helix-shaped graphite nanotubes," Science **265** (1994) 635-639.

[77] Lee, Y.H., Kim, S.G., and D. Tomanek, "Catalytic growth of single-wall carbon nanotubes: an ab initio study," Physical Review Letters 78 (1997) 2393- 2396.

[78] Cui, H., Zhou, O., and B.R. Stoner, "Deposition of aligned bamboo-like carbon nanotubes via microwave plasma enhanced chemical vapor deposition," Journal of Applied Physics **88** (2000) 6072-6074.

[79] Saito, Y., "Nanoparticles and filled nanocapsules," Carbon **33** (1995) 979-988.

[80] Kuttel, O.M., Groening, O., Emmenegger, C., and L. Schlapbach, "Electron field emission from phase pure nanotube films grown in a methane/hydrogen plasma," Applied Physics Letters **73** (1998) 2113-2115.

[81] Gao, J.S., Umeda, K., Uchino, K., Nakashima, H., and K. Muraoka, "Control of sizes and densities of nanocatalysts for nanotube synthesis by plasma breaking method," Material science and Engineering B **107** (2004) 113-118.

[82] Lin, C.H., Chang, H.L., Hsu, C.M., Lo, A.Y., and C.T. Kuo, "The role of nitrogen in carbon nanotube formation," Diamond and Related Materials **12** (2003) 1851-1857.

[83] Jung, M., Eun, K.Y., Baik, Y.G., Lee, K.R., Shin, J.K., and Sung-tae. Kim, "Effect of NH_3 environmental gas on the growth of aligned carbon nanotube in catalystically pyrolyzing C_2H_2," Thin solid films **398-399** (2001) 150-155.

[84] Lee, J.Y., and B.S. Lee, "Nitrogen induced structure control of vertically aligned carbon nanotubes synthesized by microwave plasma enhanced chemical vapor deposition," Thin solid Films **418** (2002) 85-88.

[85] Jin, S., and T.D. Moustakas, "Effect of Nitrogen on the growth of diamond films," Applied Physics Letters **65** (1994) 403- 405.

[86] Tsang, T.S, Rego, C.A., May, P.W., Ashfold, M.N.R., and K.N. Rosser, " Examination of the effects of nitrogen on the CVD diamond growth mechanism using in situ molecular beam mass spectrometry," Diamond and Related Materials **6** (1997) 247-254.

[87] Wong, W.K., Li, C.P., Au, F.C.K., Fung, M.K., Sun, X.H., Lee, C.S., Lee, S.T., and W. Zhu, "Fabrication and characterization of pure and well aligned carbon nanotubes using Methane/Nitrogen- Ammonia plasma," Journal of Physics & Chemistry B **107** (2003) 1514 – 1517.

[88] Zhong, D., Liu, S., Zhang, G., and E.G. Wang," Large-scale well aligned carbon nitride nanotube films: Low temperature growth and electron field emission," Journal of Applied Physics **89** (2001) 5939-5943.

[89] Jung, M., Eun, K.Y., Lee, J.K., Baik, Y.J., Lee, K.R., and J.W. Park, "Growth of carbon nanotubes by chemical vapor deposition," Diamond and Related Materials **10** (2001) 1235-1240.

[90] Chen, M., Chen, C.M., Koo, H.S., and C.F.Chen, "Catalyzed growth model of carbon nanotubes by microwave plasma chemical vapor deposition using CH4 and CO2 gas mixtures," Diamond and Related Materials **12** (2003) 1829-1835.

[91] Kanzow, H., and A. Ding, "Formation mechanism of single wall carbon nanotubes on liquid-metal particles," Physical Review B **60** (1999) 11180-11186.

[92] Cassell, A.M., Raymakers, J.A., Kong, J., and H.Dai, "Large scale CVD synthesis of single-walled carbon nanotubes," Journal of Physical Chemistry B **103** (1999) 6484 – 6492.

[93] Lin, C.H., Lee, S.H., Hsu, C.M., and C.T. Kuo, " Comparison on properties and growth mechanisms of carbon nanotubes fabricated by high-pressure and low-pressure plasma enhanced chemical vapor deposition," Diamond and Related Materials **13** (2004) 2147 – 2151.

[94] Juang, Z.Y., Lai, J.F., Weng, C.H., Lee, J.H., Lai, H.J., Lai, T.S., and C.H.Tsai, "On the kinetics of Carbon nanotube growth by thermal CVD method," Diamond and Related Materials **13** (2004) 2140 – 2146.

[95] Meyyapan, M., Delzeit, L., Cassell, A., and D. Hash, "Carbon nanotube growth by PECVD: a review," Plasma Sources Science and Technology **12** (2003) 205 – 216.

[96] Merkulov, V.I., Melechko, A.V., Guillorn, M.A., Lowndes, D.H., and M.L. Simpson, "Alignment mechanism of carbon nanofibers produced by plasma enhanced chemical vapor deposition," Applied Physics Letters **79** (2001) 2970 – 2972.

[97] Merkulov, V.I., Guillorn, M.A., Lowndes, D.H., Simpson, M.L., and E. Voekl, "Shaping carbon nanostructures by controlling the synthesis process," Applied Physics Letters **79** (2001) 1178 – 1180.

[99] Gao, J.S., Umeda, K., Uchino, K., Nakashima, H., and K.Muraoka, "Plasma breaking of thin films into nano-sized catalysts for carbon nanotube synthesis", Materials Science and Engineering A **352** (2003) 308-313.

[100] Tsai, S.H., Chao, C.W., Lee, C.L., and H.C. Shih, " Bias-enhanced nucleation and growth of the aligned carbon nanotubes with open ends under microwave plasma synthesis," App. Phy. Lett. **74** (1999) 3462-3464.

[101] Ebbesen, T.W., and P.M.Ajayan, "Large-scale synthesis of carbon nanotubes," Nature **358** (1992) 220-222.

[102] Qin, L.C., and S.Iijima, "Fibrilliform growth of carbon nanotubes", Mater. Lett. **30** (1997) 311 -314.

[103] Bower, C., Zhu, W., Jin, S., and O.Zhou, "Plasma induced alignment of carbon nanotubes", Applied Physics Letters **77** (2000) 830-832.

[104] Zhong, D., Liu, S., Zhang, G., and E.G.Wang, "Large scale well-aligned carbon nitride nanotube films: Low temperature growth and electron field emission", Journal of Applied Physics **89** (2001) 5939 – 5943.

[105] Zhang, Q., Yoon, S.F., Ahn, J., Gan, B., Rusli, and M.-B.Yu, "Carbon films with high density nanotubes produced using microwave plasma assisted CVD," J. Phys. Chem. Solids. **61** (2000) 1179-1183.

[106] Qin, L.C., Zhou, D., Krauss, A.R., and D.M. Gruen, "Growing carbon nanotubes by microwave plasma-enhanced chemical vapor deposition", App. Phy. Lett. **72** (1998) 3437- 3439.

[107] Bower, C., Zhou, O., Zhu, W., Werder, D.J., and S. Jin, "Nucleation and growth of carbon nanotubes by microwave plasma chemical vapor deposition," App. Phy. Lett. **77** (2000) 2767 – 2769.

[108] Choi, Y.C., Shin, Y.M., Lee, Y.H., and Byung Soo Lee, "Controlling the diameter, growth rate, and density of vertically aligned carbon nanotubes synthesized by

microwave plasma-enhanced chemical vapor deposition", App. Phy. Lett. **76** (2000) 2367-2369.

[109] Nidadavolu, A.G.R., "Synthesis of carbon nanotubes by microwave plasma enhanced CVD on silicon using iron as catalyst," M.S. Thesis, School of Mechanical and Aerospace Engineering, Oklahoma State University, Stillwater, OK (2005).

[110] Raghavan, D., "Multi-walled carbon nanotubes synthesis by microwave plasma enhanced CVD using colloidal form of iron oxide as catalyst," M.S. Thesis, School of Mechanical and Aerospace Engineering, Oklahoma State University, Stillwater, OK (2005).

[111] Thess, A., Lee, R., Nikolaev, P., Dai, H., Petit, P., Robert, J., Xu, C., Lee, Y. H., Kim, S. G., Rinzler, A. G., Colbert, D.T., Scuseria, G., Tománek, D., Fischer, J.E., and R.E. Smalley, "Crystalline Ropes of Metallic Carbon Nanotubes, "Science **273** (1996) 483.

VITA

Madhan Prasath Ramakrishnan

Candidate for the Degree of

Master of Science

Thesis: EXPERIMENTAL STUDY ON MICROWAVE ASSISTED CVD GROWTH OF CARBON NANOTUBES ON Si WAFER USING COBALT CATALYST AS A CATALYST

Major Field: Mechanical Engineering

Biographical:

Education: Received Bachelor of Engineering degree in Mechanical Engineering from Bharathiar University, Coimbatore, India in May 2000. Completed the requirements for the Master of Science degree with a major in Mechanical and Aerospace Engineering at Oklahoma State University in May 2005.

Experience: Student intern in Design section, Subermersible pumps- 5hp division, Gopalakrishna Industries, Coimbatore, India, January, 2001- December, 2001.
Graduate Research Assistant in Mechanical and Aerospace Engineering Department, Oklahoma State University, Stillwater, Oklahoma, January, 2002 - present.